WASHINGTON UNIVERSITY

Department of Physics

Dissertation Committee:
Willem H. Dickhoff, Chairperson
John W. Clark
Michael C. Ogilvie
Demetrios G. Sarantites
Lee G. Sobotka
Elizabeth R.-Stoddard

SELF-CONSISTENT GREEN'S FUNCTION STUDY OF LOW-ENERGY CORRELATIONS IN ^{16}O

by

Carlo Barbieri

A dissertation presented to the
Graduate School of Arts and Sciences
of Washington University in
partial fulfillment of the
requirements for the degree
of Doctor of Philosophy

August 2002

Saint Louis, Missouri

ABSTRACT OF THE DISSERTATION

Self-Consistent Green's Function Study
of Low-Energy Correlations in ^{16}O

by

Carlo Barbieri

Doctor of Philosophy in Physics

Washington University in Saint Louis, August 2002

Professor Willem H. Dickhoff, Chairperson

The Faddeev technique is employed to address the problem of describing the influence of both particle-particle and particle-hole phonons on the single-particle self-energy. The scope of the few-body Faddeev equations is extended to describe the motion of two-hole one-particle (two-particle one-hole) excitations. This formalism allows to sum both particle-particle and particle-hole phonons, obtained separately in the Random Phase Approximation. The appearance of spurious solutions for the present application of the Faddeev method is related to the inclusion of a consistent set of diagrams. The relevant formalism is employed to study the influence of both particle-particle and particle-hole phonons on the single-particle spectral function of ^{16}O. An iterative procedure is applied to investigate the effects of the self-consistent inclusion of the fragmentation in the determination of the phonons and the corresponding self-energy. At the same time, the excitation spectra of ^{16}O, ^{14}C and ^{14}N are obtained in a self-consistent way. The present results indicate that the characteristics of hole fragmentation are related to the low-lying states of ^{16}O. This implies that a better description of particle-hole phonons is necessary in order to improve the description of hole fragmentation. A first attempt in this direction is pursued.

Contents

List of Figures

List of Tables

Acknowledgements

My greatest thanks go to Wim Dickhoff. His guidance has made it possible to pursue this project to the end. But most of all his patience and his support during all these years have been invaluable, in may ways, not only to learn about many-body physics but also for growing as a physicist. I am indebted to him for all that I know about this field. I wish to extend my thanks to the people of the nuclear physics group and those who have served on my committee, Lee Sobotka, Demetrios Sarantites, Libby and especially John Clark.

I am also very grateful to Herbert Müther, for his hospitality during my stay at the university of Tübingen. I thank Mike Ogilvie for his advice from which I have learned as well.

Many things have happened during these three years in St.Louis and for sure it wouldn't have been the same without all the people that I met. Silvina, Hui-fen and Francesca will always be among my dearest friends. All the others are nothing less.

A very special thanks goes to my grandmother, *Maria*. She is mom's mom and by definition the second most beautiful woman in the world (the first place goes to mom, obviously). When they told her that I was leaving my home town she said: "Uff... even if I tried I know I couldn't keep him here. So what can I do?" But she was smiling and I will always remember this, because if I didn't have her long ago I probably would not be writing this thesis today.

Ringraziamenti

I miei più sinceri ringraziamenti vanno a Wim Dickhoff per la guida ed il sostegno avuti. Essi non solo hanno reso possibile il completamento di questo lavoro ma sono anche stati fondamentali per apprendere la fisica dei molti corpi per crescere come ricercatore. Desidero estendere i miei ringraziamenti anche ai membri della commissione, Lee Sobotka, Demetrios Sarantites, Libby ed in particolare John Clark.

Sono grato a Herbert Müther per la sua ospitalità durante la mia permanenza all'unitversità di Tübingen e a Mike Ogilvie per alcune chiacchierate da cui ho imparato molto.

Sebbene sia un poco retorico dire ciò, molte cose sono successe durante questi tre anni passati a St. Louis e sicuramente tale esperienza non sarebbe stata la stessa senza tutte le persone che ho conosciuto. Silvina, Hui-fen e Francesca saranno sempre tra i miei più cari amici, lo stesso vale per tutti gli altri.

Un grazie molto speciale a mia nonna *Maria*, lei è senza dubbio la seconda donna più bella al mondo (la prima è sempre la mamma). Quando le hanno detto che sarei partito ha sbuffato un pò e ha detto: "...e mi sa gon da fag? Tant u va istes...." Però sorrideva e mi ricorderò sempre di questo, perchè se oggi sono qui a scrivere questa tesi è anche grazie al fatto di aver avuto lei tempo addietro.

Chapter 1

Introduction and Motivation

1.1 Motivation

Correlations in the nucleus produce a substantial reduction of the occupation probability of single-particle (sp) shells with respect to the independent-particle model (IPM) prediction. A substantial part of this depletion is due to the coupling to high-lying excitations reached by the strong short-range and tensor components of the nucleon-nucleon interaction [1, 2]. At low energy, the presence of various collective modes may result in a rearrangement of the sp strength distribution around the Fermi energy [3]. Experimentally, these features can be observed in the $(e, e'p)$ reaction as a reduction of the absolute spectroscopic factors for the knockout of a nucleon from a valence shell, as the strong fragmentation of the spectral strength for more deeply bound sp states, and by the appearance of small fragments associated with sp states that are empty in the IPM. Studies of $(e, e'p)$ reactions have determined absolute spectroscopic factors in many closed-shell nuclei [4, 5, 6] demonstrating that the removal probability for nucleons from these systems is reduced by about 35% with respect to the shell-model predictions. More recently, also $(e, e'NN)$ reactions, that involve the emission of two nucleons from the target, have become feasible [7, 8]. The latter were motivated by the possibility to directly study the high-momentum components, produced by short-range and tensor correlations (SRTC), between pairs of nucleons at low energy. Such experiments are now able to disentangle the most relevant lowest states of the residual $A-2$ nucleus [9] which are also influenced by the presence of low-energy correlations.

The theoretical study of one- and two-hole spectral functions to understand the results of the above reactions, requires substantial efforts in computational many-body physics and does not always give a complete explanation of the observed data. In particular, the nucleus of ^{16}O is still not completely understood at the microscopic level and theoretical calculations of its properties still fail in two ways.

First, the experimental spectroscopic strength [10] for the knockout of a proton

	experiment	GF-sr	VMC	CBF	GF [18]	GF [19]
$Z_{p_{3/2}}$	0.50–0.64	0.91	0.90	0.90	0.85	0.76
$Z_{p_{1/2}}$	0.54–0.72	0.89		0.90	0.83	0.77

Table 1.1: The experimental and theoretical values for the absolute hole spectroscopic factors of the principal $p_{1/2}$ and $p_{3/2}$ orbitals. Reported is the range of values obtained from different analysis of the experimental data. The theoretical results have been obtained by employing different techniques, such as Green's function approach to study short-range correlations (GF-sr) [13], variational Monte Carlo (VMC) [14], correlated basis function (CBF) [15] and other applications of Green's function theory that include long-range effects (GF) [18, 19]. The effects of the center of mass motion are not included in any of these theoretical results and are known to produce a 7% increase of the spectral strength.

from both the $p_{1/2}$ and $p_{3/2}$ shells corresponds to about 60%. Table 1.1 gives an overview of the present experimental and theoretical values. The uncertainty in the experimental values is a consequence of the sensitivity to the model adopted for treating the final-state interactions. In general, the outgoing proton is described by a wave distorted by a complex optical potential which describes the corresponding elastic proton scattering data. This introduces an uncertainty in these spectroscopic factors since the $(e, e'p)$ reaction probes the interior of the nucleus, where elastic proton scattering is less sensitive. The inclusion of a relativistic description of the outgoing proton in the analysis of the data can further change these results somewhat [10, 11, 12]. An assignment of a 5 to 10% error for the experimental absolute spectroscopic factors appears quite reasonable at this time. Several theoretical studies have focused on the effect of short-range correlations [13, 14, 15] and computed spectroscopic factors directly for ^{16}O. All these works yield a strength reduction of about 10% in general agreement with expectations based on nuclear-matter calculations [1]. Center-of-mass corrections are known to raise the spectroscopic factor by about 7% [16, 17], resulting in a substantial disagreement with data. The effects of long-range correlations (LRC) were studied in Refs. [18, 19]. The inclusion of LRC in these works is limited to the Tamm-Dancoff (TDA) approximation for the intermediate two-particle−one-hole (2p1h) and two-hole−one-particle (2h1p) states in

the nucleon self-energy using the G-matrix as a residual interaction. The reduction of the $p_{1/2}$ and $p_{3/2}$ spectroscopic factors due to these LRC is about 15%. In the calculations of Ref. [19], a combined treatment of LRC and SRTC was obtained. The resulting $p_{1/2}$ and $p_{3/2}$ spectroscopic factors correspond to 77% and 76% of the sp strength, respectively, without inclusion of center-of-mass corrections. Short-range effects were included by employing the energy-dependence of the Brueckner G-matrix in the corresponding self-energy contribution. The resulting disagreement with the experimental data appears to be about 15-20% after considering the center of mass effects. Some allowance for the uncertainty of the extraction of the spectroscopic factors should be factored in. Looking at the overall picture, a comparison between the quoted results suggests that the quenching produced by SRTC appears to be well established. At the same time, the results of Refs. [18, 19] clearly show that a substantial improvement can be obtained by the inclusion of LRC. The latter are identified as an essential ingredient that is needed for a complete understanding of the discrepancy with the experimental data.

The second issue regarding ^{16}O concerns a satisfactory understanding of the fragmentation of the sp strength at low energy. In particular, the experiments show that the spectral strength for the emission of a $p_{3/2}$ proton is split in one big peak and a few smaller ones [10]. The latter are found at a slightly higher missing energy and carry a reasonable amount of strength: of the 60% observed mean-field strength, about 5% is distributed in these small peaks while the rest is in the main fragment. This feature is not reproduced by the results of Refs. [18, 19], where all the strength is concentrated in one single peak. Other experimentally observed hole fragments, like the $d_{5/2}$ and $s_{1/2}$ found at about -17.4 MeV missing energy, are not reproduced as well. The full one-hole spectral function for small missing energies was computed in Ref. [19] and the results were subsequently used as a starting point for the study of the ^{16}O(e,e′pp) reaction [20, 21]. The high-momentum components of the two-hole overlap function caused by short-range effects were also included by adding the proper defect functions computed directly for the ^{16}O nucleus [22]. These calculations led to a proper description of the experimental cross section for two proton emission [7, 8] to the ground state of ^{14}C. In spite of these successes, the one- and two-hole spectral functions still miss some key features of the fragmentation and do not describe all the relevant low-lying states of the residual nuclei ^{15}N and ^{14}C. The spectrum of ^{14}C contains two low-lying isovector 2^+ levels that can be reached by two-nucleon emission, but only one of them is reproduced by the above theoretical calculations. This missing state represents the main discrepancy between

the theoretical and experimental ^{16}O(e,e′pp) cross sections [8]. The need for a theoretical description of the 2^+ splitting will become more compelling in the near future, since the high resolution of the experiments performed at MAMI can now distinguish clearly between the corresponding final states [9, 23]. It is interesting to note that the transition to both of the 2^+ states can be interpreted as the knockout of two protons from a $p_{1/2}$ and a $p_{3/2}$ state. Although this has not been directly investigated before, it is natural to suppose that a connection exists between the spectrum of ^{14}C and the fragmentation of the $p_{3/2}$ strength in ^{15}N. The presence of a very low-lying 2^+ state in ^{16}O can also play a role. It is worth noting that the fragmentation of the $p_{3/2}$ strength, in turn, can be interpreted as a $p_{3/2}$ hole in either the ground state of ^{16}O or one of its low-lying positive parity states. Thus, there exists an intimate connection between various excited levels of ^{16}O and those of its neighbors. Since these spectra and transition amplitudes are naturally linked to each other, a formalism in which all of them are obtained in a self-consistent way is desirable, if not necessary, to resolve the above issues. Such self-consistent calculations have so far been restricted to second-order contributions to the self-energy using a Skyrme force for the effective interaction [24]. Such a treatment of LRC in ^{16}O is inadequate since it does not include any residual interaction between the intermediate 2p1h and 2h1p states in the self-energy.

The merit of the calculations of Refs. [18, 19] was that the interaction between the 2p1h states (and 2h1p states) was summed to all orders. Thus a simultaneous description of the effects of both particle-hole (ph) and hole-hole (hh) (as well as particle-particle (pp)) collective excitations was achieved, including the interplay between them. These collective excitations, though, were accounted for only at the TDA level. An extension of these calculations beyond TDA is not a trivial problem and presents serious difficulties [25]. On the other hand, in order to account for the coupling to collective excitations that are actually observed in ^{16}O it is necessary to at least consider a random phase approximation (RPA) description of the isoscalar negative parity states [26]. The situation is even more complicated if one wants to reproduce the low-lying isoscalar positive parity states. For example the first 0^+ and 2^+ excitations are known to contain relevant 4-particle–4-hole (4p4h) components [27]. For these states an RPA approach is not enough and an even more complicated treatment will be required [28]. A similar situation has to be faced in order to account for two-particle correlations in the medium. Sizable collective effects are present in the pp and hh excitations involving tensor correlations for isoscalar and pair correlations for isovector states. Also in this case, an RPA

treatment would be relevant.

This thesis aims to extend the calculation of Ref [19] in two ways. First, we want to account for the collectivity in the ph and pp (hh) channels at least at the RPA level. The second goal is to achieve a self-consistent description of these correlations. The importance of the last point can be understood by noting that the observed fragmentation and depletion of the sp strength in ^{16}O is quite substantial. Thus, it is reasonable to expect that these features are also important in the description of the excitations that contribute to the self-energy. To account for them one requires a self-consistent formulation where the dressing of the nucleons is incorporated in the description of the collective excitations (that ultimately leads to the dressing itself). For this reason the present work will be formulated using self-consistent Green's function (SCGF) theory. This type of self-consistency must also be considered in describing pairing correlations in semi-magic nuclei [29, 30]. The problem of properly describing the excitation spectra of ^{16}O, going beyond the RPA scheme, represents one of the main missing ingredients in the present calculations. This will be addressed separately, still within the framework of SCGF.

1.2 Technical Issues

The consistent treatment of ph and pp(hh) phonons in the sp self-energies represents a non-trivial many-body problem [31, 32, 33] and is the main technical issue that was addressed in the present work.

A formalism in which both pp and ph phonons are treated at the RPA level in the self-energy was proposed in Ref. [34]. This work focused on the two-time two-particle one-hole (2p1h) propagator and generated a formulation that reduces to either including the pp RPA or the ph RPA phonons in the self-energy when ph or pp vertices are omitted, respectively. This expansion, however, was obtained using some drastic assumptions and disregarding some of the constraints that arise when propagators in different diagrams of the expansion are connected. Related to this issue is the appearance of unphysical solutions for the 2p1h propagator that have been discussed in [25]. Results in [25] have therefore been obtained mostly for the TDA treatment of the 2p1h propagator. Moreover, this approximation was obtained by employing mean-field (single-pole) sp propagators. In the present self-consistent treatment, which sums fully dressed propagators, this approach is no longer possible.

To proceed with the inclusion of both pp and ph collectivity in the nucleon self-energy it is important to note that the naive summation of diagrams containing

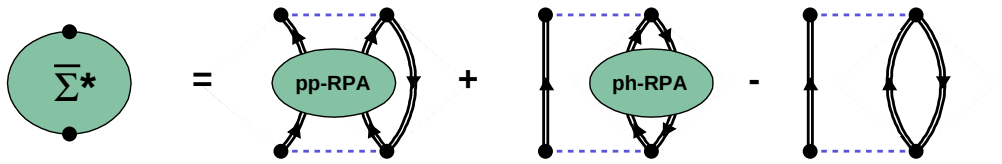

Figure 1.1: Example of an approximation for the self-energy. Although this approximation contains both ph and pp correlations it would generate incorrect results, due to the need of subtracting the second order term to avoid double counting.

both pp and ph phonons leads to serious inconsistencies. This approximation is depicted in Fig. 1.1. The last of the three diagrams on the right hand side is already contained in each of the other two and must therefore be subtracted to avoid double counting. This subtraction introduces spurious poles in the Lehmann representation of the self-energy and generates meaningless solutions of the Dyson equation. In addition, each of the first two terms in Fig. 1.1 ignores the Pauli correlations between the freely propagating line and the quasi-particles forming the phonons, as noted in [3]. In the present work a formalism is pursued which sums the contribution of the pp and ph phonons to the self-energy to all orders avoiding the subtraction of the second-order diagram. The treatment of Pauli correlations is improved over methods that employ ph RPA phonons in the self-energy since all exchange terms at the 2p1h level are consistently included.

Other approaches have been proposed in the literature that attempt to extend the nature of the phonon correlations included by performing massive summations of diagrams [31, 32, 33, 35]. Nevertheless, a consistent resummation of both pp and ph phonons to all orders has not been achieved in these papers. The main problem in pursuing such an infinite summation of diagrams for the 2p1h propagator, which includes both pp and ph RPA correlations, is related to the fact that a two-body interaction can invert the sense of propagation of only two lines (i.e. change at most two particles into two holes and vice versa) while the third line continues to propagate in the original direction. In this way, a propagator depending on more than two times is generated. It is therefore necessary first to consider an exact

formulation involving the four-time Green's function for the 2p1h propagator. Direct application of four-time propagator equations presumably will remain impractical for the forseeable future. Appropriate approximations to this equation are therefore necessary to construct the relevant two-time Green's functions which contains the sought after correlations. The approach pursued in this thesis consists in computing the RPA phonons in the pp and ph channels, separately, and then summing them to all orders employing a Faddeev technique [36, 37]. This led to a formalism that has been proposed recently in Refs. [38, 39]. The resulting self-energy contains the inclusion of these pp(hh) and ph RPA phonons to all orders and therefore allows for an improved description of the influence of LRC on the sp propagator. In turn, the results for the hole (and particle) spectral functions can be employed in a subsequent dressed RPA (DRPA) calculation and then iterated to investigate the effects of self-consistency on the fragmentation.

A nontrivial problem in the implementation of the Faddeev equations is the appearance of spurious solutions [40, 41] which also have to be considered for the 2p1h propagator. As pointed out in Ref. [42], the spurious eigenstates are easy to recognize for the three-body problem since they also diagonalize the unperturbed Hamiltonian. Their main features are that their eigenvalues are known and that their wave-function amplitudes sum up to zero. The situation is more complicated when the Faddeev technique is employed in a many-body formulation. In particular, the fulfillment of closure relations for pp and ph amplitudes is related to the behavior of the spurious Faddeev eigenstates. Without a consistent treatment of this relation the spurious solutions will mix with the physically meaningful ones. Applying the Faddeev technique to the many-body problem, it is important to solve for all physical solutions that contribute to the self-energy. Thus, it is necessary to develop a formalism in which the spurious solutions are correctly separated from the physical ones.

A relevant feature of the Faddeev approach is that it can be naturally extended to include correlation effects that go beyond the standard (D)RPA level. For example, one may consider to employ the extended RPA (ERPA) equations [43] to include the effects of 2p2h states in ^{16}O. Nevertheless, in order to properly generate the low-lying excitation spectrum these equations have to be extended at least to a level that includes the coupling of different phonons, following the approach proposed in Ref. [28]. A self-consistent treatment of the resulting equations would automatically include effects due to 3p3h and higher configurations. This type of calculation, however, is still in its infancy stage and the inclusion of the resulting

phonons into the Faddeev scheme is beyond the scope of this thesis.

The practical implementation of the present Faddeev scheme results in a set of equations that require a substantial amount of computational effort. Nevertheless, they can be solved in practice for the system of interest in this thesis.

1.3 Outline

In Chapter 2 the concept of Green's functions of a many-body system and the framework of SCGFs are introduced. The latter approach represents the basis underlying the calculations of the present thesis and provides the way to account for the effects of nuclear fragmentation. In general, the nuclear Hamiltonian contains sizable three-body forces [44] that are needed in order to correctly reproduce the binding energy of systems with three or more nucleons. Such interactions include contributions from two-pion exchange diagrams that involve excitations of a delta particle as well as effective terms that account for short-range interactions of the three nucleons. In the present work we are mainly interested in long-range effects, that involve small excitation energies. As a consequence, one should not expect any relevant contribution of delta excitations to the low-lying spectrum of ^{16}O. For this reason three-body forces will not be considered in the present work.

Following the philosophy of the SCGF approach, the DRPA equations for ph and pp (hh) motion will be discussed in Section 2.3 and then will be employed to generate the interaction kernel of the Faddeev equations, which are introduced in Section 2.4. In order to apply the formalism presented in Chapter 2 to a real system, further manipulations are required. These have practical importance but no further discussion of them is strictly necessary to understand the calculation and the physics associated with the results of this thesis. To avoid discontinuity in the discussion, the rest of the formalism will be presented in the appendices. In particular, Appendix A will deal with the (D)RPA equations and their extension to include two-phonon states. In Appendix B the Faddeev equations will be discussed in detail, paying particular attention to the issues related to the spurious solutions. Although so far only the 2p1h propagator has been mentioned, it should be understood that the corresponding two-hole one-particle (2h1p) propagator must be included in the calculation of the nucleon self-energy. In the present work no coupling terms are considered that transform the 2p1h into the 2h1p propagators (or vice versa). For this reason the same technique can be used for both propagators and we will use the generic 2p1h case to discuss the theory throughout this thesis.

The Faddeev formalism is applied to ^{16}O in Chapter 3. These calculations are

performed within a truncated model space and a G-matrix interaction is employed as an effective interaction. Effects of short-range correlations are included by taking into account the energy dependence of the G-matrix, as in Ref. [19]. Contributions from either three-body interactions or relativistic effects still play a role in determining the spin-orbit splitting of states close to the Fermi level. This can be taken into account in an effective way, as explained in Section 3.1.2. The results of Section 3.2 for the hole spectral function have already been published in Ref. [45]. Further results, pertaining to the ph and hh phonons, are presented in the following sections. It is shown that a proper description of the ph propagator is needed in order to fully understand the fragmentation properties of the sp spectral function. Chapter 4 deals with the extension of the ph RPA equation and represents a first step to obtain a complete description of the spectrum of ^{16}O. Two-phonon contributions are embedded into the ERPA formalism and the resulting formalism is applied to study the ph propagator. Conclusions are drawn in Chapter. 5.

Chapter 2

Formalism

The aim of this chapter is to present the formalism employed to study the spectral function of ^{16}O. The interaction used in the calculations will be of G-matrix type and its energy dependence will be taken into account at the level of the Hartree-Fock term, in order to properly account for the effects of short-range correlations. Nevertheless, the results presented in this chapter have general validity. Therefore the formalism will be discussed in terms of a general two-body interaction, $\hat{V}$.

The general definition of Green's functions and their relation to spectral functions is given in Section. 2.1. In the next section, we describe the Dyson-Schwinger expansion for the one-body propagator and review the concept of the self-consistent Green's function (SCGF) approach. At this point, a set of different approximations to the self-energy are possible, corresponding to different truncations of the expansion in terms of dressed Feynman diagrams. Section 2.3 describes the (dressed) random phase approximation, or (D)RPA, which will be applied to evaluate the particle-particle (pp) (hole-hole (hh)) and particle-hole (ph) propagators. These will be the basic building blocks used to develop the Faddeev RPA approximation, in Section 2.4. Several technical details are relegated to the appendices. In particular, the approach used to solve the Faddeev equations and the existence and treatment of their spurious solutions are discussed thoroughly in Appendix B.

As the present work is intended for the study of low-lying excitations in finite systems, the formalism presented here is geared towards a discrete basis representation of the many-body propagators. A more general and exhaustive introduction to second quantization in many-body theory can be found in Refs. [46]-[52].

2.1 Green's Function of a Many-Body System: Definition and Relation to Experimental Quantities

We consider a finite system of A fermions interacting by means of a two-body interaction $\hat{V}$. The total Hamiltonian can then be written as

$$\hat{H} \;=\; \sum_{\alpha\beta} t_{\alpha\beta}\; c^{\dagger}_{\alpha} c_{\beta} \;+\; \tfrac{1}{4} \sum_{\alpha\beta\gamma\delta} V_{\alpha\beta,\gamma\delta}\; c^{\dagger}_{\alpha}\; c^{\dagger}_{\beta}\; c_{\delta}\; c_{\gamma}\;, \tag{2.1}$$

where $c^{\dagger}_{\alpha}$ (c_{α}) are the creation (destruction) operators of a particle in the state α, $V_{\alpha\beta,\gamma\delta}$ are the antisymmetrized two-body matrix elements of $\hat{V}$, and $t_{\alpha\beta}$ correspond to the matrix elements of the kinetic energy operator. Here and in the following, $\{\alpha\}$, $(\alpha = n_{\alpha}, l_{\alpha}, j_{\alpha}, m_{\alpha}, \tau_{\alpha})$ refer to a complete set of single-particle (sp) orbitals. In principle, three-body forces also contribute to the nuclear Hamiltonian. As explained in Section 1.3 these will not be considered in this thesis and therefore we do not include three-body operators in Eq. (2.1).

The one-body propagator (also known as two-point Green's function) of the A-body system with ground state $|\Psi^{A}_{0}\rangle$ is defined as [46, 47]

$$g_{\alpha\beta}(\tau) \;=\; -\,i\,\langle \Psi^{A}_{0}|\; T[c_{\alpha}(\tau) c^{\dagger}_{\beta}(0)]\; |\Psi^{A}_{0}\rangle\;, \tag{2.2}$$

where $T[\ldots]$ is the time-ordering operator and $c^{\dagger}_{\alpha}(t)$ and $c_{\alpha}(t)$ now correspond to operators in the Heisenberg picture, with time dependence

$$c_{\alpha}(t) \;=\; e^{iHt}\; c_{\alpha}\; e^{-iHt}\;. \tag{2.3}$$

Note that $\hbar$ is set equal to 1.

The sp propagator characterizes the evolution of a system containing one additional particle (for $\tau > 0$) or a system with one less particle ($\tau < 0$). It contains information on the expectation value of any one-body operator in the ground state $|\Psi^{A}_{0}\rangle$, as well as additional information on the systems with $A \pm 1$ particles. To see this, it is useful to insert a complete set of $A+1$ $\{|\Psi^{A+1}_{n}\rangle\}$ and $A-1$ $\{|\Psi^{A-1}_{k}\rangle\}$ eigenstates of the Hamiltonian $\hat{H}$. Then one can introduce the integral representation of the step function and Fourier transform the time variable τ to energy space. The result is the spectral, or Lehmann, representation [53] of the sp propagator (2.2),

$$g_{\alpha\beta}(\omega) \;=\; \sum_{n} \frac{(\mathcal{X}^{n}_{\alpha})^{*}\;\; \mathcal{X}^{n}_{\beta}}{\omega - \varepsilon^{+}_{n} + i\eta} \;+\; \sum_{k} \frac{\mathcal{Y}^{k}_{\alpha}\;\left(\mathcal{Y}^{k}_{\beta}\right)^{*}}{\omega - \varepsilon^{-}_{k} - i\eta}\;, \tag{2.4}$$

where the quantities $\mathcal{X}^{n}_{\alpha}$ and ε^{+}_{n} ($\mathcal{Y}^{k}_{\alpha}$ and ε^{-}_{k}) represent the spectroscopic amplitudes and the excitation energies –with respect to the A-body ground state– for the excited

states of a system with $A+1$ ($A-1$) particles. These quantities are defined in detail as follows

$$\begin{aligned} \mathcal{X}_\alpha^n &\equiv \langle \Psi_n^{A+1} | c_\alpha^\dagger | \Psi_0^A \rangle \ , \\ \mathcal{Y}_\alpha^k &\equiv \langle \Psi_k^{A-1} | c_\alpha | \Psi_0^A \rangle \ , \\ \varepsilon_n^+ &\equiv E_n^{A+1} - E_0^A \ , \\ \varepsilon_k^- &\equiv E_0^A - E_k^{A-1} \ . \end{aligned} \tag{2.5}$$

In Eqs. (2.4), (2.5) and in the following, we use the indices n and k to enumerate the fragments associated with the one-particle and one-hole excitations, respectively.

The Lehmann representation (2.4) contains all the eigenvalues of the excited states of the systems with $A+1$ and $A-1$ particles as well as their spectroscopic amplitudes for transitions to those states that are relevant for comparison with experimental data. This involves all the states that have non-zero transition amplitudes (i.e. non-zero residues) to the A-body ground state, thus also those which have predominantly 2p1h, 2h1p or more complex nature.

From Eq. (2.4) it is possible to extract the one-hole spectral function

$$\begin{aligned} S_\alpha^h(\omega) &= \frac{1}{\pi} \, Im \; g_{\alpha\alpha}(\omega) \\ &= \sum_k \left| \langle \Psi_k^{A-1} | c_\alpha | \Psi_0^A \rangle \right|^2 \ \delta(\omega + E_k^{A-1} - E_0^A) \\ &= \sum_k \left| \mathcal{Y}_\alpha^k \right|^2 \ \delta(\omega - \varepsilon_k^-) \ . \end{aligned} \tag{2.6}$$

The absolute spectroscopic factors Z_k for the removal of a nucleon from the A particle system, while leaving the residual nucleus in its k-th excited state, is obtained as

$$Z_k \ = \ \sum_\alpha |\langle \Psi_k^{A-1} | c_\alpha | \Psi_0^A \rangle|^2 \ = \ \sum_\alpha \left| \mathcal{Y}_\alpha^k \right|^2 \ . \tag{2.7}$$

The occupation number for a given sp state α is given by

$$n_\alpha \ = \ \langle \Psi_0^A | c_\alpha^\dagger c_\alpha | \Psi_0^A \rangle \ = \ \sum_k \left| \mathcal{Y}_\alpha^k \right|^2 \ , \tag{2.8}$$

while the total number of particles is

$$A \ = \ \sum_\alpha n_\alpha \ . \tag{2.9}$$

Another quantity of interest is the four-point Green's function, defined as

$$g^{4-pts}_{\alpha\beta,\gamma\delta}(t_1,t_2;t_3,t_4) \;=\; -\,i\,\langle\Psi^A_0|\;T[c_\beta(t_2)c_\alpha(t_1)c^\dagger_\gamma(t_3)c^\dagger_\delta(t_4)]\;|\Psi^A_0\rangle\;. \tag{2.10}$$

This can be reduced to a two-time quantity to obtain the polarization propagator

$$\Pi_{\alpha\beta,\gamma\delta}(\tau) \;=\; g^{4-pts}_{\delta\alpha,\gamma\beta}(\tau^+;0^+,\tau,0) - \langle\Psi^A_0|c^\dagger_\beta c_\alpha|\Psi^A_0\rangle\langle\Psi^A_0|c^\dagger_\gamma c_\delta|\Psi^A_0\rangle \tag{2.11}$$

which describes ph fluctuations with respect to the ground state $|\Psi^A_0\rangle$. This quantity contains all essential information about one-body nuclear excitations, as is more apparent from its Lehmann representation

$$\begin{aligned}\Pi_{\alpha\beta,\gamma\delta}(\omega) \;&=\; \sum_{n\neq 0}\frac{\langle\Psi^A_0|c^\dagger_\beta c_\alpha|\Psi^A_n\rangle\;\langle\Psi^A_n|c^\dagger_\gamma c_\delta|\Psi^A_0\rangle}{\omega-(E^A_n-E^A_0)+i\eta}\\ &\quad-\sum_{n\neq 0}\frac{\langle\Psi^A_0|c^\dagger_\gamma c_\delta|\Psi^A_n\rangle\;\langle\Psi^A_n|c^\dagger_\beta c_\alpha|\Psi^A_0\rangle}{\omega-(E^A_0-E^A_n)-i\eta}\;.\end{aligned} \tag{2.12}$$

Another two-time reduction of Eq. (2.10) is the two-particle propagator

$$g^{II}_{\alpha\beta,\gamma\delta}(\tau) \;=\; g^{4-pts}_{\alpha\beta,\gamma\delta}(\tau,\tau^+;0^+,0) \tag{2.13}$$

whose spectral representation

$$\begin{aligned}g^{II}_{\alpha\beta,\gamma\delta}(\omega) \;&=\; \sum_{n}\frac{\langle\Psi^A_0|c_\beta c_\alpha|\Psi^{A+2}_n\rangle\;\langle\Psi^{A+2}_n|c^\dagger_\gamma c^\dagger_\delta|\Psi^A_0\rangle}{\omega-(E^{A+2}_n-E^A_0)+i\eta}\\ &-\;\sum_{k}\frac{\langle\Psi^A_0|c^\dagger_\gamma c^\dagger_\delta|\Psi^{A-2}_k\rangle\;\langle\Psi^{A-2}_k|c_\beta c_\alpha|\Psi^A_0\rangle}{\omega-\left(E^A_0-E^{A-2}_k\right)-i\eta}\;.\end{aligned} \tag{2.14}$$

contains the spectroscopic amplitude and excitation energies for transitions to states with $A\pm 2$ particles.

In their Lehmann representations, $\Pi(\omega)$ and $g^{II}(\omega)$ contain all the relevant information regarding ph and pp(hh) collective excitations. These represent the correlations whose influence on the spectral function we aim to account for in the present work.

2.2 Dyson Equation and SCGF Method

Although not strictly necessary in the present approach, it is customary to introduce an appropriate mean-field potential $\hat{U}$ to localize the nucleons and split

the Hamiltonian into an unperturbed one-body part $\hat{H}_0 = \hat{T} + \hat{U}$ and a residual interaction $\hat{H}_1 = \hat{V} - \hat{U}$. The eigenfunctions of $\hat{H}_0$ form a complete set $\{\alpha'\}$ of sp orbitals with energy $\varepsilon_{\alpha'}$:

$$\hat{H}_0 \ \varphi_{\alpha'} \ = \ \sum_{\beta'} \left(t_{\alpha'\beta'} + U_{\alpha'\beta'}\right) \ \varphi_{\beta'} \ = \ \varepsilon_{\alpha'} \varphi_{\alpha'} \ , \tag{2.15}$$

so that, the Hamiltonian (2.1) is rewritten as

$$\begin{aligned} \hat{H} \ &= \ \hat{H}_0 + \hat{H}_1 \\ &= \ \sum_{\alpha'} \varepsilon_{\alpha'} \ c^{\dagger}_{\alpha'} c_{\alpha'} \ + \ \left(\hat{V} \ - \ \hat{U}\right) \ . \end{aligned} \tag{2.16}$$

It must be noted that, in principle, the set of orbitals $\{\alpha'\}$ that diagonalize $\hat{H}_0$ does not need to correspond to the set $\{\alpha\}$ used to expand the exact propagators (2.2), (2.4) and (2.10). Nevertheless, in the following it will be simpler to assume that they coincide $\{\alpha = \alpha'\}$.

Then, the one-body Green's function associated with the ground state of $\hat{H}_0$ (which is an independent-particle model, i.e. a Slater determinant wave function) has the following Lehmann representation:

$$g^0_{\alpha\beta}(\omega) \ = \ \delta_{\alpha,\beta} \left\{ \frac{\theta(\alpha - F)}{\omega - \varepsilon_\alpha + i\eta} \ + \ \frac{\theta(F - \alpha)}{\omega - \varepsilon_\alpha - i\eta} \right\} \ , \tag{2.17}$$

where $\theta(\alpha - F)$ ($\theta(F - \alpha)$) is equal to to 0 (1) if α is an occupied state and it is 1 (0) otherwise.

To find an equation for the complete one-body Green's function (2.4), one can consider the equation of motion for an operator in the Heisenberg picture,

$$i \frac{\partial \hat{\mathcal{O}}_H(t)}{\partial t} \ = \ \left[\hat{\mathcal{O}}_H(t), \hat{H}\right] \ . \tag{2.18}$$

By applying the latter to the creation and destruction operators of Eq. (2.2) and in the corresponding equation that defines $g^0(\tau)$ (in terms of $\hat{H}_0$), one obtains the Dyson equation [46],

$$g_{\alpha\beta}(\tau) \ = \ g^0_{\alpha\beta}(\tau) \ + \ g^0_{\alpha\gamma}(\tau - t_1) \left(\Sigma^\star_{\gamma\delta}(t_1 - t_2) - U_{\gamma\delta} \ \delta(t_1 - t_2)\right) g_{\delta\beta}(t_2) \ , \tag{2.19}$$

where the therm $-U_{\gamma\delta}$ comes from the contribution to the residual interaction (Eq. (2.16)) and $\Sigma^\star_{\alpha\beta}(\tau)$ is the irreducible self-energy. Here and in the following, we employ the convention of summing over all repeated indices and integrate from $-\infty$ to $+\infty$ over all repeated time variables, unless specified otherwise.

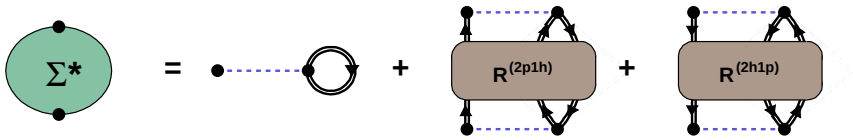

Figure 2.1: Diagrams contributing to the irreducible self-energy $\Sigma^\star$. The double lines represent dressed sp propagators and dashed lines correspond to the two-body interaction $\hat{V}$. The first term is the Hartree-Fock potential while the others represent the 2p1h/2h1p or higher contributions that are to be approximated through the Faddeev TDA/RPA equations, see Sec.2.4.

In general, $\Sigma^\star_{\alpha\beta}(\tau)$ can be represented as the sum of a one-body Hartree-Fock potential and terms that describe the coupling between the sp motion and more complex excitations [54]. This can be seen by applying once more the equation of motion for $g(\tau)$, with the result

$$\Sigma^\star_{\alpha\beta}(\tau) \;=\; \Sigma^{HF}_{\alpha\beta}\;\delta(t_1-t_2) \;+\; V_{\alpha\lambda,\mu\nu}\;R_{\mu\nu\lambda,\gamma\delta\varepsilon}(\tau^-,\tau,\tau^+;0^+,0,0^-)\;V_{\gamma\delta,\beta\varepsilon}\;. \qquad (2.20)$$

This separation is depicted by the diagrams of Fig. 2.1.

The (time-independent) Hartree-Fock part of the self-energy $\Sigma^{HF}_{\alpha\beta}$ can be computed in terms of the solution $g_{\alpha\beta}(\tau)$ itself

$$\Sigma^{HF}_{\alpha\beta} = \int \frac{d\omega}{2\pi i}\; e^{+i\omega\eta^+}\; V_{\alpha\gamma,\beta\delta}\; g_{\gamma\delta}(\omega)\;\;. \qquad (2.21)$$

The 2p1h propagator $R(\tau)$, appearing in the last term of Eq. (2.20), contains the sum of all so-called one-particle irreducible diagrams which cannot be separated by cutting a single line. Thus $R(\tau)$ describes only those contributions that involve the propagation of at least 2p1h ($\tau > 0$) or 2h1p ($\tau < 0$) at the same time. These contributions correspond to the last two diagrams of Fig. 2.1. It is at the level of $R(\tau)$ that the correlations involving interactions between different collective modes need to be included.

The diagrams included in $R(\tau)$ correspond to a subset of those contained in the 2p1h Green's function, $g^{2p1h}_{\mu\nu\lambda,\alpha\beta\gamma}$, defined below. The relation between $R(\tau)$ and

g^{2p1h} is given by [54]

$$R_{\mu\nu\lambda,\alpha\beta\gamma}(t_1,t_2,t_3;t_4,t_5,t_6) = g^{2p1h}_{\mu\nu\lambda,\alpha\beta\gamma}(t_1,t_2,t_3;t_4,t_5,t_6) - g^{4-pts}_{\mu\nu,\lambda\eta}(t_1,t_2;t_3,t')\, g^{-1}_{\eta\sigma}(t'-t'')\, g^{4-pts}_{\gamma\sigma,\alpha\beta}(t_6,t'';t_4,t_5)\ , \tag{2.22}$$

in which $g^{-1}_{\eta\sigma}$ is the inverse of the one-body Green's function (2.2), g^{4-pts} is the 4-point propagator defined in Eq. (2.10) and g^{2p1h} is the 6-point Green's function defined as

$$g^{2p1h}_{\mu\nu\lambda,\alpha\beta\gamma}(t_1,t_2,t_3;t_4,t_5,t_6) = -i\ \langle\Psi^A_0|\ T[c^\dagger_\lambda(t_3)c_\nu(t_2)c_\mu(t_1)c^\dagger_\alpha(t_4)c^\dagger_\beta(t_5)c_\gamma(t_6)]\ |\Psi^A_0\rangle\ . \tag{2.23}$$

It must be noted that the propagator R (2.22) appears in Eq. (2.20) only after it has been specialized to two times. Eqs. (2.22) and (2.23) give the most general definition since it will be useful to the discussion of the formalism of Sec. 2.4. There, a set of equations that give the two-time $R(\tau)$ directly will also be discussed.

2.2.1 Calculation of the Single-Particle Green's Function

The Dyson equation (2.19) is more easily solved after it has been Fourier transformed to its energy representation

$$g_{\alpha\beta}(\omega) = g^0_{\alpha\beta}(\omega)\ +\ \sum_{\gamma\delta} g^0_{\alpha\gamma}(\omega)\left(\Sigma^\star_{\gamma\delta}(\omega) - U_{\gamma\delta}\right) g_{\delta\beta}(\omega)\ \ . \tag{2.24}$$

One can substitute the Lehmann representations (2.4) and (2.17) into Eq. (2.24) and then extract the residues of the poles ε^+_n and ε^-_k. Taking a given hole pole ε^-_k as an example, this procedure gives [30]

$$\begin{aligned} \omega\ \mathcal{Y}^k_\alpha &= \sum_\beta \left(\varepsilon_\alpha\delta_{\alpha\beta} - U_{\alpha\beta} + \Sigma^\star_{\alpha\beta}(\omega)\right)\mathcal{Y}^k_\beta\Big|_{\omega=\varepsilon^-_k} \\ &= \sum_\beta \left(t_{\alpha\beta} + \Sigma^\star_{\alpha\beta}(\omega)\right)\mathcal{Y}^k_\beta\Big|_{\omega=\varepsilon^-_k}\ , \end{aligned} \tag{2.25}$$

where Eq.(2.15) has been used in the last line. This represents an eigenvalue equation for the hole spectroscopic amplitudes and the relative missing energies (2.5). Here it is seen that the irreducible self-energy $\Sigma^\star_{\gamma\delta}(\omega)$ acts as an effective, energy-dependent, potential.

It should be noted that the contribution of the one-body interaction $\hat{U}$ completely cancels the corresponding term included in the sp spectrum $\varepsilon_{\alpha'}$ of $\hat{H}_0$ in equation (2.25), leaving only matrix elements of the kinetic energy operator of the original Hamiltonian (2.1). Thus, without any change in the results, one can drop the $-U$ term in Eqs. (2.19) and (2.24) and solve the Dyson equation directly in terms of an unperturbed propagator $g^0(\omega)$, which is associated only with the kinetic energy term.

To obtain the normalization condition for the spectroscopic amplitudes one can expand the Dyson equation (2.24) in terms of ω around a given pole ε_k^-, consider the coefficient of order zero and then make use of the conjugate of the eigenvalue equation (2.25) . This results in the following normalization condition [55, 56, 30]

$$Z_k = \sum_\alpha \left|\mathcal{Y}_\alpha^k\right|^2 = 1 + \sum_{\alpha,\beta} \left(\mathcal{Y}_\alpha^k\right)^* \left.\frac{\partial \Sigma^\star_{\alpha\beta}(\omega)}{\partial \omega}\right|_{\omega=\varepsilon_k^-} \mathcal{Y}_\beta^k \,, \tag{2.26}$$

which also determines the value of the absolute spectroscopic factor (2.7). The same relations (2.25) and (2.26) apply to the one-particle component of $g(\omega)$ as well, giving solutions for $(\mathcal{X}_\alpha^n)^*$ and ε_n^+.

2.2.2 Self-Consistent Green's Function Approach

As is apparent from Eqs. (2.20) and (2.21), the exact irreducible self-energy $\Sigma^\star(\omega)$ is completely independent on the choice of the unperturbed Hamiltonian $\hat{H}_0$. Obviously, the same applies to the solution of the Dyson equation. Nevertheless, the choice of $\hat{H}_0$ is important in the simplest realization of perturbation theory, where $\Sigma^\star(\omega)$ is expanded in a Feynman diagram series, depending on the mean-field IPM propagator $g^0_{\alpha,\beta}(\omega)$ and on the vertices of the residual interaction [46, 47].

A different approach is to provide an expansion of the irreducible self-energy that depends only on the exact propagator $g(\omega)$. This can be achieved either by considering the equation of motion (2.18) for $g(\omega)$ [57] or working directly with the effective action functional [48]. The result is an exact formulation relating each many-body Green's function to the exact propagators of higher order. This generates a hierarchy of relations between the two-, three- and A-body Green's function, of which Eqn. (2.19) and (2.22) are the first examples. The relevant feature of this approach is that it allows one to devise a Feynman diagram expansion for the irreducible self-energy that depends only on the exact propagator $g(\omega)$ and not on its uncorrelated approximation $g^0(\omega)$. Of course, this is obtained at the price of increased difficulties in practical calculations.

In the nuclear case, there exists a strong coupling between the sp degree of freedom and both low-lying collective states and high-lying states. The coupling to the latter is related to the strong short-range repulsion in the nuclear force. These couplings generate the fragmentation of sp strengths. The size of the fragmentation observed experimentally suggests that this feature must already be included in the description of these couplings. In other words, the correlated one-body propagators need to be considered in the construction of the nucleon self-energy. Thus, the second of the two approaches is highly desirable for the purposes of this thesis.

This formalism provides a scheme in which one- and two-body spectral functions can be evaluated in terms of an already dressed sp Green's function. This allows the possibility of including, already from the start, the features of the sp motion that go beyond a mean-field description. Once such features are included in the input propagator, their effects on the one- and two-body motion will be automatically included in the calculations. It is important to observe that the expansion of the irreducible propagator $R_{\mu\nu\lambda,\gamma\delta\varepsilon}(\omega)$ in Eq. (2.20), derived employing the equation of motion, is given in terms of the dressed one-body propagator. Thus, in principle, it is the exact solution of the many-body problem that is supposed to be employed in the Faddeev calculations described below.

The first term in the expansion of the self-energy with respect to the dressed propagator is depicted in Fig. 2.1 and describes the interaction of a nucleon with the dressed particles in the system. By approximating the self-energy to include only this diagram one is left with the Hartree-Fock theory. This represents the simplest realization of the above formulation.

The approach of self-consistent Green's function theory consists in starting with an approximation for the input Green's function (usually a Hartree-Fock propagator or other independent particle model). From this, an approximation for the irreducible 2p1h propagator $R(\tau)$ and for the irreducible self-energy can be constructed. Then, the solution of the Dyson Eq. (2.24) will give a better approximation of the s.p. propagator that can be employed in the second calculation. In the calculations of this thesis, the self-energy was obtained by evaluating both the pp and the ph propagators and then coupling them through a Faddeev expansion, as described in Secs. 2.3 and 2.4. As shown in Fig. 2.2, the whole procedure is iterated several times until consistency is found between two successive solutions (i.e. between the input propagator and the solution that it generates).

The attractive feature of SCGF is not only restricted to the fact that the effects of fragmentation are included in the calculations. Also, solutions for the one-body,

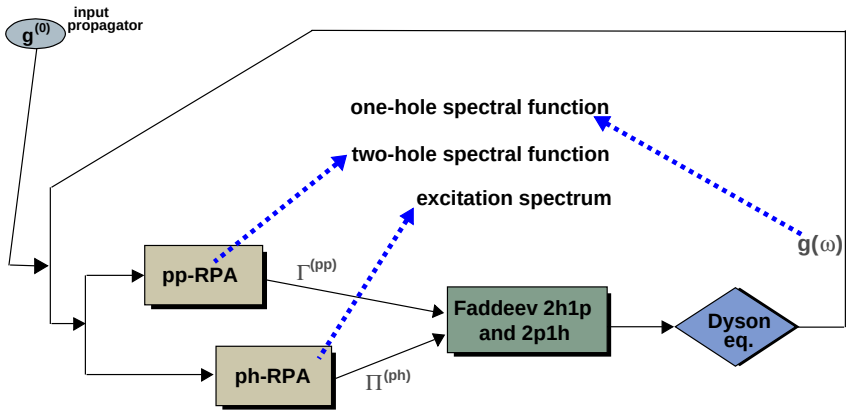

Figure 2.2: Iteration scheme used to reach self-consistency between the input propagator and the result of the Dyson equation. At each iteration new approximations for the one- and two- body propagators (2.4), (2.12) and (2.14) are obtained. In this thesis the nuclear self-energy is generated by means of the Faddeev equations, as explained in Sec. 2.4.

two-body and higher-order propagators are generated all at the same time, the relative effects of each one on the others being taken into account.

One may note that the final self-consistent solutions will not depend in any way on $\hat{H}_0$ and on its eigenstates $\{\alpha'\}$ (2.15) (but it will still depend on the truncation of the basis $\{\alpha\}$ used to expand the propagators). Still, a good choice for the unperturbed propagator g^0 can be usefully employed as input to the first iteration.

Obviously, the exact form of the sp propagator $g(\omega)$ is very complex, containing many poles and a continuum. Such richness of details cannot be easily included in the above calculation unless some approximation is adopted to simplify $g(\omega)$ at each intermediate iteration [29, 30]. In the present thesis this is certainly possible, since the main interest is in the low-energy behavior of the sp motion and the few poles that contain the main sp strength are expected to be much more relevant than the others. This also allows to limit the calculation to a relatively small model space while taking into account short-range effects by means of a G-matrix effective interaction. These details will be discussed more completely in Sec. 3.1, for the present application.

2.3 Dressed TDA and RPA Equations

The information on the excitation of the A-particle core and on the $A\pm2$ particle systems are contained, respectively, in the polarization and two-particle propagators defined in equations (2.12) and (2.14). In the present work these quantities have been evaluated by employing the Tamm-Dancoff (TDA) and random-phase (RPA) approximations.

2.3.1 Polarization Propagator

Taking the polarization propagator as an example, one can define the *free* ph propagator $\Pi^f(\omega)$ by coupling two excitations of particle and hole type, not interacting with each other. Graphically, this corresponds to two dressed sp lines propagating with opposite direction in time. By applying Feynman diagram rules [46], one obtains the following Lehmann representation for $\Pi^f(\omega)$:

$$\begin{aligned}\Pi^f_{\alpha\beta,\gamma\delta}(\omega) &= -i\int\frac{d\omega_1}{2\pi}(-1)\; ig_{\alpha\gamma}(\omega+\omega_1)\; ig_{\delta\beta}(\omega_1) \\ &= \sum_{n,k}\frac{\left(\mathcal{X}^n_\alpha\mathcal{Y}^k_\beta\right)^*\;\mathcal{X}^n_\gamma\mathcal{Y}^k_\delta}{\omega-\left(\varepsilon^+_n-\varepsilon^-_k\right)+i\eta} \;-\; \sum_{n,k}\frac{\mathcal{Y}^k_\alpha\mathcal{X}^n_\beta\;\left(\mathcal{Y}^k_\gamma\mathcal{X}^n_\delta\right)^*}{\omega+\left(\varepsilon^+_n-\varepsilon^-_k\right)-i\eta}\,. \end{aligned} \tag{2.27}$$

In the last line of Eq. (2.27), the forward- and the backward-going contributions describe the propagation of a particle-hole and hole-particle type excitation, respectively. Thus they are identical apart from a time reversal transformation.

In order to account for the collective excitations present in the A-body system, we need to take into account the interactions between the two lines propagating in $\Pi^f(\omega)$. This can be done by solving the following equation

$$\Pi_{\alpha\beta,\gamma\delta}(\omega) \;=\; \Pi^f_{\alpha\beta,\gamma\delta}(\omega) \;+\; \Pi^f_{\alpha\nu,\beta\mu}(\omega)\; V_{\mu\nu,\rho\epsilon}\;\Pi_{\rho\epsilon,\gamma\delta}(\omega)\,, \tag{2.28}$$

which is depicted in Fig.2.3 in terms of Feynman diagrams. Eq. (2.28) implicitly generates a series of diagrams in which the particle and the hole interact to all orders, any number of times. The resulting expansion is depicted in Figs.2.4 and 2.5, in terms of unperturbed propagators. Consistent with the aim of performing a self-consistent calculation, Eqs. (2.27) and (2.28) have been formulated in terms of the full, dressed, sp propagator $g(\omega)$, Eq. (2.4). However, when an unperturbed, IPM, Green's function $g^0(\omega)$ (2.17) is used as input, the approximations depicted in this section reduce to the standard TDA and RPA [58].

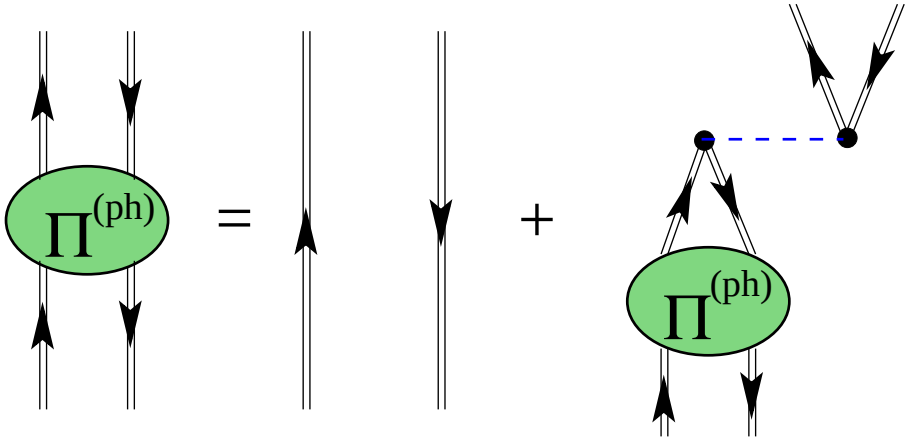

Figure 2.3: Feynman diagram representation of the DRPA equation for the polarization propagator $\Pi(\omega)$.

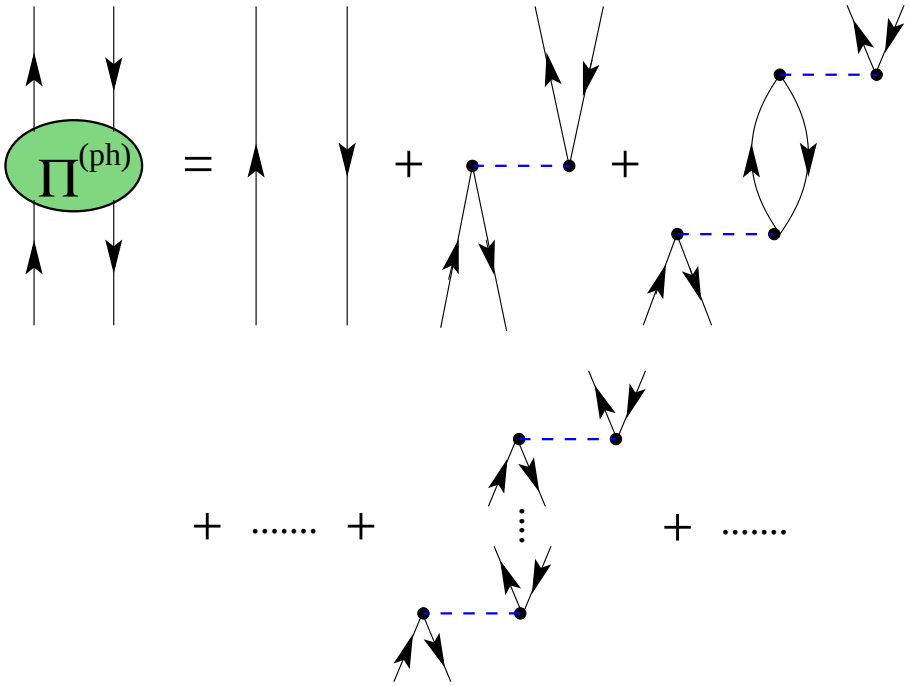

Figure 2.4: Diagrammatic expansion of the ph propagator $\Pi(\omega)$ in TDA. An implicit time ordering is intended for these diagrams. Dressing all the sp lines would result in the DTDA.

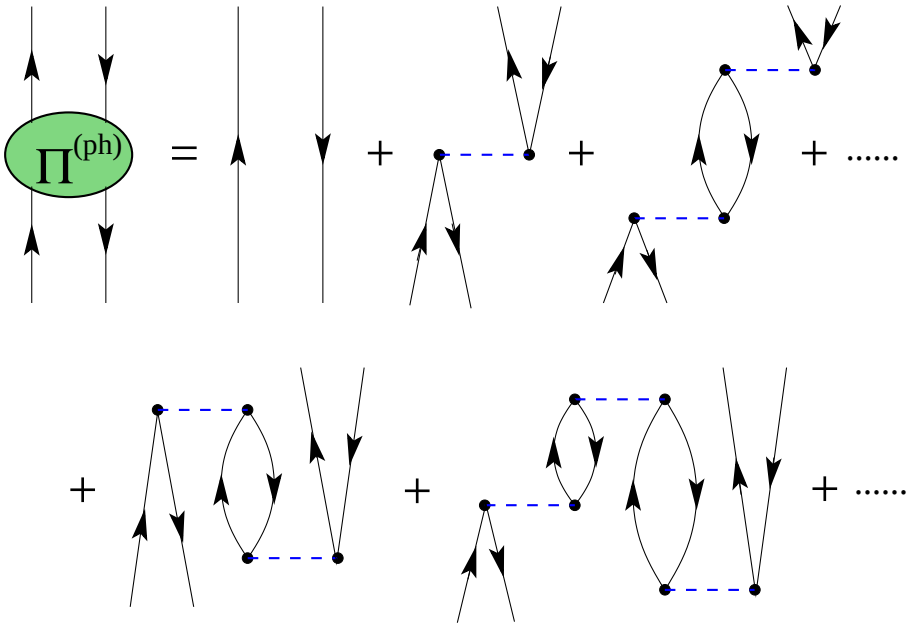

Figure 2.5: Diagrammatic expansion of the ph propagator $\Pi(\omega)$ in RPA. This contains the whole phTDA series plus diagrams involving the inversion of the propagation time. Dressing all the sp lines results in the DRPA.

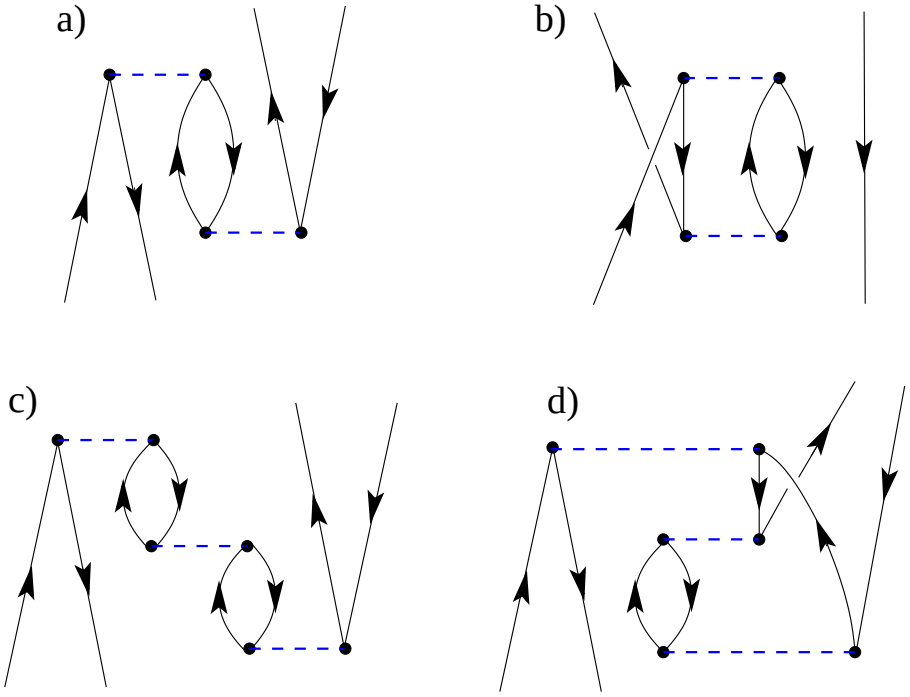

Figure 2.6: Diagrams a) and c) give examples of contributions to the RPA expansion. These corresponds to the creation of two additional ph excitations to generate an intermediate 3p3h states. The diagrams b) and d) are Pauli exchange corrections to a) and d) respectively, but they are discarded in the RPA approximation. Diagram b) can be accounted for if the DRPA approach is used, however, this does not apply to d).

It must be noted that a simpler realization of Eq. (2.28) consists in including only forward-going propagation, that is to include —in place of $\Pi^f(\omega)$— only the first term in the second line of Eq. (2.27). This consists in the so called Dressed Tamm-Dancoff Approximation (DTDA), depicted in Fig. 2.4 (where an explicit time ordering is assumed and the dressing of sp Green's functions must be understood).

When the full $\Pi^f(\omega)$ (2.27) is considered in Eq. (2.28) one obtains the Dressed Random Phase Approximation (DRPA). The relevant diagrammatic expansion is the one of Fig. 2.5. Clearly, the whole TDA series is contained in the RPA one. Besides this contribution, the backward-going component of $\Pi^f(\omega)$ allows to generate diagrams containing more that a single ph excitation at each time. These refer to contributions in which additional intermediate ph states are generated and eventually annihilated by two-body interactions.

In general, the interparticle distance between nucleons inside the nucleus is of the order of the nucleon size itself. In this sense the nuclear medium can be considered a rather dense system. Besides, the nuclear interaction has a strong character. Thus it is not surprising that intermediate n-particle–n-hole excitations (with $n \geq 2$) play an important role [3, 26]. Still, it must be realized that not all the possible diagrams obtained from each other by Pauli exchange are included in the RPA series. Fig. 2.6 gives two examples of diagrams that are summed by RPA and of Pauli exchange corrections to them that are neglected. The philosophy underlying the use of RPA relies on the assumption that the corrections coming from Pauli correlations sum up in a random way and tend to cancel each other (whence the name "random phase"). The improvement obtained by including RPA correlations is generally more relevant than the error generated by the (smaller) violation of the Pauli principle. For this reason RPA is a useful approximation scheme. It must be kept in mind, however, that in systems containing strong collective and/or pairing correlations the effects of Pauli violation may sum up in coherent way, invalidating the RPA approach. Typically this situation is signaled by the appearence of a pair of complex eigenvalues of Eq. (2.28) together with diverging solutions for the ph spectroscopic amplitudes.

One may also note, see Fig 2.5, that in the undressed RPA only intermediate 3p3h states or higher are generated, the 2p2h contribution being completely discarded. The dressing of propagators implicitly includes more diagrams that can include some 2p2h states and partially fix the Pauli violations, as in Fig. 2.6.

2.3.2 Two-body Propagator

The two-body propagator (2.14) was also computed by employing the (dressed) TDA and RPA equations. In this case, the zero-order contribution consists of two lines propagating in the same direction in time. The Lehmann representation for the dressed case is now

$$\begin{aligned} g^{II,f}_{\alpha\beta,\gamma\delta}(\omega) &= -i \int \frac{d\omega_1}{2\pi}\, ig_{\alpha,\gamma}(\omega-\omega_1)\, ig_{\beta,\delta}(\omega_1) \\ &= \sum_{n_1,n_2} \frac{\left(\mathcal{X}^{n_1}_{\alpha}\mathcal{X}^{n_2}_{\beta}\right)^{*}\, \mathcal{X}^{n_1}_{\gamma}\mathcal{X}^{n_2}_{\delta}}{\omega - \left(\varepsilon^{+}_{n_1} - \varepsilon^{+}_{n_2}\right) + i\eta} - \sum_{n_1,n_2} \frac{\mathcal{Y}^{k_1}_{\alpha}\mathcal{Y}^{k_2}_{\beta}\, \left(\mathcal{Y}^{k_1}_{\gamma}\mathcal{Y}^{k_2}_{\delta}\right)^{*}}{\omega - \left(\varepsilon^{-}_{k_1} - \varepsilon^{-}_{k_2}\right) - i\eta}\,, \end{aligned} \tag{2.29}$$

where the forward and backward part refer to the (independent) propagation of two particle and of two hole lines, respectively.

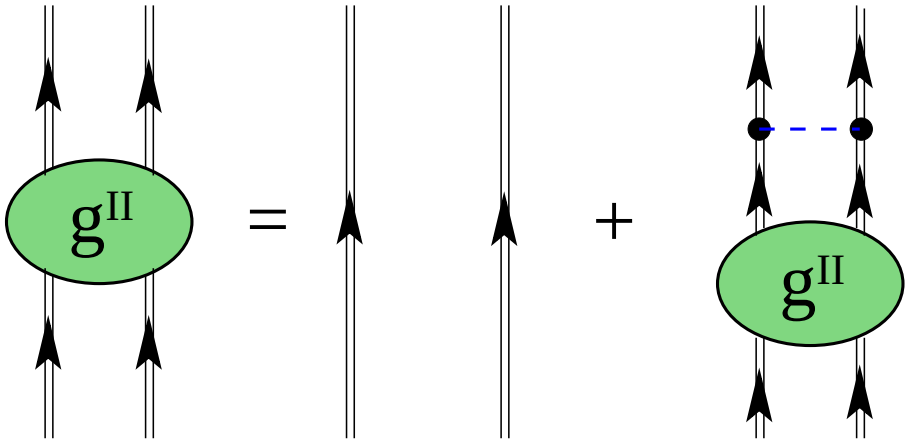

Figure 2.7: DRPA equation for the two-particle propagator $g^{II}(\omega)$.

The ppDRPA equation is given by

$$g^{II}_{\alpha\beta,\gamma\delta}(\omega) \;=\; \left(g^{II,f}_{\alpha\beta,\gamma\delta}(\omega) - g^{II,f}_{\beta\alpha,\gamma\delta}(\omega)\right) \;+\; \frac{1}{2} g^{II,f}_{\alpha\beta,\mu\nu}(\omega)\, V_{\mu\nu,\rho\epsilon}\, g^{II}_{\rho\epsilon,\gamma\delta}(\omega)\,, \qquad (2.30)$$

where the factor $\frac{1}{2}$ is the symmetry factor required by Feynman rules [46]. Eq. (2.30) is depicted in terms of Feynman diagrams in Fig. 2.7 and generates a series of diagrams analogous to that of Fig. 2.5.

As in the ph case, the corresponding ppDTDA approximation is obtained by considering propagation only in one time direction. This corresponds to employing only the first (second) term in the last line of Eq.(2.29) into Eq. (2.30) when solving for the pp (hh) part of g^{II}.

The solution of RPA/TDA equations (2.28) and (2.30) requires the extraction of the poles of the final propagator and follows the same path as for solving the Dyson equation. This is discussed in more detail in Section A.1 for the pp case. The ph equation allows a competely analogous treatment and it is also discussed in Section A.3.1. The TDA and RPA propagators described in this section are used in the following to generate the interaction kernels for the Faddeev equations.

2.4 Simultaneous Treatment of ph and pp(hh) Phonons

One of the aims of the present work is to include the effects of both ph and hh collective excitations into the nuclear self-energy, while describing them at least at

the RPA level. Both ph and pp(hh) phonons, Eqs.(2.12) and (2.14), can be straightforwardly included in a separate manner by coupling them to a freely propagating particle or hole line, respectively [3]. Nevertheless the simultaneous inclusion of both contributions is not trivial.

Naively, the easiest approach would be that of summing the contribution of both diagrams, as depicted in Fig. 1.1. Unfortunately this approximation leads to serious inconsistencies. As noticed in Chapter 1, the last of the three diagrams on the right hand side is already contained in each of the other two and must therefore be subtracted to avoid double counting. The minus sign in front this term introduces spurious poles in the Lehmann representation of the self-energy and generates meaningless solutions of the Dyson equation. This may also prevent in some cases the proper normalization of the spectroscopic amplitudes. The latter feature can be understood by considering a possible solution near such a spurious pole. The normalization is determined by the derivative of the self-energy at this energy, Eq. (2.26), and will not yield a correct result on account of the additional minus sign when the third diagram dominates. Besides this, it is also apparent that the contribution of the type p+(ph) and (pp)+h represent different couplings of the same 2p1h excitation. Thus the approach of Fig. 1.1 tends to overestimate the effects of contributions that are already properly accounted for by both diagrams. Finally, the second term in Fig. 1.1 ignores the exchange correlations between the freely propagating line and the quasi-particles forming the ph phonon, as discussed e.g. in [3]. This results in a violation of the Pauli principle already at the 2p1h and 2h1p level.

These issues can be overcome only by performing an all order summation that allows the contribution of the pp and ph phonons to be mixed together, generating diagrams like the one depicted in Fig. 2.8. This would also include the exchange between the first two lines, thus improving the treatment of Pauli correlations since all exchange terms at the 2p1h level are consistently included. This can be achieved by employing the formalism of the Faddeev equations [38, 39]. This approximation is the one applied in this thesis and it will be described in the rest of this Chapter and in Appendix B.

It must also be observed that in Fig. 1.1 violations of Pauli exchange come from higher order excitations as well and are present also in the first diagram, which involves pp(hh) phonons. These are intrinsically introduced by the standard RPA equations and therefore will appear also in the present Faddeev formalism. Nevertheless, they involve only 3p2h (3h2p) and higher order contributions and will

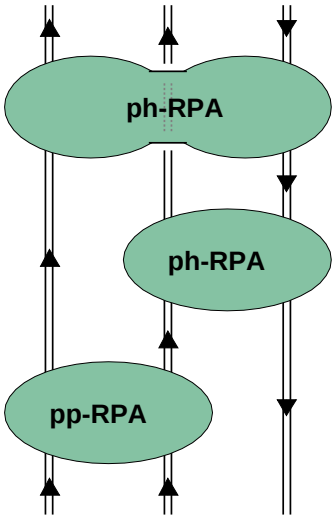

Figure 2.8: Example of diagrams that are summed to all orders by means of the Faddeev equations.

not be discussed any further in this chapter. An improved treatment would require the extension of the formalism to Extended RPA phonons [43, 59] and the complete solution of the 3p2h (3h2p) excitation problem, which is beyond the scope of the present work.

2.4.1 Bethe-Salpeter Equation for the $2p1h$ ($2h1p$) Propagation

The propagator $R_{\mu\nu\lambda,\alpha\beta\gamma}$ is the solution of the following equation which has a similar form as the Bethe-Salpeter equation for pp and ph propagators

$$\begin{aligned} & R_{\mu\nu\lambda,\alpha\beta\gamma}(t_1,t_2,t_3;t_4,t_5,t_6) \\ &= g_{\mu\alpha}(t_1-t_4)g_{\nu\beta}(t_2-t_5)g_{\gamma\lambda}(t_6-t_3) - g_{\nu\alpha}(t_2-t_4)g_{\mu\beta}(t_1-t_5)g_{\gamma\lambda}(t_6-t_3) \\ &\quad + g_{\mu\mu'}(t_1-t'_1)g_{\nu\nu'}(t_2-t'_2)g_{\lambda'\lambda}(t'_3-t_3) \\ &\quad \times K_{\mu'\nu'\lambda',\alpha'\beta'\gamma'}(t'_1,t'_2,t'_3;t'_4,t'_5,t'_6)\, R_{\alpha'\beta'\gamma',\alpha\beta\gamma}(t'_4,t'_5,t'_6;t_4,t_5,t_6)\,, \end{aligned} \tag{2.31}$$

which is shown in Fig. 2.9 in terms of Feynman diagrams. The interaction vertex, also shown in Fig. 2.9, is given by

$$\begin{aligned} & K_{\mu\nu\lambda,\alpha\beta\gamma}(t_1,t_2,t_3;t_4,t_5,t_6) \\ & \quad = \; K^{(ph)}_{\nu\lambda,\beta\gamma}(t_2,t_3;t_5,t_6)g^{-1}_{\mu\alpha}(t_1-t_4) \; + \; K^{(ph)}_{\mu\lambda,\alpha\gamma}(t_1,t_3;t_4,t_6)g^{-1}_{\nu\beta}(t_2-t_5) \\ & \qquad + \; K^{(pp)}_{\mu\nu,\alpha\beta}(t_1,t_2;t_4,t_5)g^{-1}_{\gamma\lambda}(t_6-t_3) \; + \; K^{(pph)}_{\mu\nu\lambda,\alpha\beta\gamma}(t_1,t_2,t_3;t_4,t_5,t_6) \; . \end{aligned} \tag{2.32}$$

In Eq. (2.32), $K^{(pp)}$ and $K^{(ph)}$ represent the pp and ph irreducible vertices while $K^{(pph)}$ is the 2p1h irreducible vertex. It was already noted that in Eq. (2.20) the propagator $R_{\mu\nu\lambda,\alpha\beta\gamma}$ is only required at two times and therefore its complete knowledge, as given by (2.22), is not necessary to solve the Dyson equation. On the other hand, the dependence on the time variables t_1, t_2 and t_3 is intrinsic in the Bethe-Salpeter Eq. (2.31), thus requiring that at least a 4-times object be employed to solve for the 2p1h motion exactly.

Equations (2.19), (2.20) and (2.31) together form a set of coupled equations, where the same propagator, which solves the Dyson equation (2.19), appears as input in the Bethe-Salpeter equation (2.31). If the irreducible vertices $K^{(pp)}$, $K^{(ph)}$ and $K^{(pph)}$ are also expressed in terms of the $g_{\alpha\beta}(\tau)$, then Eqs. (2.19) and (2.31) will generate a self-consistent expansion. Obviously, Eq. (2.31) and the irreducible vertex (2.32) represent the exact solution for R and therefore require a suitable approximation.

2.4.2 Faddeev-Bethe-Salpeter Equations

Eq. (2.31) can be reduced to a set of coupled equations in a way similar to the method proposed by Faddeev to solve the three-body problem [36, 60]. The inclusion of pp and ph RPA phonons in a consistent way requires this Faddeev approach since it provides a natural framework for correctly iterating quantities that have already been summed to all orders like the RPA phonons. In the present work we will neglect the contribution of the irreducible $K^{(pph)}$ term in Eq. (2.32) since it leads to the coupling of higher order particle-hole terms than already considered in the following. We will therefore require only three Faddeev components. Following standard notation in the literature [37], $R^{(i)}_{\mu\nu\lambda,\alpha\beta\gamma}$ will represent the component related to all diagrams ending with a vertex between legs j and k with (i,j,k) cyclic permutations of $(1,2,3)$. We will employ the convention in which the third leg propagates in the opposite direction with respect to the first two. The Faddeev

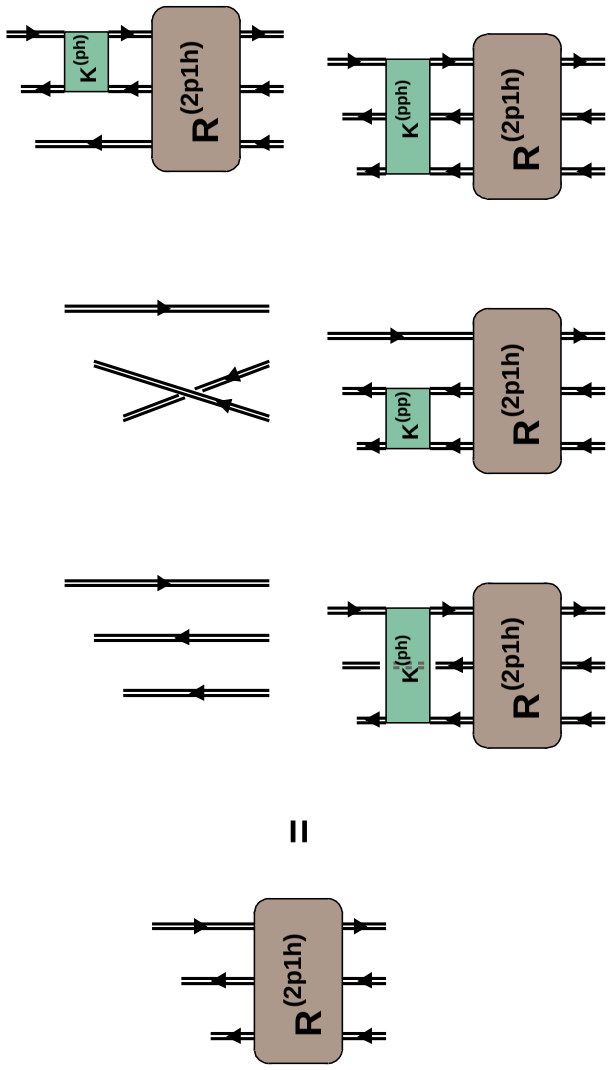

Figure 2.9: Bethe-Salpeter equation (2.31) for the 2p1h propagator with vertices given by (2.32). The irreducible interaction vertices for the pp and two ph channels are denoted by $K^{(pp)}$ and $K^{(ph)}$, respectively. The irreducible vertex involving all three lines simultaneously is denoted by $K^{(pph)}$.

components $R^{(i)}$ can be written in terms of the 2p1h propagator R and the contribution of the three dressed but noninteracting sp propagators. This definition is given in detail here for all three components, omitting explicit reference to the time variables for convenience of notation

$$R^{(1)}_{\mu\nu\lambda,\alpha\beta\gamma} = g_{\nu\epsilon}g_{\rho\lambda}\ K^{(ph)}_{\epsilon\rho,\eta\sigma}\ R_{\mu\eta\sigma,\alpha\beta\gamma} + \frac{1}{2}\left(g_{\mu\alpha}\ g_{\nu\beta}\ g_{\gamma\lambda} - g_{\nu\alpha}\ g_{\mu\beta}\ g_{\gamma\lambda}\right) , \tag{2.33}$$

$$R^{(2)}_{\mu\nu\lambda,\alpha\beta\gamma} = g_{\mu\epsilon}g_{\rho\lambda}\ K^{(ph)}_{\epsilon\rho,\eta\sigma}\ R_{\eta\nu\sigma,\alpha\beta\gamma} + \frac{1}{2}\left(g_{\mu\alpha}\ g_{\nu\beta}\ g_{\gamma\lambda} - g_{\nu\alpha}\ g_{\mu\beta}\ g_{\gamma\lambda}\right) , \tag{2.34}$$

$$R^{(3)}_{\mu\nu\lambda,\alpha\beta\gamma} = g_{\mu\epsilon}g_{\nu\rho}\ K^{(pp)}_{\epsilon\rho,\eta\sigma}\ R_{\eta\sigma\lambda,\alpha\beta\gamma} + \frac{1}{2}\left(g_{\mu\alpha}\ g_{\nu\beta}\ g_{\gamma\lambda} - g_{\nu\alpha}\ g_{\mu\beta}\ g_{\gamma\lambda}\right) . \tag{2.35}$$

The factor $\frac{1}{2}$ in Eqs. (2.33-2.35) properly takes into account the exchange symmetry between the parallel lines in the Faddeev equations. With these definitions the full propagator (2.22) is given by

$$R_{\mu\nu\lambda,\alpha\beta\gamma} = \sum_{i=1,2,3} R^{(i)}_{\mu\nu\lambda,\alpha\beta\gamma} - \frac{1}{2}\left(g_{\mu\alpha}\ g_{\nu\beta}\ g_{\gamma\lambda} - g_{\nu\alpha}\ g_{\mu\beta}\ g_{\gamma\lambda}\right) . \tag{2.36}$$

The Faddeev equations now take the following form

$$\begin{aligned} R^{(i)}_{\mu\nu\lambda,\alpha\beta\gamma} &= \frac{1}{2}\left(g_{\mu\alpha}\ g_{\nu\beta}\ g_{\gamma\lambda} - g_{\nu\alpha}\ g_{\mu\beta}\ g_{\gamma\lambda}\right) \\ &+ g_{\mu\mu'}\ g_{\nu\nu'}\ g_{\lambda'\lambda}\ \Gamma^{(i)}_{\mu'\nu'\lambda',\mu''\nu''\lambda''}\ \left(R^{(j)}_{\mu''\nu''\lambda'',\alpha\beta\gamma} + R^{(k)}_{\mu''\nu''\lambda'',\alpha\beta\gamma}\right) , \ i = 1,2,3 \end{aligned} \tag{2.37}$$

where the $\Gamma^{(i)}_{\mu\nu\lambda,\alpha\beta\gamma}$ vertices obey the following symmetry relations and are defined by

$$\begin{aligned} &\Gamma^{(1)}_{\mu\nu\lambda,\alpha\beta\gamma}(t_1,t_2,t_3;t_4,t_5,t_6) = \\ &\qquad \Gamma^{(2)}_{\nu\mu\lambda,\beta\alpha\gamma}(t_2,t_1,t_3;t_5,t_4,t_6) = g^{-1}_{\mu\alpha}(t_1-t_4)\ \tilde{\Gamma}^{(ph)}_{\nu\lambda,\beta\gamma}(t_2,t_3;t_5,t_6) , \end{aligned} \tag{2.38}$$

$$\begin{aligned} &\Gamma^{(3)}_{\mu\nu\lambda,\alpha\beta\gamma}(t_1,t_2,t_3;t_4,t_5,t_6) = \\ &\qquad \Gamma^{(3)}_{\nu\mu\lambda,\beta\alpha\gamma}(t_2,t_1,t_3;t_5,t_4,t_6) = g^{-1}_{\gamma\lambda}(t_6-t_3)\ \tilde{\Gamma}^{(pp)}_{\mu\nu,\alpha\beta}(t_1,t_2;t_4,t_5) . \end{aligned} \tag{2.39}$$

The gamma matrices $\tilde{\Gamma}^{(pp)}$ and $\tilde{\Gamma}^{(ph)}$ are the four-point functions that solve the Bethe-Salpeter equation for the pp and ph motion. These vertex functions contain the pp and ph phonons and can be written as

$$\begin{aligned} \tilde{\Gamma}^{(pp)}_{\gamma\delta,\alpha\beta}(t_1,t_2;t_3,t_4) &= K^{(pp)}_{\gamma\delta,\alpha\beta}(t_1,t_2;t_3,t_4) \\ &+ \tilde{\Gamma}^{(pp)}_{\gamma\delta,\mu\nu}(t_1,t_2;t'_1,t'_2)\ g_{\mu\eta}(t'_1-t'_3)\ g_{\nu\sigma}(t'_2-t'_4)\ K^{(pp)}_{\eta\sigma,\alpha\beta}(t'_3,t'_4;t_3,t_4) , \end{aligned} \tag{2.40}$$

$$\tilde{\Gamma}^{(ph)}_{\gamma\delta,\alpha\beta}(t_1,t_2;t_3,t_4) \;=\; K^{(ph)}_{\gamma\delta,\alpha\beta}(t_1,t_2;t_3,t_4) \tag{2.41}$$
$$+\;\; \tilde{\Gamma}^{(ph)}_{\gamma\delta,\mu\nu}(t_1,t_2;t_1',t_2')\; g_{\mu\eta}(t_1'-t_3')\; g_{\sigma\nu}(t_4'-t_2')\; K^{(ph)}_{\eta\sigma,\alpha\beta}(t_3',t_4';t_3,t_4)\;.$$

which generalize the DRPA equations (2.28) and (2.30).

Apart from neglecting the $K^{(2p1h)}$ vertex, Eq. (2.37) is otherwise a complete equation for the 2p1h propagator. This general equation involves quantities which depend on several times and is therefore too complex to be solved numerically. In order to construct a manageable approximation scheme that includes the relevant physical ingredients two simplifications will be considered in this section. The first one involves the restriction to two-time pp and ph vertices that include the respective RPA contributions in these channels. This approximation is the minimum step that maintains the simultaneous inclusion of both pp and ph collective low-lying excitations in describing the sp propagator. Extension of the formalism to include correlation beyond the DRPA approach are also possible. An example will be considered in Chapter 4. Second, it is necessary to simplify Eq. (2.37) to include only two-time Green's functions. This procedure no longer allows the inversion of the the propagation direction of all three lines together. As a result, the Faddeev equations split up in two separate expansions for the 2p1h and the 2h1p components. Although the hole spectral function is of primary interest for comparison with experimental data, it must be stressed that both 2p1h and 2h1p components are needed to generate the self-consistent solution for the sp propagator. Since the formalism involved is the same for both components, we will describe only the forward-going (2p1h) expansion. The equations for the 2h1p case are completely analogous.

2.4.3 Reduction to a Two-time Kernel

To construct the present approximation scheme, it is more convenient to use the spectral representation for propagators. Employing the bare interaction $V_{\alpha\beta,\gamma\delta}$ for the vertices $K^{(pp)}$ and $K^{(ph)}$, the Bethe-Salpeter equations (2.40) and (2.41) reduce to the DRPA equations [61, 59]. The solutions of these equations depend only on two times. These pp and ph phonons correspond to the dressed version of the phonons that are considered in Ref. [3] (see also Fig. 1.1). These excitations describe the correlations that we aim to iterate to all orders and, subsequently, to include in the self-energy as explained in the introduction. These DRPA solutions can then be substituted in Eqs. (2.38) and (2.39) to generate the $\Gamma^{(i)}$ matrices to be used in the Faddeev expansion. Both the forward- and backward-going components of the DRPA solutions are included into the expansion as illustrated in Fig. 2.10.

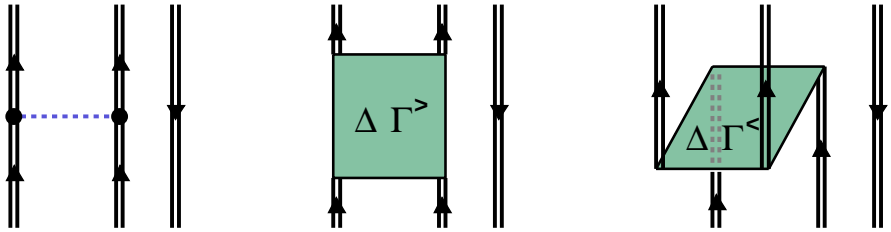

Figure 2.10: Diagrams that are included in the definition of the vertex for the pp channel. Here $\Delta\Gamma^{>}$ and $\Delta\Gamma^{<}$ are the forward- and backward-going part of the energy dependent contribution to the pp DRPA vertex (A.2). The contribution of these three diagrams can be factorized in an expression of the form $G^{0>}\,\Gamma^{(3)}\,G^{0>}$ only after having redefined the propagators $G^{0>}$ and $\Gamma^{(3)}$ to depend also on the particle and hole fragmentation indices (n,n',k). The last diagram has a smaller effect on the physical solutions of the problem, although it is essential for the elimination of spurious solutions.

This is crucial in order to eliminate the spurious solutions of the Faddeev equations as explained in Appendix B.2.2.

The working expression for the $\Gamma^{(i)}$ matrices, which depends on only two times (or equivalently one energy), is given in some detail in Appendix A.2. Here we only need to stress that the resulting $\Gamma^{(i)}$'s cannot invert the freely propagating line from hole to particle or vice versa, *i.e.* they cannot connect the 2p1h amplitudes with the 2h1p ones. For this reason, the pp and ph phonons will be summed only in one time direction in a TDA way contributing separately to the 2p1h and 2h1p propagators. The reader may notice that two contributions of the type shown in Fig. 2.11 can connect the 2p1h and the 2h1p propagators. The inclusion of such terms leads to the simultaneous propagation of two phonons which requires an extension of the approximation presented in here. Since these terms are expected to contribute only in higher order, we will neglect them in the following. We note that the collective RPA correlations in the pp and ph channels have already been computed through Eqs. (2.40) and (2.41) and therefore remain properly included in our approximation.

The remaining complication, related to the use of dressed propagators, concerns the interactions vertices (2.38) and (2.39). As explained in Appendix A.2, the $\Gamma^{(i)}$ and the propagators $R^{(i)}$ need to be redefined in such a way that their matrix elements also depend on the indices $(n,\ n',\ k)$, which label the fragments of the

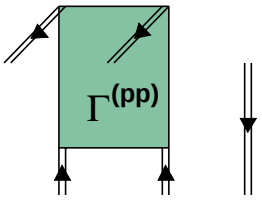

Figure 2.11: A combination of two diagrams of the type shown here can be used to connect the 2p1h and 2h1p propagators. Diagrams like these are not included in the present approximation scheme. Nevertheless, their contribution appears in the normalization of spectroscopic amplitudes. Explicit time-ordering is implied in this diagram.

propagators. This implies that the eigenvalue equations will involve summations on both the sp indices (α, β, γ) and the ones corresponding to the fragmentation, (n_α, n_β, k_γ). The 2p1h propagator and its Faddeev components, as defined in Eqs. (2.22) and (2.33-2.35), are recovered only at the end by summing the solutions over all values of (n_α, n_β, k_γ) and (n_μ, n_ν, k_λ).

Putting together all the above considerations, the resulting approximation to the Faddeev equations (2.37) can be rewritten in a way where all the propagators involved depend only on one energy variable (or two time variables). The forward-going part of this expansion can be written as follows

$$
\begin{aligned}
& R^{(i)}_{\mu n_\mu \nu n_\nu \lambda k_\lambda, \alpha n_\alpha \beta n_\beta \gamma k_\gamma}(\omega) \\
& \quad = \quad \frac{1}{2}\left(G^{0>}_{\mu n_\mu \nu n_\nu \lambda k_\lambda, \alpha n_\alpha \beta n_\beta \gamma k_\gamma}(\omega) - G^{0>}_{\nu n_\nu \mu n_\mu \lambda k_\lambda, \alpha n_\alpha \beta n_\beta \gamma k_\gamma}(\omega) \right) \\
& \qquad + \; G^{0>}_{\nu n_\nu \mu n_\mu \lambda k_\lambda, \mu' n'_\mu \nu' n'_\nu \lambda' k'_\lambda}(\omega) \; \Gamma^{(i)}_{\nu' n'_\nu \mu' n'_\mu \lambda' k'_\lambda, \mu'' n''_\mu \nu'' n''_\nu \lambda'' k''_\lambda}(\omega) \\
& \qquad\quad \times \quad \left(R^{(j)}_{\mu'' n''_\mu \nu'' n''_\nu \lambda'' k''_\lambda, \alpha n_\alpha \beta n_\beta \gamma k_\gamma}(\omega) \; + \; R^{(k)}_{\mu'' n''_\mu \nu'' n''_\nu \lambda'' k''_\lambda, \alpha n_\alpha \beta n_\beta \gamma k_\gamma}(\omega) \right) \; , \\
& \qquad\qquad\qquad\qquad\qquad\qquad\qquad\qquad\qquad\qquad i = 1, 2, 3 \; . \qquad (2.42)
\end{aligned}
$$

In Eq. (2.42), $G^{0>}$ is the forward-going part of the 2p1h propagator for three dressed but noninteracting lines. Using notations (2.5) we have

$$
G^{0>}_{\mu n_\mu \nu n_\nu \lambda k_\lambda, \alpha n_\alpha \beta n_\beta \gamma k_\gamma}(\omega) \; = \; \delta_{n_\mu, n_\alpha} \; \delta_{n_\nu, n_\beta} \; \delta_{k_\lambda, k_\gamma} \; \frac{\left(\mathcal{X}^{n_\mu}_\mu \mathcal{X}^{n_\nu}_\nu \mathcal{Y}^{k_\lambda}_\lambda \right)^* \; \mathcal{X}^{n_\alpha}_\alpha \mathcal{X}^{n_\beta}_\beta \mathcal{Y}^{k_\gamma}_\gamma}{\omega - (\varepsilon^+_{n_\alpha} + \varepsilon^+_{n_\beta} - \varepsilon^-_{k_\gamma}) + i\eta} \; . \qquad (2.43)
$$

Eqs. (2.42), together with the $\Gamma^{(i)}$'s given in Appendix A.2, approximate the general "Faddeev-Bethe-Salpeter" expansion to a tractable set of equations involving only two-time objects. It is important to note that these equations are still expressed in terms of the self-consistent solution $g_{\alpha\beta}(\omega)$ and include both pp and ph RPA phonons in a correct way. Thus they maintain all the features relevant for the physics we aim to describe.

As far as the physics is concerned, the material presented in this chapter gives a complete description of the ingredients that enter the calculations of this thesis. The use of the Faddeev equations allows one to account for the nuclear fragmentation and for both ph and hh(pp) phonons, simultaneously. The latter can be evaluated either at the RPA or TDA level. Although this formalism is practicable, Eqs. (2.42) require further manipulations before they can actually be solved numerically [38]. This added formalism is important for practical applications but it is not necessary to discuss the physical results presented in the next chapters. For this reason it is treated in the Appendices.

Chapter 3

Results

Following the iteration scheme of Chapter 2, the polarization and two-body propagators are computed first. Then, these results are employed to solve the Faddeev equations. The last step consists in evaluating the irreducible self-energy, Eq. (2.20), and to solve the Dyson equation. This calculation is carried out using both TDA and RPA equations and employing an IPM Green's function input like Eq. (2.17). This allows one to study the relative importance of RPA effects on the spectral functions. Subsequently, the dressed output propagator is employed as a starting point of a new calculation and the results are iterated a few more times. This elucidates the effects of self-consistency on fragmentation by employing DRPA phonons to provide the most complete treatment of correlations.

In order to apply the formalism of Chapter 2 to a finite nucleus like ^{16}O, it is necessary to make use of a limited model space and, accordingly, to employ an corresponding effective interaction. At the same time a prescription is needed to contain the number of poles that are generated at each iteration. These details are explained in Sec. 3.1, before discussing the results in the following sections.

3.1 Details of the Implementation for ^{16}O

3.1.1 Model Space and G-Matrix Interaction

The present calculations were performed within a finite set of harmonic oscillator states, representing the sp orbitals that are most relevant for low-lying excitations. Both the (D)RPA, the Faddeev and the Dyson equations were solved within a model space including all the first four major shells (from $1s$ to $2p1f$) plus the $1g_{9/2}$. The harmonic oscillator parameter was chosen to be b=1.76 fm. For the $1p$ states, this value reproduces properly the quasihole wave function computed in Ref.[62]. As a consequence of the truncation of the model space a Brueckner G-matrix was used as a microscopic effective interaction. This was derived from a Bonn-C potential [63] and computed according to Ref. [22]. The solution of the Bethe-Goldstone

equation includes the high-momentum intermediate states that are necessary for the treatment of SRTC. The Pauli operator used in the calculation of the G-matrix excludes all the intermediate states that are part of the model space, in which the LRC are explicitly computed [18]. This double-partitioning procedure avoids double counting of the pp ladder-diagram contributions to the self-energy (such as those, for example, included in the first diagram on the right hand side of Fig. 1.1). The results of Refs. [64, 43], suggest that this model space is large enough to properly account for the low-energy collective states that we are mainly interested in, while the SRTC are accounted for through the G-matrix effective interaction. These calculations also show that screening effects, such as those included by dressing the sp propagator, improve the convergence of results with respect to the dimension of the model space. The Bonn-C potential employed in this work does not include any charge independence breaking term and the Coulomb interaction between protons was not taken into account as well. Therefore the same results were obtained for both neutron and proton spectral functions.

As explained below, the energy dependence of the G-matrix was completely taken into account in the evaluation of the BHF part of the self-energy and in computing the normalization of spectral amplitudes. A G-matrix evaluated at a fixed starting energy was instead employed when solving the Faddeev equations. In this case a value of -25 MeV has been chosen as a suitable average of the most important 2h1p states that are of interest here. The only exception was made in computing the first 0^+ excited state for ^{16}O, as explained below.

3.1.2 Brueckner-Hartree-Fock Self-energy

After the G-matrix interaction has been substituted for the bare potential $\hat{V}$, the first diagram on the right-hand side of Fig. 2.1 represents the Brueckner-Hartree-Fock (BHF) contribution to the self-energy and acquires an energy dependence due to the use of the G-matrix. Its analytical expression is

$$\Sigma^{BHF}_{\alpha\beta}(\omega) = i \sum_{\gamma\delta} \int \frac{d\omega'}{2\pi} G_{\alpha\gamma,\delta\beta}(\omega+\omega') g_{\gamma\delta}(\omega') \; . \tag{3.1}$$

This contribution is needed in order to generate the correct sp energies for the main shells. It should be noted that Eq. (3.1) is expressed in terms of the self-consistent solution $g_{\gamma\delta}(\omega)$. If instead an IPM input is used, the approximated Hartree-Fock contribution may not be sufficient to put the main hole and particle fragments at the right place in energy. Rather, a self-consistent solution of the BHF equations should

be employed to evaluate Eq. (3.1). For example, in Ref. [19], the BHF equations were solved in advance. Then, the set of precomputed sp energies was used in the rest of the calculations. Also, one must note that a relevant contribution to the spin-orbit splitting between the $1p_{1/2}$ and $1p_{3/2}$ shells comes from relativistic effects or three-body forces [65, 66]. These contributions are not considered here.

In the present work, this issue was solved by adding an auxiliary one-body term to the BHF self-energy (3.1). This potential was chosen to be diagonal in the model space basis and was used to shift the sp energies for the fragments close to the Fermi energy. These corrections were needed during the first iterations, when the IPM starting point was used, and the parameters were fitted to reproduce the correct missing energies for the knockout and the addition of a proton. Once self-consistency is achieved, the BHF term of Eq. (3.1) generates correctly the contribution to the sp energies that come from two-body interactions . Accordingly, in our calculation the corrections applied to the s and d shells became negligibly small after a few iterations. The p shells continue to require an adjustment of 2.7 MeV for $1p_{1/2}$ and -0.7 MeV for $1p_{3/2}$, respectively. This is quantitatively in agreement with the need for a contribution from three-body forces as obtained in Ref. [65].

The BHF contribution (3.1) is also relevant for the normalization of the spectral amplitudes. The normalization condition (2.26) remains valid in the G-matrix approach but now an additional contribution to the derivative of $\Sigma^\star(\omega)$ comes from the energy dependence of the BHF term (3.1). In Ref. [19], it was shown that this accounts for a proper treatment of the depletion induced by SRTC at least for the normally occupied shells in the IPM. In the present work, the energy dependence of the BHF contribution was taken into account both in solving the Dyson equation and in the normalization of the (hole) spectral amplitudes. In the case of quasiparticle amplitudes this effect could not being taken into account. This is a consequence of the fact that for positive energies the G-matrix becomes a complex quantity and its calculation is not a trivial problem. In our case, the algorithm of Ref. [22] works only for negative energies. Therefore a constant value of $G(\omega)$ (computed for ω=-5 MeV) was adopted for all positive energies.

3.1.3 Iterative Procedure

The solution to the Dyson equation (2.24) contains a large number of fragments, most of which are quite small. A fully self-consistent solution requires a method in which the sp strength is binned over a large energy domain [24]. The number of poles and the resulting 2p1h and 2h1p configurations are then too numerous for a

practical solution of the Faddeev equations. To obtain some insight into the effects of self-consistency we have chosen to limit the number of fragments in such a way that the ones closer to the the Fermi level are kept intact. This approximation appears to be well founded and it is confirmed by our results, which show that the low-energy structure is principally determined by the main fragments. The following procedure was employed to limit the number of poles in $g(\omega)$. For each value of the angular momenta ℓ and j, we have kept two poles above and two below the Fermi energy. When two poles on one side of the Fermi energy were included, the fragment closest to the Fermi energy was kept, including its location and strength. Thus, for the levels near the Fermi energy, the principal quasiparticle (quasihole) fragment was kept intact. The rest of the strength was collected in the remaining pole at a location determined by weighing the remaining fragment energies with the corresponding strength. The only exception to this was made for the f and g shells for which only one effective hole pole was kept. The resulting dressed propagator still contains all the relevant low-energy fragmentation and at the same time it has a number of poles small enough to be used as input to another Faddeev DRPA calculation.

A last prescription employed in the present calculations needs to be discussed. As noted in Sec. 2.3, for too attractive interactions, the RPA approach can give rise to instabilities. This situation is particularly critical when a realistic nuclear interaction is applied to compute the isoscalar 0^+ channel [26] of ^{16}O. In performing our calculations with a dressed propagator, the phDRPA equations gave an unstable solution for the first 0^+ excited state. Naturally, the instability of the lowest ph 0^+ state tends to disappear when a more negative starting energy is chosen for the G-matrix since such a choice reduces the attraction in this channel. Since the first 0^+ state is of particular importance, we decided not to simply discard the unstable solution but to compute it in a regime where the instability disappears, adopting the following procedure. A stable solution for the spectroscopic amplitudes of this state was obtained by solving the ph DPRA equations with a G-matrix at a starting energy of -110 MeV. Then, the energy of the state was kept fixed at the experimental energy of 6.05 MeV. The solution obtained, was then substituted for the unstable one. All the remaining 0^+ levels were properly computed with a G-matrix at -25 MeV.

Obviously, such a prescription is somewhat artificial and should be avoided in future calculations. When improved phonons are considered, the RPA equations tend to yield stable results and allow for more attractive interactions [43]. Therefore,

Shell	TDA	RPA
$d_{3/2}$	0.866	0.838
$s_{1/2}$	0.882	0.842
$d_{5/2}$	0.894	0.875
$p_{1/2}$	0.775	0.745
$p_{3/2}$	0.766	0.725

Table 3.1: Spectroscopic factors for ^{16}O as computed in both TDA and RPA schemes using an IPM input. Listed are the strengths of the main (particle or hole) fragments for the five levels close to the Fermi energy. All values are given as a fraction of the corresponding IPM value.

such improvement of the phonon calculation is expected to eliminate the need for this artificial step. Most probably, this calculation will require a proper treatment of the coupling between pairs of ph phonons [28] together with an approach to reduce the effects of Pauli violation in the DRPA equation. This may require a further extension of the formalism of Chapter 2 and is the topic of planned future work [67]. Nevertheless, a first attempt in this direction is described in Chapter 4 of this thesis.

3.2 Results for the Single-particle Motion

3.2.1 Effects of RPA Correlations

By using an IPM ansatz as input propagator, the Faddeev equations have been applied to obtain the self-energy of ^{16}O in both TDA and RPA approximations. The resulting self-energy was then used in the Dyson equation (2.24) to obtain the sp spectral functions for the removal (one-hole) and addition (one-particle) of a nucleon. The values of the spectroscopic factors for the main particle and hole shells close to the Fermi energy are reported in Table 3.1. The hole strengths given by TDA are 0.775 for $p_{1/2}$ and 0.766 for $p_{3/2}$, in close agreement with the results of Ref. [19] (to which the present TDA calculation is equivalent). The introduction of RPA correlations reduces these values and brings them down to 0.745 and 0.725, respectively. This result reduces the discrepancy with the experiment by about 4% and shows that collectivity beyond the TDA level is relevant to explain the quenching of spectroscopic factors. Since the present formalism does not account for

	TDA		RPA	
Shell	Particle	Hole	Particle	Hole
$2p_{1/2}$	0.983	0.014	0.980	0.017
$2p_{3/2}$	0.980	0.016	0.978	0.018
$1d_{3/2}$	0.959	0.038	0.945	0.051
$2s_{1/2}$	0.954	0.039	0.916	0.074
$1d_{5/2}$	0.961	0.035	0.946	0.049
$1p_{1/2}$	0.102	0.828	0.128	0.804
$1p_{3/2}$	0.076	0.856	0.107	0.828
$1s_{1/2}$	0.044	0.888	0.057	0.876
Total occ.		14.95		15.06

Table 3.2: Occupation and depletion numbers for the most relevant shells of ^{16}O as computed in both TDA and RPA schemes using an IPM input. All the results are given as a fraction of the corresponding IPM value. Also shown is the result for the total number of nucleons obtained by summing over all the hole fragments.

center-of-mass effects, the above quantities need to be increased by about 7% before they are compared with the experiment [16, 17]. It should be noted that the present RPA results describing the ph and pp (hh) spectrum suffer from the usual problems associated with RPA. One such feature, as already noted above for the ph 0^+ state, is the appearance of at most one collective state for a given J^π, whereas many low-lying isoscalar natural parity states are observed experimentally. This feature implies that especially the ph spectrum does not provide a very good description of the experimental data. One may therefore expect that further improvements of the description of the RPA phonons themselves will close the gap with the experimental data further.

Together with the main fragments, the Dyson equation produces also a large number of solutions with small spectroscopic factors. For the one-hole spectral function, this strength extends down to about -130 MeV. This background partly represents the strength that is removed from the main peaks and shifted to medium missing energies. The energy dependence of the G-matrix accounts for another 10% effect in pushing the strength of the mostly occupied shells to high energies in the particle domain. We note that the location of this strength cannot be explicitly calculated in the present approach but corresponds to very large energies [1]. The

occupation number coming from both the background contribution at negative energies, as well as from the main hole fragments is displayed in Table 3.2 for the most important shells. Summing these numbers together with the occupation of the main peaks and weighing them by a factor of $2(2j+1)$, one gets a total number of particles equal to about 15 nucleons. This violation of particle number is a consequence of the energy dependence of the G-matrix. The remaining strength is then accounted for by the presence of high-momentum components due to SRTC not explicitly calculated in the present scheme. The present result therefore also gives an estimate of the number of these high-momentum particles that are shifted to even higher missing energies (more negative hole poles). These high-momentum components are included in the results of Refs. [13, 62] and their strength agrees with the number of missing nucleons in the present calculation. The effects of SRTC on the reduction of quasihole spectroscopic factors are thus properly included, through the energy dependence of the G-matrix interaction.

Fig. 3.1 displays the TDA and RPA one-hole spectral function for the $p_{1/2}$ and $p_{3/2}$ states. In this figure the theoretical spectral function is binned in order to make a comparison with the experimental results. These results demonstrate that neither of the two approaches explains the breaking of the main $p_{3/2}$ peak when an input IPM propagator is used. The main difference between the two results are the 4% smaller peaks obtained in the RPA approach. The results for positive parity shells are shown in Fig. 3.2. The solid bars refer to results for orbital angular momentum $\ell = 2$ and the open bars to $\ell = 0$, respectively. We observe that the RPA approach generates two hole peaks with angular momenta $d_{5/2}$ and $s_{1/2}$ at small missing energy. These peaks are found separated from the rest of strength at -15.6 and -15.8 MeV respectively, which differ from the experimental value by about 2 MeV. These "weak" fragments have relatively small spectroscopic factors and represent the particle orbitals that would characterize the excitation spectrum of the $A+1$ system but that are found to be empty in an IPM wave function of the $A-1$ nucleus. As a consequence of correlations in the ground state of the original ^{16}O such sp states become partially occupied and are shifted down to energies comparable to those of the hole states. The existence of these states is a characteristic of many closed shell nuclei (and their neighbors) throughout the nuclear table [68] . The RPA predicts a spectroscopic factor of 0.1% for $d_{5/2}$ which is smaller than the experimental value of 1.9%. This represents an improvement with respect to the TDA, where such a fragment is not reproduced at all. The agreement is better for the $s_{1/2}$ fragment for which the theory predicts 3.0% and the experimental value

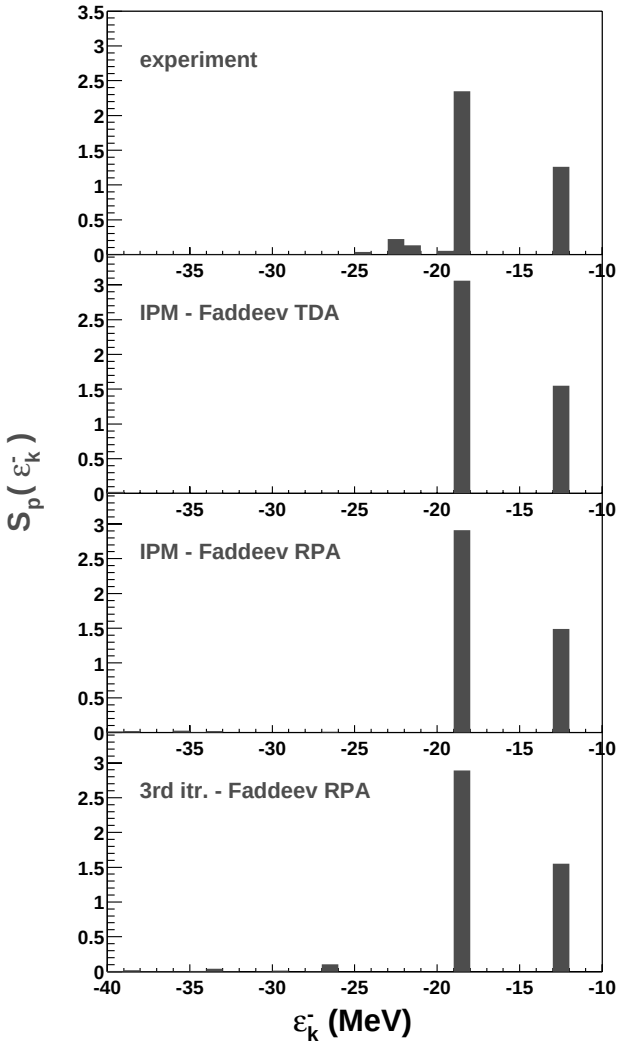

Figure 3.1: One-proton removal strength as a function of the hole sp energy $\varepsilon_k^- = E_0^A - E_k^{A-1}$ for ^{16}O and angular momentum $\ell = 1$. The experimental values are taken from [10]. The theoretical results have been calculated in both TDA and RPA approximation with an IPM model input. The bottom panel includes the results of iterating the fragmentation pattern through the construction of DRPA phonons.

is 1.8%. We note, however, that the experimental analysis of these states [10] is expected to suffer from the same uncertainties discussed in Chapter 1 for the main fragments [11, 12]. Due to the small value of their spectroscopic factors the experimental error seems too big to make a reliable comparison with the results of the present model. At energies below -20 MeV, the experimental $s_{1/2}$ strength is distributed almost continuously and increases as the energy approaches the region corresponding to giant resonances. In the present calculation, based on a finite number of discrete states, the theory predicts a fragmentation over fewer isolated peaks with higher spectroscopic strengths.

3.2.2 Effects of Fragmentation

The RPA results were iterated a few times, with the aim of studying the effects of fragmentation on the RPA phonons and, subsequently, on the spectral strength. This was done by employing the prescription for representing the strength distribution with effective poles that is described in Sec. 3.1.3. The negative parity hole spectral function resulting from the third iteration is shown in the lower panel of Fig. 3.1. The main difference between these results and the one obtained by using an IPM input is the appearance of a second smaller $p_{3/2}$ fragment at -26.3 MeV. This peak rises in the first two iterations and appears to become stable in the last ones, with a spectroscopic factor of 2.6%. This can be interpreted as a peak that describes the fragments seen experimentally at slightly lower energy. This is the first time that such a fragment is obtained in calculations of the spectral strength. Further insight into the appearance of this strength is discussed in Sec. 3.4.

A second effect of including fragmentation in the construction of the RPA phonons is to increase the strength of the main hole peaks. The spectroscopic factors for the main p peaks, as obtained from the first four iterations, are reported in Table 3.3. The $p_{1/2}$ strength increases from the 0.745 obtained with IPM input to 0.776, essentially cancelling the improvement gained by the introduction of RPA correlations over the TDA ones. The main peak of the $p_{3/2}$ remains at 0.722 but the appearance of the secondary fragment slightly increases the overall strength at low energy as well. This behavior can be understood by realizing that with an IPM input most of the phonons are somewhat more collective than the ones obtained from employing dressed propagators with the exception of the special case of the ph 0^+. As a result, one can expect a reduced effect of RPA correlations when fragmentation is included in the construction of the phonons. This feature has also been observed in other self-consistent calculations of the sp spectral strength, for example

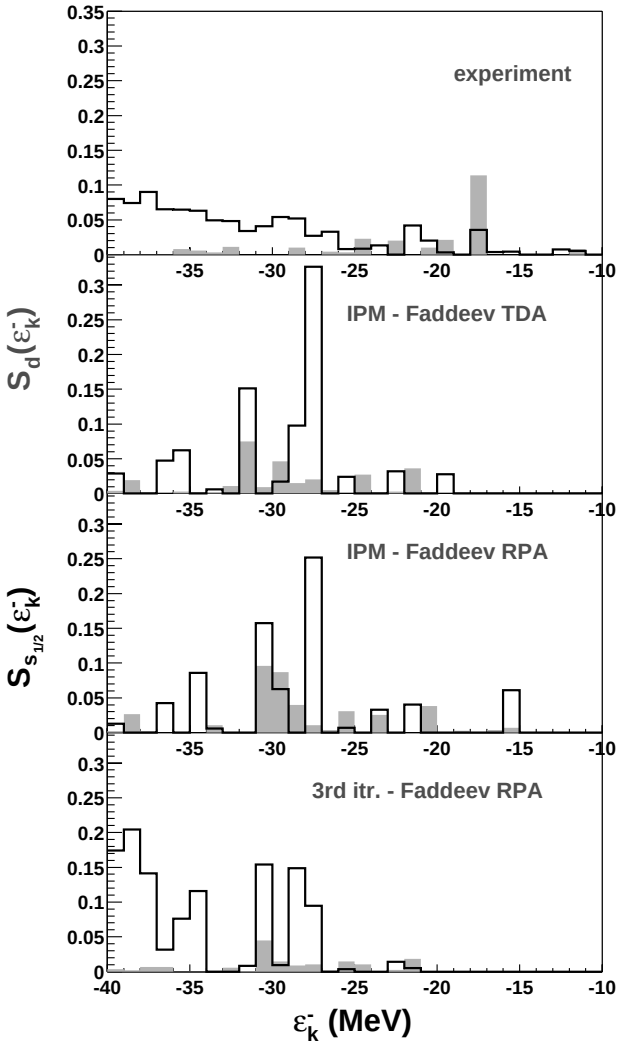

Figure 3.2: One-proton removal strength as a function of the hole sp energy $\varepsilon_k^- = E_0^A - E_k^{A-1}$ for ^{16}O and positive parity final states. The solid bars correspond to results for orbital angular momentum $\ell = 2$, while the thick lines refer to $\ell = 0$. The experimental values are taken from [10]. The theoretical results have been calculated in both TDA and RPA approximation with an IPM model input. The bottom panel includes the effect of fragmentation on the construction of the DRPA phonons after three iterations.

Shell	1st itr.	2nd itr.	3rd itr.	4th itr.
$Z_{p_{1/2}}$	0.775	0.777	0.774	0.776
$Z_{p_{3/2}}$	0.725	0.727	0.722	0.724
	0.015	0.027	0.026	0.026
$n_{d_{3/2}}$	0.025	0.025	0.026	0.025
$n_{d_{5/2}}$	0.020	0.021	0.021	0.020
$n_{p_{1/2}}$	0.850	0.848	0.848	0.848
$n_{p_{3/2}}$	0.870	0.871	0.870	0.871
$n_{s_{1/2}}$	0.911	0.914	0.916	0.930
Total occ.	14.56	14.57	14.58	14.63

Table 3.3: Hole spectroscopic factors (Z_α) for knock out of a $\ell = 1$ proton from ^{16}O and occupation numbers (n_α) for different angular momenta of the nucleon. These results refer to the first four iterations of the DRPA equations. All the values are given as a fraction of the corresponding IPM value and in the case of $\ell = 0$ and $\ell = 1$ are summed over the principal h.o. quantum numbers belonging to the model space (i.e. $s_{1/2}$ stands for the sum of $1s_{1/2}$ and $2s_{1/2}$, similarly for $p_{1/2}$ and $p_{3/2}$). Also included is the total number of nucleons for each iteration.

in nuclear matter [69]. Obviously, this makes the disagreement with experiments a little worse and additional work is needed to resolve the disagreement with the data. Nevertheless it is clear that fragmentation is a relevant feature of nuclear systems and that it has to be properly taken into account. It is also worth nothing that already after a few iterations, all the main quantities of Table 3.3 tend to stabilize and sustain themselves in a self-consistent way.

Table 3.3 also shows the total number of particles obtained at each iteration (derived by summing over the hole strength). This result corresponds to about 14.6 nucleons when fragmentation is included. This gives an estimate for the overall occupancy of high-momentum states of about 10%, in agreement with direct calculations of SRTC [13, 62]. We observe that this estimate is different from the results for the IPM input quoted in Table 3.2. We associate this difference with the

energy dependence of the G-matrix which is sampled differently in both cases. In the IPM calculation the lowest three shells are included at the harmonic oscillator level. Upon iteration, which involves the changing BHF contribution, the admixture of the other s and p shells is included and will generate a slightly different effect related to the energy dependence of the G-matrix since different matrix elements are sampled in each case. We note here that for this reason there is also a distinct difference between the quasiparticle and quasihole strengths near the Fermi energy as shown in Table 3.1 of about 10%. This same difference appears in the summed strengths appearing in Table 3.2. In both cases there appears more strength in the particle domain than is appropriate for the effect of SRTC. In the present approach we cannot treat this effect for particle shells properly since the G-matrix of Ref. [22] is constructed only for negative energy. The derivative of the energy dependence of the G-matrix at energies relevant for particle states will therefore not reflect the true depletion due to SRTC. For this reason the summed strength for the particle states is close to 1 in Table 3.2.

The results of the third iteration are also given in Fig. 3.2 for the relevant positive parity spectral functions. We note that the $s_{1/2}$ and $d_{5/2}$ hole fragments at -15 MeV are no longer generated by these iterated calculations. Also, as a consequence of dressing the input propagator, more poles are produced as solutions of the Dyson equation (2.24). This allows for a better distribution of the $s_{1/2}$ strength at medium missing energies. Similar results have been obtained in the self-consistent second-order calculation for ^{48}Ca in Ref. [24]. Presumably, a more complete representation of the strength in the input propagator would further improve the $\ell = 0$ strength distribution.

3.2.3 One-Particle Spectral Function

The results for the one-particle spectral function are shown in Fig. 3.3 for final states of positive parity. In this picture the solid and open bars refer to d and s states, respectively. These comprise the first shells above the Fermi energy and their spectral function contains the principal particle peaks. As explained in Section 3.1.2, these fragments were forced to be at their experimental energies during the initial TDA and RPA calculations. During the following iterations, the contribution of Brueckner-Hartree-Fock potential (3.1) properly generates the energy shifts that are needed to place these peaks at the right place. As a consequence no correction was added to sp energies obtained in the Dressed RPA calculation and agreement with experimental values was still obtained, as shown by the bottom picture of Fig. 3.3.

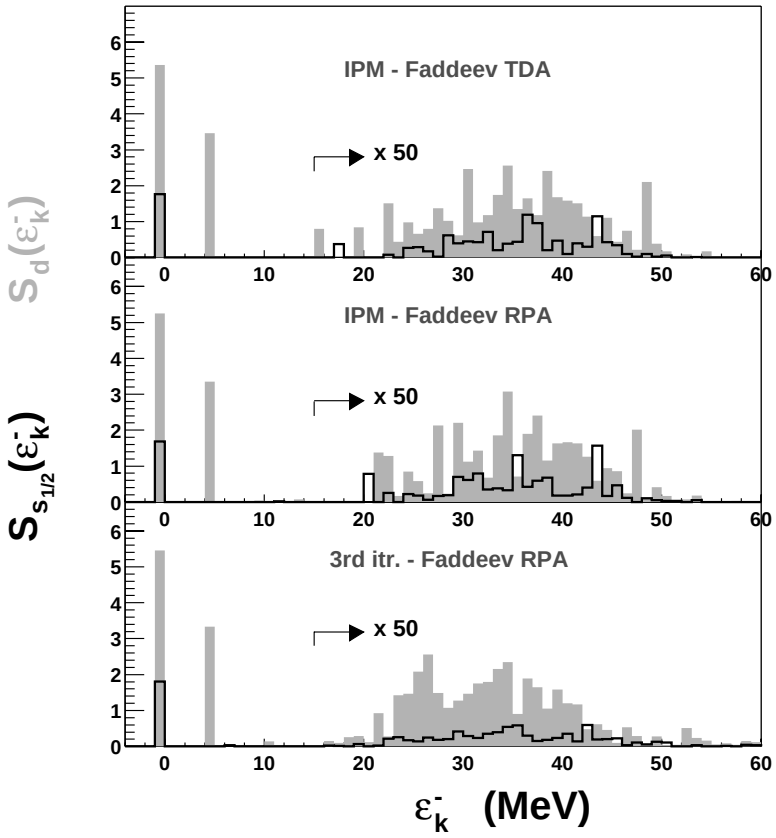

Figure 3.3: One-proton addition strength as a function of sp energy $\varepsilon_n^+ = E_n^{A+1} - E_0^A$ for ^{16}O and positive parity final states. The solid bars correspond to results for orbital angular momentum $\ell = 2$, while the thick lines refer to $\ell = 0$. The theoretical results have been calculated in both TDA and RPA approximation with an IPM model input. The bottom panel includes the effect of fragmentation on the construction of the DRPA phonons after three iterations. The particle strength located above 15 MeV has been multiplied by a factor of 50.

Shell	IPM/TDA.	IPM/RPA.	3rd itr.
$Z_{s_{1/2}}$	0.882	0.842	0.903
	0.004	0.008	0.015
$n_{r,s_{1/2}}$	0.106	0.123	0.099
$Z_{d_{5/2}}$	0.894	0.875	0.909
$n_{r,d_{5/2}}$	0.067	0.071	0.069
$Z_{d_{3/2}}$	0.866	0.838	0.832
		0.018	0.036
$n_{r,d_{3/2}}$	0.083	0.089	0.105

Table 3.4: Particle spectroscopic factors (Z_α) for addition of a $\ell = 0$ or $\ell = 2$ proton to ^{16}O and contribution to the depletion numbers ($n_{r,\alpha}$) from the residual strength at medium energies. These results refer to the initial TDA and RPA calculations and to the third iteration. All the values are given as a fraction of the corresponding IPM value and in the case of $\ell = 0$ are summed over the principal h.o. quantum numbers belonging to the model space (i.e. $s_{1/2}$ stands for the sum of $1s_{1/2}$ and $2s_{1/2}$).

The values of the total spectroscopic strengths for the main s and d peaks is given in Table 3.4 for the same cases of Fig. 3.3. As explained above, these values do not take into account SRTC effects and therefore are expected to be 10% lower if an energy-dependent G-matrix would be used also for positive energies. As for the hole case, the effects of RPA correlations tend to increase the collectiveness of the system and therefore to raise the occupation number of the main particle orbitals (that are empty in the IPM). The corresponding effect on the one-particle spectral function is a strength reduction of the relative quasiparticle peaks by about 3%. Fragmentation screens this effect and increases the total spectroscopic strength back to about the initial TDA values. The only exception is the $d_{3/2}$ peak which has a reduced spectroscopic factor, while an additional fragment is generated in a way analogous to the breaking of the $p_{3/2}$ hole fragment. We also note that an additional $s_{1/2}$ fragment is generated and sustained by both RPA and dressing effects. The $s_{1/2}$ and $d_{3/2}$ secondary fragments have small spectroscopic factor and can barely be seen in Fig. 3.3. In the ph DRPA, their poles were found at 6.42 and 10.9 MeV, respectively.

All the remaining strength that has been obtained solving the Dyson equation is located at medium energies, above 15 MeV. This consists of a large number of fragments with small spectroscopic factors that are distributed up to about 55 MeV. The relative strength is shown in Fig. 3.3 increased by a factor of 50, in order to make it visible. Table 3.4 shows that at least 10% of the total particle strength is located in this portion of the spectrum and another 10% would be moved to even higher energies by SRTC. This behavior is also found for the hole spectral function for p states, where the medium energy strength is shifted down to energies not visible in Fig. 3.1. For particle energies above 50 MeV, more strength is present in real nuclei, due to SRTC, but cannot be computed in the present approach.

The one-particle spectral function for negative parity final states is plotted in Fig. 3.4 where solid and empty bars refer to f and p states, respectively. These strengths correspond to the pf shells, which are found higher in energy. In this case, the fragmentation is substantial at the energies of the corresponding sp orbitals for these shells. This results in a spreading of the main particle strength in an energy interval between 5 to 30 MeV. A smaller portion of the fragmentation, corresponding to about 10%, is also found at intermediate energies above 35 MeV. As can be seen in Fig. 3.4, the distribution of the latter is somewhat similar in TDA and RPA calculations. Dressing the input propagator makes this spreading more uniform and extends it to both lower and higher energies. Also in this case the high-energy tail of the strength distribution, expected from SRTC, is missed by the present calculations.

A comparison of Figs. 3.3 and 3.4 can give more insight into the limits of the iterative procedure discussed in Section 3.1.3. The single fragments at medium energies are very small and, separately, do not produce any measurable effect on low-energy correlations. Nevertheless, due to the large number of fragments a considerable part of the strength (more than 10%) is contained in this region. Obviously, this should be taken into account at least in an effective way. To do this, we collected all these fragments in a single pole that contains the sum of all of them. As an example, in the case of Fig. 3.3 the three s and d principal fragments were kept as calculated, while the rest of the distribution was substituted with three effective peaks at 39.7 for $s_{1/2}$, at 37.8 for $d_{5/2}$ and at 31.0 MeV for $d_{5/2}$. These are the centroids of the relative distributions of the fragments. The total spectral strengths for these orbitals were 0.114, 0.069 and 0.141, respectively. We note that the application of such a prescription to the pf distribution of Fig. 3.4 is more troublesome. Still the lower panel shows that it is possible to separate some p and f fragments that are

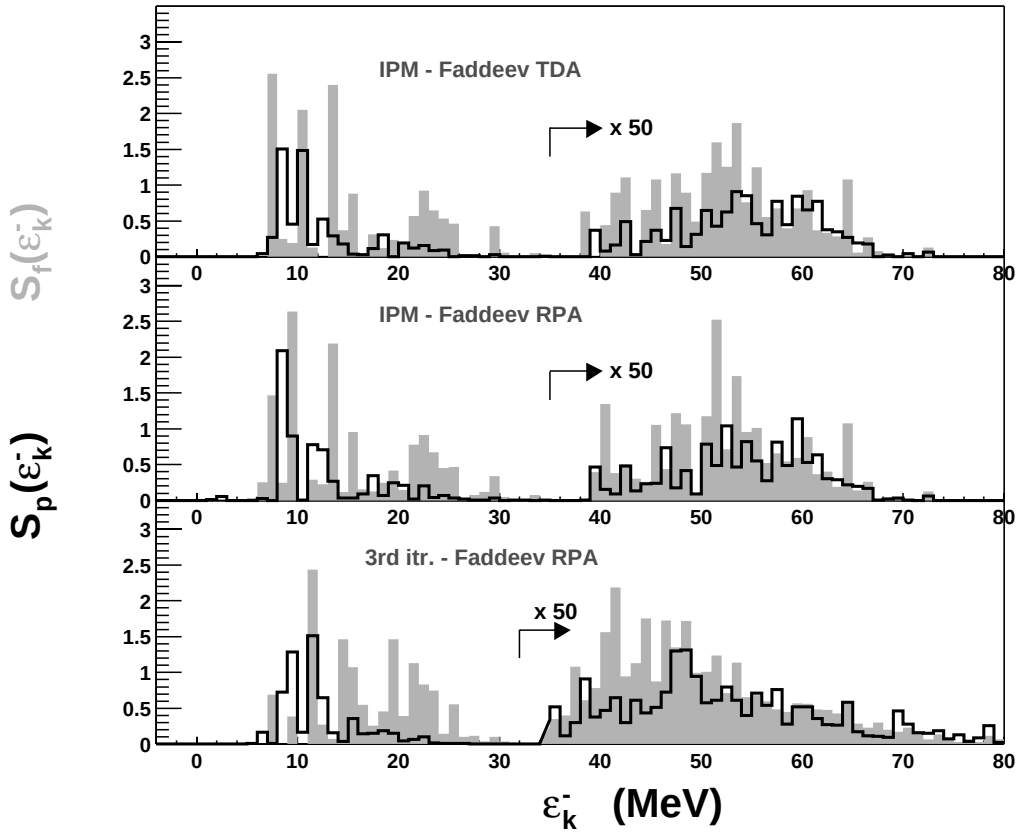

Figure 3.4: One-proton addition strength as a function of the hole sp energy $\varepsilon_n^+ = E_n^{A+1} - E_0^A$ for ^{16}O and negative parity final states. The solid bars correspond to results for orbital angular momentum $\ell = 3$, while the thick lines refer to $\ell = 1$. The theoretical results have been calculated in both TDA and RPA approximation with an IPM model input. The bottom panel includes the effect of fragmentation on the construction of the DRPA phonons after three iterations. The particle strength located above 35 MeV has been multiplied by a factor of 50.

bigger than the others. All of the remaining strength was collected in four effective poles for $p_{3/2}$, $p_{1/2}$, $f_{7/2}$ and $f_{5/2}$ states. Although this approach is less satisfactory for pf shell, it is needed in order to keep the dimension of the Faddeev eigenvalue equation within a tractable size. The focus of this work is on the low-energy behavior of the hole spectral function. Moreover, the p and sd fragments close to the Fermi energy are the principal quantities that determine the LRC structure of ^{16}O. Thus at the higher energies where the p and f particle fragments are found, the above prescription is adequate for the purposes of this thesis. In any case, a proper calculation of the particle spectral function at medium energies would require a continuum representation of the one-body spectral function.

3.3 Collective Phonons

3.3.1 Excitation Spectrum of ^{16}O

The excitation spectrum of ^{16}O has been extracted from the Lehmann representation of the polarization propagator, Eq. (2.12). The results for the lowest isoscalar excited states, obtained in terms of an IPM input propagator, are compared with experiment in Fig. 3.5. The TDA reproduces only the negative parity states. The 1^- is found at 9.60 MeV while the 3^- is at 9.07 MeV. This corresponds to about 2-3 MeV above the experimental values. The situation is improved when the RPA equations are solved. This brings down the energies to 9.13 and 7.14 MeV, respectively, and gives a better agreement for the 3^- state. More dramatic is the behavior of the first 0^+ excited level. The lowest 0^+ eigenvalue obtained from TDA is found at 14.9 MeV. This energy is rather high and cannot be easily interpreted as a low lying eigenvalue. Instead, the RPA equation gives a solution at 9.46 MeV. In general, the effect of RPA is to produce a more attractive interaction that makes the first excited states more collective and brings them down to lower energies. The fact that this effect is more relevant for the 0^+ state is in accordance with the experience from shell-model calculations, where up to $4\hbar\omega$ configurations are needed to reproduce low-energy positive parity states of ^{16}O [70, 27]. Such configurations contain 2p2h and 3p3h states that are completely missed by the standard TDA equation but are partially included in the RPA, as discussed in Section 2.3.1.

A further rearrangement of the ph spectrum is obtained when the effects of fragmentation are included. This is shown in the last column of Fig. 3.5, where the ph DRPA results from the third iteration are reported. The excitation energies for the first 1^- and 3^- levels rise to 10.8 and 9.42 MeV, thus worsening the agreement

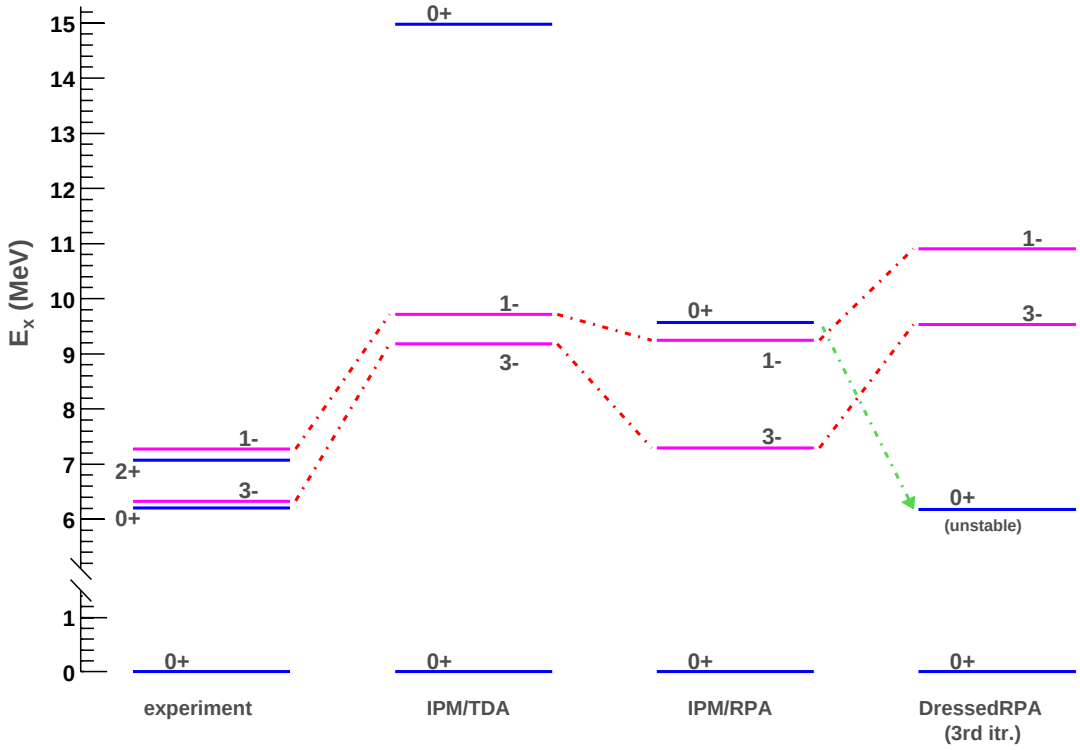

Figure 3.5: Results for the first isoscalar excited states of ^{16}O. The second and third columns are obtained from an IPM propagator, by solving TDA and RPA equations respectively. The last column refers to the ph DRPA propagator obtained during the the third iteration. The results are compared to the experiment in the first column. The unstable 0^+ state in phDRPA has been artificially set to the experimental energy.

	experiment	IPM/TDA	IPM/RPA	DRPA (3rd itr)
$T=0,\ 2^-$	12.53	12.58	12.63	12.04
$T=0,\ 0^-$	10.96	10.63	10.04	11.64
$T=1,\ 3^-$		13.94	13.85	12.95
$T=1,\ 1^-$	13.09	13.11	13.04	12.80

Table 3.5: Higher excited states obtained from TDA and (D)RPA compared to empirical values. Experimentally, several more excited states of ^{16}O are found at these energies but that are not reproduced by the present calculations.

with data. This is an effect of dressing the sp propagator, which introduces a screening of the interaction and therefore reduces collective effects. This points to a need for a more attractive G-matrix interaction. We mention here that the present G-matrix is calculated without any binding correction of the sp energies for particle states which could have some influence on the strength of the effective interaction. These results also suggest that more correlation effects should be taken into account to bring the lowest negative parity states to the right place in energy. The case of the first 0^+ state is anomalous. The introduction of fragmentation makes this channel even more collective and already at the first iteration unstable, imaginary eigenvalues are obtained. This behavior with respect to fragmentation effects is quite surprising and counterintuitive. One possible explanation may be related to the variety of configurations that mix to form this level. It may happen that the ph interaction turns out to be repulsive for part of the involved contributions. If the screening effects are stronger for these matrix elements than for the attractive ones, the net effect would still be an increase of collectivity. In any case, this anomaly is a clear indication of the complexity in the structure of the first 0^+ state. Calculations that properly go beyond the phDRPA level will be required to solve this puzzle. In order to pursue an iterative calculation, the unstable solution was replaced according to the prescription of Sec. 3.1.3, as shown in Fig. 3.5.

Other negative parity levels are correctly reproduced in both TDA and RPA at higher excitation energies. The most important are the isoscalar 0^- and 2^- found at about 10-12 MeV and the isovector 1^- and 3^- at 11-13 MeV. These are not shown in Fig. 3.5. The results for all of them are in fair agreement with the experiment and with previous calculations [26], as can be seen from Table 3.5.

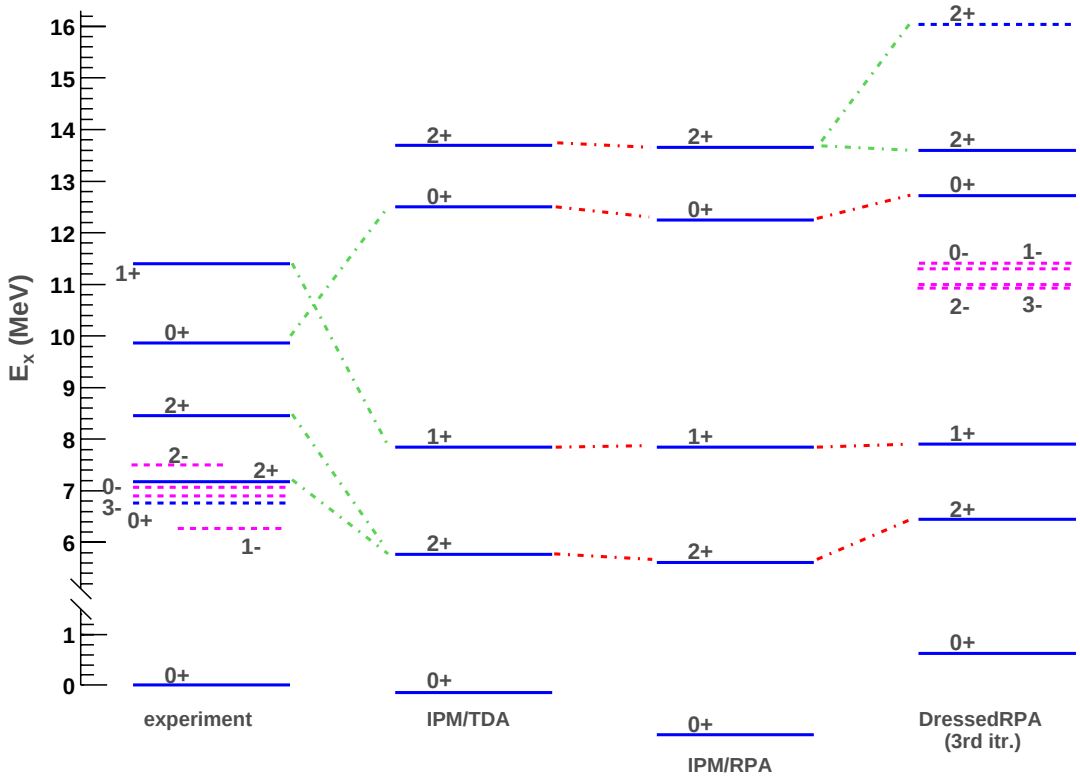

Figure 3.6: Lowest excited level of ^{14}C as obtained from TDA and (D)RPA calculations. The theory is compared to the experimental results in the first column. The levels drawn with a dashed line have a small total spectroscopic strength and therefore they would be little populated in two-nucleon transfer reactions.

3.3.2 Excitation Spectra for ^{14}C and ^{14}N

The solution for the two-particle propagator contains information on the excitation spectra of the system with $A-2$ nucleons. In particular the isovector and isoscalar channels give the lowest excited states for ^{14}C and ^{14}N, respectively. The excitation spectrum of ^{14}C is shown in Fig. 3.6. The levels have been extracted from the poles $\varepsilon^{\Gamma+}_{k-}$ of the two-body propagator (2.14) and have been shifted to be compared with the experimental excitation energies. This requires to consider the experimental separation energies for extracting two protons from ^{16}O (cf. the last of Eqs. (A.3)).

The results for positive parity levels from TDA and RPA, with an IPM input, are basically equivalent to the ones of Ref. [20], where a hh DRPA equation was solved. The excited 0^+ and 1^+ states are reproduced but with energies far from the experimental ones and in the wrong order. In spite of this discrepancy the relative spectral amplitudes have been successfully applied to study the ^{16}O$(e,e'pp)$ cross section [21, 8]. Less satisfactory are the solutions for the 2^+ channel. Experimentally a pair of 2^+ levels is observed below 9 MeV. The theory reproduces only one of them and at lower energy. As discussed in Chapter 1, these low-lying states are of two-proton–hole type and are characterized by a $(p_{3/2}, p_{3/2})^{-1}$ configuration. For this reason, it has been argued that the splitting of the 2^+ states could be directly related to the splitting of the $p_{3/2}$ hole fragment in ^{15}N. This conjecture does not seem to be confirmed by the pp DRPA calculation shown in the last column of Fig. 3.6. The latter refers to the third iteration and therefore a dressed sp propagator with $p_{3/2}$ breaking was employed (2nd itr. column of Table 3.3). Curiously enough, the results show a splitting of the high 2^+ state at about 14 MeV, rather than for the lowest one. Furthermore the second fragment is at higher energy and carries very little strength. We have checked the relation with the one-hole spectral function by suppressing the second $p_{3/2}$ fragment in the input propagator and then repeating the same calculation with the main $p_{3/2}$ only. In this case only one 2^+ state is found around 14 MeV. It must be observed that the splitting of $p_{3/2}$ fragments in ^{15}N is not completely described in the present calculations. This suggests that the $p_{3/2}$ breaking may still play some role in the determination of the 2^+ states of ^{14}C if improvement in the present calculation is achieved. Nevertheless, it also appears reasonable to suspect that the above mechanism may not be sufficient to explain the 2^+ puzzle and that other configurations may come in to play. Two-phonon configurations that couple either the excited 2^+ levels of ^{14}C to the lower 0^+ phonons in the ^{16}O core or the ground state of ^{14}C to the 2^+ state in ^{16}O, may play this role. Another candidate can be the coupling of the two weak $d_{5/2}$ and $s_{1/2}$ hole fragments discussed in Sections 3.2.1 and 3.4.

Finally we note that the experimental spectrum of ^{14}C includes a few states with quantum numbers 0^+ at 6.59, 1^- at 6.09 and 3^- at 6.73 MeV, which are hardly populated in two-proton transfer experiments [7, 8, 71, 72]. These are clearly reminiscent of the low-lying states of ^{16}O with the same quantum numbers and can be interpreted as excitations of the ^{16}O core in ^{14}C as well. In this sense they are "weak" levels analogous to the ones discussed in Section 3.2.1 for the hole spectral function. The TDA and RPA calculations, based on an IPM ansatz, do

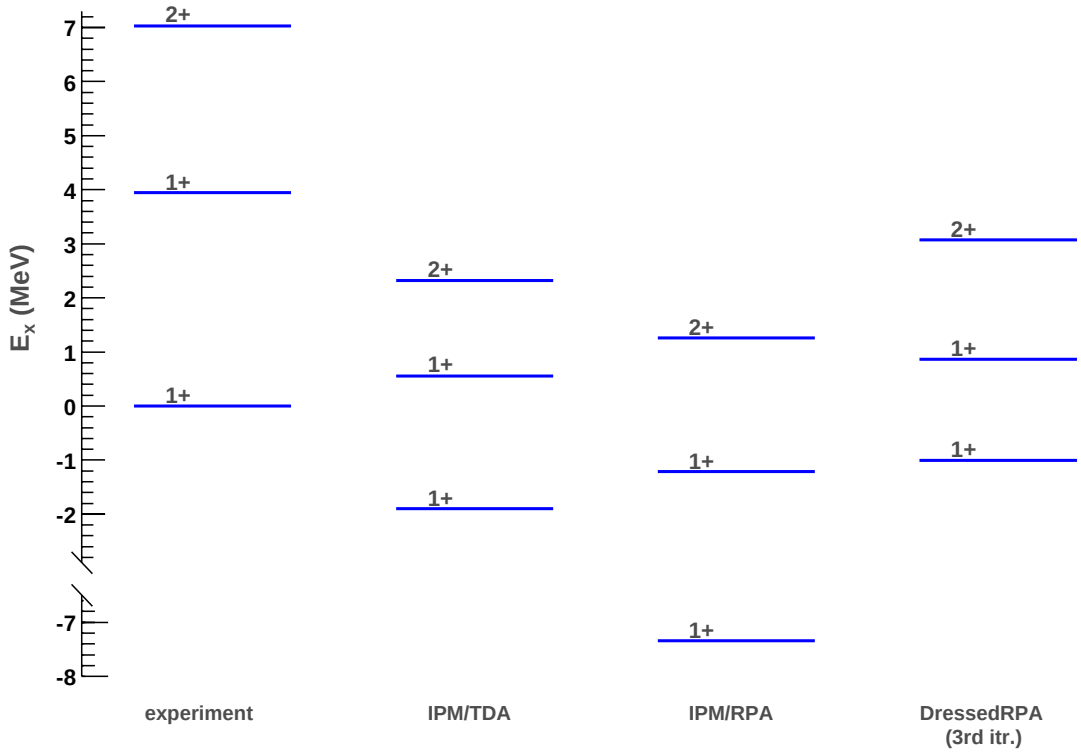

Figure 3.7: Lowest excited levels of ^{14}N as obtained from TDA and (D)RPA calculations. The theory is compared to the experimental results shown in the first column.

not reproduce these levels. Though a few negative parity levels with small total spectral strength are obtained in hh DRPA.

The experimental and theoretical spectra of ^{14}N are compared in Fig. 3.7 for the ground states and the principal isoscalar states. Note that the excitation energies are plotted with respect to the experimental ground state of ^{14}N, which requires a shift of the theoretical results by the separation energy of a proton and a neutron from the ^{16}O core. In our calculation, the Coulomb interaction was completely neglected but the one-hole spectral function that enter the hh DRPA (and hh TDA) calculations where fitted to reproduce the proton-hole energies. If neutron-hole energies were employed for one of the legs in the hh propagator, Eq. (2.29), higher theoretical energies for the ground state would be found. This explains why the IPM/TDA and the DRPA results in Fig. 3.7 are systematically somewhat lower than experiment.

It makes sense, however, to compare the relative excitation energies. The theory predicts 2.54 Mev for the 1^+ state and 4.22 MeV for 2^+ in IPM/TDA, and 1.86 MeV for 1^+ and 4.07 MeV for 2^+ in hhDPRA. These are both 2 and 3 MeV lower than the experimental values of 3.95 and 7.03, respectively. The results from IPM/RPA should not be taken too seriously since the ground state is affected by the closeness of the pairing instability of the RPA.

Finally we note the behavior of the ground state energies for both ^{14}C and ^{14}N with respect to the different approximations employed. Figs. 3.6 and 3.7 show that the lowest levels obtained in IMP/RPA are more collective and lower in energy than the corresponding TDA results. When fragmentation is included, the ground state level is brought back up as a consequence of screening, eventually reaching a higher energy than the IMP/TDA one. This effect is remakable for ^{14}N, in which the undressed RPA calculation is at the limit of breakdown and the ground state energy is unrealistically shifted down to -7.3 MeV. In the hh DRPA calculation, this pathology is not present and the ground state is found at a realistic value.

3.4 Coupling Between Collective Phonons and sp Motion

A deeper insight into the mechanisms that generate the fragmentation pattern can be gained by looking directly at the connection between the spectral function and some specific collective states. To clarify this point we repeated the third iteration using exactly the same input but without replacing the unstable ph 0^+ state, which was instead discarded. The resulting p hole spectral function is shown in the upper panel of Fig. 3.8. In this calculation no breaking of the $p_{3/2}$ peak is obtained. Instead a single peak is found with a spectroscopic factor equal to 0.75 which corresponds to the sum of the two fragments that are obtained when the 0^+ state is taken into account. This result can be interpreted by considering the $p_{3/2}$ fragments as a hole in the ground state and the first excited 0^+ state of the ^{16}O core, respectively. If the latter two levels are close enough to each other in the calculation, a mixing between the two configurations can occur and a second smaller fragment is generated. When the excited 0^+ state is removed from the calculation or, like in the TDA approach, is found far above the experimental energy, the calculation can reproduce only one single peak. Obviously, it is understood from the dressed results of Fig. 3.1 that further improvements have to be made in other to describe properly the strength and the missing energy of the smaller fragments. A candidate to consider in this improvement is the role of the first 2^+ state in ^{16}O, which can also couple to generate $p_{3/2}$ hole fragments but was not included here since it cannot

be obtained by the present ph DRPA calculation, at least not at low enough energy.

The other two low-lying states of ^{16}O that may be of some relevance are the isoscalar 1^- and 3^-. These excitations are reproduced reasonably well by RPA type calculations [26] but are typically found at higher energies than the experimental ones. In the present case the 3^- and 1^- are shifted to even higher values by screening effects, like in the ph DRPA result of Fig 3.5. The lower panels of Fig. 3.8 show the results for the even parity spectral functions that are obtained if the third iteration is repeated while shifting the 3^- alone or both 3^- and 1^- down to their experimental values. In this case, a $d_{5/2}$ hole peak is obtained at low missing energy. This result is also quantitatively more satisfactory that what was obtained in the RPA calculation based on the IPM, since in this case it is found at -17.7 MeV (in agreement with experiment) and with a spectroscopic strength of 0.5%. It is interesting to note that the shifting of the 3^- collective state does not produce any other noticeable change in the theoretical spectral function. The same applies if also the 1^- is shifted.

It appears therefore that the main impediment for further improvements of the description of the experimental hole spectral function is associated with the deficiencies of the RPA (DRPA) description of the excited states. One important problem is the appearance of at most one collective phonon for a given J^π, T combination. Experimentally, several low-lying isoscalar 0^+ and 2^+ excited states are observed at low energy in ^{16}O as well as additional 3^- and 1^- states. A possible way to proceed would be to first concentrate on an improved description of the collective phonons by extending the RPA to explicitly include the coupling to two-particle−two-hole (2p2h) states. Such an extended RPA procedure has been applied in heavier nuclei with considerable success [64, 43]. In order to be relevant for ^{16}O, this approach requires an extension in which the coherence of the 2p2h states is included in the form of the presence of two-phonon excitations. Such contributions arise naturally when the response is calculated by using the Baym-Kadanoff construction of the irreducible ph interaction which is based on a self-consistent treatment of the self-energy [73]. This is will be the topic of Chapter 4, where a first attempt to pursue such calculations is described.

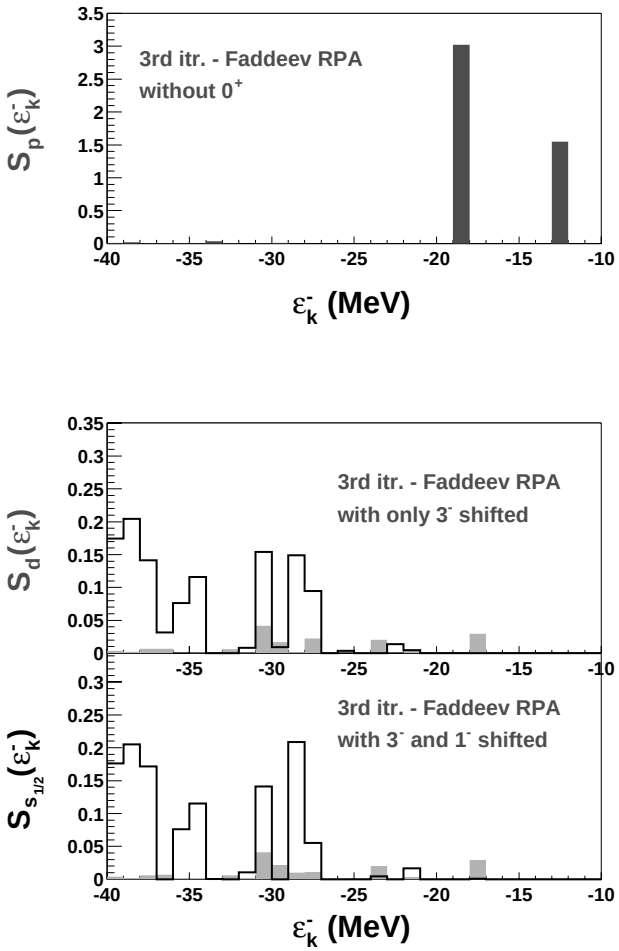

Figure 3.8: One-proton removal strength resulting from repeating the third iteration with a modified ph propagator. The upper panel refers to the results for $\ell = 1$ when the lowest 0^+ state of ^{16}O is excluded. The lower panels give the $\ell = 0$ (thick curve) and $\ell = 2$ (solid bar) results obtained when the 3^- alone or both the 3^- and 1^- states are shifted to their experimental energies.

Chapter 4

Two-phonon Effects in ^{16}O

The results of Chapter 3 demonstrate strong correlations between the excitation spectrum of ^{16}O and its one-hole spectral function, which describes the excitations of the residual $A-1$ nucleus. At the same time the description of the ^{16}O spectrum, as obtained in phDRPA, is not completely satisfactory. While the isoscalar, 3^- and 1^- states can be obtained roughly at the right experimental energies, the 0^+ is found to be highly unstable and the low-lying 2^+ is not reproduced at all. This suggests the presence of correlation effects in the $T = 0$ positive parity channel that are not included in the standard RPA expansion. Obviously, a proper treatment of the ^{16}O core is needed also in order to improve the results for the sp spectral function.

From a shell model point of view, it is well known that the first 0^+ state contains relevant 4p4h holes components [27, 70]. These contributions are accounted for by (D)RPA only in a very partial way and are among the diagrams that suffer from the violation of the Pauli principle (see Fig 2.6). With this consideration in mind, one may not be surprised by the instability of the 0^+ channel and by the fact that the dressing of sp propagators fails to screen the ph interaction in this channel (as one would intuitively expect). In any case, a reliable study of the importance of Pauli violations in isoscalar positive parity states needs to be performed in future work, before any definitive statement can be made. An alternative point of view to this problem was suggested in Ref. [28]. There it is argued that predominant contribution to the low 0^+ and 2^+ states can be understood as a coupling of the negative parity 3^- and 1^- states. Such contributions can indeed generate correctly the quantum number of the rotational band of ^{16}O and of the first 0^+ level. Obviously, this picture is coherent with the above one, since the diagrams that involve couplings of two phonons both contain 2p2h and higher excitations and fix part of the Pauli breaking generated by (D)RPA. The SCGF approach differs from shell model calculations because it is based on the coupling of complete dressed propagators (i.e. states that are already superpositions of several selected npnh configurations).

In this chapter we apply a formalism developed by Baym and Kadanoff to con-

sistently include the effects of two-phonon contributions to the ^{16}O core. This will result in a further extension of the 'Extended RPA' (ERPA) formalism of Refs. [64, 43].

4.1 Beyond phDRPA

4.1.1 Baym-Kadanoff and ERPA

The Bethe-Salpeter equation (2.41) for the ph vertex can be obtained by considering the functional derivatives of the effective action. In particular one can choose to derive directly an equation for the ph propagator, which includes the external legs [43],

$$\begin{aligned}\Pi_{\alpha\beta,\gamma\delta}(t_1,t_2;t_3,t_4) \;&=\; -ig_{\alpha\gamma}(t_1-t_3)g_{\delta\beta}(t_4-t_2) \;+ \\ &-ig_{\alpha\mu}(t_1-t_5)g_{\nu\beta}(t_6-t_1)\; K^{(ph)}_{\mu\nu,\epsilon\rho}(t_5,t_6;t_7,t_8)\; \Pi_{\epsilon\rho,\gamma\delta}(t_7,t_8;t_3,t_4)\;, \qquad (4.1)\end{aligned}$$

where $\Pi(t_1,t_2;t_3,t_4)$ is the obvious generalization of Eq. (2.11) to include the complete dependence on four times.

The ph irreducible vertex $K^{(ph)}$ contains all the 4-point diagrams that cannot be split by cutting a single line. As shown in Ref. [73], this can be derived as a functional derivative of the irreducible self-energy $\Sigma^{\star}$[1]

$$K^{(ph)}_{\alpha\beta,\gamma\delta}(t_1,t_2;t_3,t_4) \;=\; \frac{\delta\;\Sigma^{\star}_{\alpha\beta}(t_1,t_2)}{\delta\;g_{\gamma\delta}(t_3,t_4)}\;. \qquad (4.2)$$

Baym and Kadanoff [73, 74] developed a scheme, based on the above equations, that allows one to construct a conserving approximation to $\Pi(\{t_i\})$ once a particular approximation to the self-energy has been made. They showed that the ph propagator is assured to satisfy the principal conservation laws as long as both g and $K^{(ph)}$ in Eq. (4.1) are derived from the same approximation to the self-energy (by means of the Dyson equation and Eq. (4.2), respectively)[2]. In terms of Feynman diagrams, Eq. (4.2) states that the expansion for $K^{(ph)}$ is obtained by taking every diagram that contributes to the irreducible self-energy and cutting a line in every

[1] The functional derivative with respect to the propagator $g(\tau)$ can be related to the second derivative with respect an the auxiliary field (cf. Eq. (2.2)). Since the self-energy is already obtained as a second derivative of the effective action, Eq. (4.2) is essentially a fourth derivative, i.e. a 4-point irreducible vertex.

[2] Vice versa, the sp propagator g is itself a conserving quantity whenever the corresponding self-energy is obtained, self-consistently, from a proper approximation of the 4-point Green's function [73].

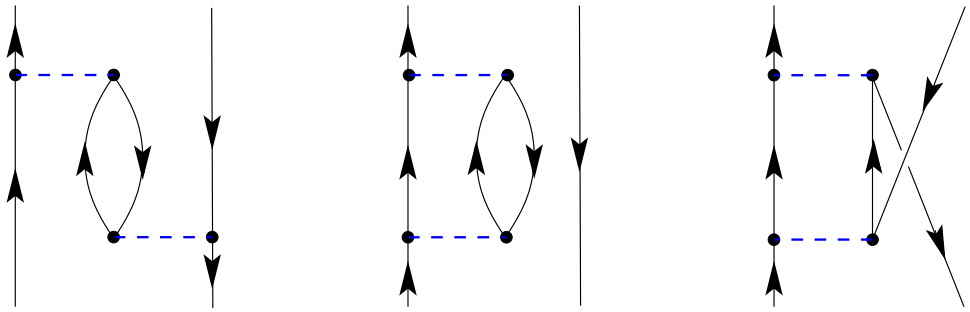

Figure 4.1: Examples of diagrams contributing to the forward-going propagation in standard ERPA. They are referred as screening, self-energy insertion and ladder diagrams, respectively. The last two are related by Pauli exchange of the free hole line with the hole that propagates inside the second-order self-energy term. Note that the Dressed RPA equations automatically account for the effect of the self-energy while completely ignoring the ladder and screening contribution.

possible way. Obviously, substituting the whole Faddeev expansion of Section 2.4 into Eq. (4.2) would result in an unpractically large number of diagrams to be considered. One can still use Eq. (4.2) to derive a set of different approximations to $K^{(ph)}$ that consistently go beyond the RPA approach.

The easiest approach consists in applying Eq. (4.2) to the sole Hartree-Fock contribution (2.21). The result, $K^{(ph)}_{\alpha\beta,\gamma\delta} = V_{\alpha\delta,\beta\gamma}$, is the usual kernel of the (D)RPA equations and leads directly to the formalism discussed in Sections 2.3 and A.1. The immediate extension to the RPA formalism consists in including also the second-order contribution to the self-energy (which is the last diagram of Fig. 1.1). This approach leads to the Extended RPA (ERPA) formalism of Refs. [64, 43, 59]. The interesting feature of ERPA is that it includes diagrams with intermediate 2p2h states and consistently accounts for all the Pauli exchange contributions up to the 2p2h level. Fig. 4.1 gives some examples of diagrams that are included in this

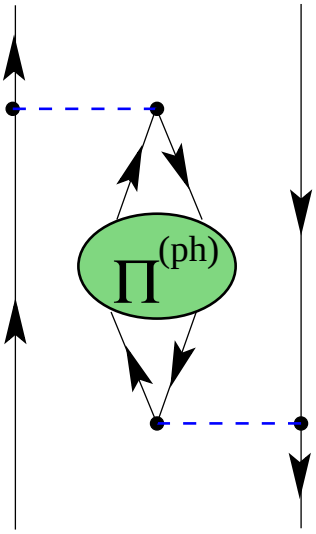

Figure 4.2: The screening of the ph interaction comes from diagrams involving the exchange of a complete phonon.

expansion. Of particular interest is the first one, which represents a contribution to the screening of the ph interaction. It must be noted that this diagram contains only the lowest order contribution. The complete screening would require a series of all order interactions between the additional ph state [55], as shown in Fig. 4.2. This corresponds to allowing the particle and the hole to exchange the phonons of the system. The latter have a low "mass" and therefore can provide a long-range contribution to the residual interaction.

At this level, the ERPA approach accounts for the creation and immediate destruction of 2p2h contributions on top of the normal ph propagation. Contributions of 2p2h type are expected to be relevant in ^{16}O and therefore they should also be allowed to interact to all orders and sustain themselves without being forced

to instantaneously annihilate in a ph state. A further extension of the input to Eq. (4.2) would allow to include part of these contributions. This can be seen by considering a self-energy in which a single ph propagator has been inserted, i.e. the second diagram on the right hand side of Fig.1.1[3]. This approximation was initially suggested in Ref. [28] and results in substituting the intermediate 2p2h state generated by ERPA with two independent ph phonons. The latter propagate simultaneously and are coupled to the simpler ph states by a single interaction. Two possible contributions are shown in Fig. 4.3, in terms of dressed Green's functions. If the two intermediate phonons have been computed using the (D)RPA equations, they will already provide a reasonable description of the lowest isoscalar 3^- and 1^- excited states. These can be sufficient to generate the most important positive parity states. Particularly attractive is the coupling of two 3^- phonons, $3^- \otimes 3^- = 0^+ \oplus 2^+ \oplus 4^+ \oplus 6^+$, that can generate a contribution to the first rotational band of ^{16}O. Couplings involving the 1^- are also expected to give contributions to the low 0^+ and 2^+ states.

It is not difficult to see that different diagrams similar to those in Fig. 4.3 can be obtained through Pauli exchange of the phonon's external lines. In total there are sixteen possible contributions, corresponding to all the possibilities of connecting two phonons to a ph state by means of a single interaction, both in the upper and lower part of the diagram. In the calculations of Section 4.2, we compute all sixteen possibilities and add them to the the forward- and backward-going parts of the phDRPA series. Obviously, both the standard ERPA contributions of Fig. 4.1 and the complete screening, Fig. 4.2, are included in the approximation of Fig. 4.3. Moreover a SCGF approach, based on dressed input Green's function is applied. Thus, the formalism introduced here is an extension of (and goes well beyond) the calculations of Refs. [64, 43, 59, 55]. However, to avoid complications in the notation, we will still refer to it as "Extended RPA" or as "two-phonon ERPA" whenever confusion may arise.

It is worth noting that the inclusion of all the sixteen diagrams of Fig. 4.3 account for the Pauli corrections to the 2p2h states formed by the phonon's external legs. This guarantees the correct properties of the intermediate states that are included into the calculations. Nevertheless, not all the 2p2h Pauli correlations are properly accounted for since no exchange is possible between the lines propagating

[3]The first diagram in Fig.1.1, which is a pp(hh) phonon insertion would lead to other contributions that are similar to those treated in the next section but that are not expected to be as relevant as the present ones. These contributions are not considered in this thesis.

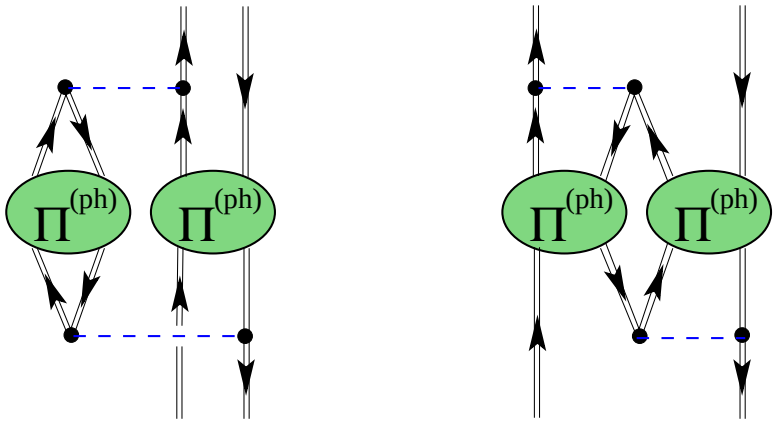

Figure 4.3: Examples of contributions involving the coupling of two independent ph phonons. The first one includes the screening diagram of Fig 4.2. In total, there are sixteen possible diagrams of this type, obtained by considering all the possible coupling to a ph state. The two-phonon ERPA equations (4.6) sum all of them in terms of dressed propagators.

inside the two separate phonons. The situation here is very similar to that of the 2p1h Pauli breaking in the diagrams of Fig. 1.1: to overcome it and to include all the possible correlations one should perform a complete all order summation of 2p2h states, for example by developing 2p2h Faddeev-Yakubovsky formalism. The same expansion would be obtained by employing the 2p1h Faddeev propagator (2.36) in deriving $K^{(ph)}$ from Eq. (4.2). Obviously, such calculations would completely fulfill the requirements of the Baym-Kadanoff formalism but it goes far beyond the scope of the present work and will not be attempted here. Moreover, it is not yet clear, given our present knowledge, whether a massive all order summation of 2p2h diagrams would actually provide a relevant contribution to the spectrum of ^{16}O.

Finally, we observe that the standard ERPA calculations of Refs. [43, 59] were performed by including also diagrams like the second one of Fig. 4.4. These have the

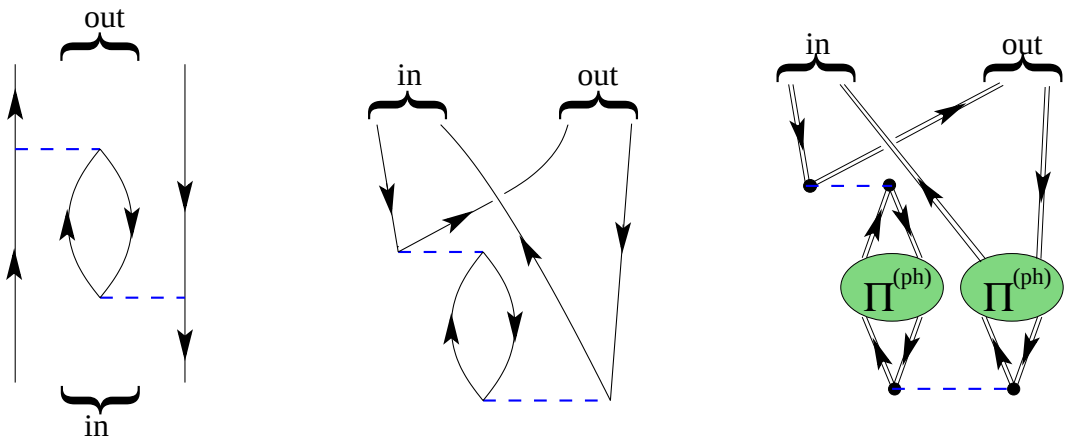

Figure 4.4: Example of direct and time inversion diagrams that appear in the standard ERPA expansion. Both of them come for the same 4-time screening diagram. The last picture shows the corresponding two-phonon extension of the time inversion contribution. Note that the second diagram contributes to the Pauli exchange contribution of Fig. 2.6 d).

property of inverting the direction of propagation in time in the usual RPA fashion. One may note that by combining this diagram with a single ph interaction, the Pauli exchange diagram of Fig. 2.6 d) is reproduced. Thus, time inversion diagrams in ERPA could sensibly reduce the Pauli violations also for 3p3h and higher states. These contributions were not yet included in the calculation described below and will be considered in future work.

4.1.2 Two-phonon Contribution to the ph Propagator

To include the diagrams of Fig. 4.3, we need to perform some further manipulation of Eq. (4.1). As in Section 2.4.3, the main issue is that one needs to reduce the Bethe-Salpeter equation to a form that involves only two-time quantities. in order

to do this, one has to promote the quantum numbers $\{n, k\}$, labelling particle and hole fragments, to external indices. Moreover, it must be observed that reducing the kernel $K^{(ph)}$ to a two-time quantity, a given contribution can generate different types of diagrams according to which time direction is chosen for the incoming and outgoing ph pair. Fig. 4.4 gives an example for the case of the screening diagrams. Therefore, one must consider the two-time diagrams that come from a single 4-time contribution to $K^{(ph)}$ and add them to Eq. (4.1) in a separate way. For our purposes, it is easier to start from the DRPA equation (2.28) and upgrade it to include the diagrams of interests.

In the present chapter we are only interested in including the two-phonon contribution in the forward-, Fig. 4.3, or backward-going time direction. We do not consider the time inversion term other than the one coming from the standard (D)RPA expansion. We start by splitting the free ph propagator (2.27) into its forward- and backward-going part, denoted by $^>$ and $^<$, respectively

$$\Pi^f(\omega) \longrightarrow \Pi^{f\,>}(\omega) \;+\; \Pi^{f\,<}(\omega)\,. \tag{4.3}$$

By performing this substitution in the DRPA equation (2.28) one obtains a similar separation for the complete propagator

$$\Pi(\omega) \longrightarrow \Pi^{>}(\omega) \;+\; \Pi^{<}(\omega)\,, \tag{4.4}$$

where $^>$ and $^<$ now refer to the sense of propagation of the final lines only

$$\begin{aligned} \Pi^{>}(\omega) &= \Pi^{f\,>}(\omega) \;+\; \Pi^{f\,>}(\omega)\; V\; \Pi(\omega) \\ \Pi^{<}(\omega) &= \Pi^{f\,<}(\omega) \;+\; \Pi^{f\,<}(\omega)\; V\; \Pi(\omega)\,. \end{aligned} \tag{4.5}$$

The latter still represent the standard DRPA equations. The last step consists in substituting Eq. (4.4) into (4.5) and adding the two-phonon contributions. The result are the ERPA equations,

$$\begin{aligned} \Pi^{>}(\omega) &= \Pi^{f\,>}(\omega) \;+\; \Pi^{f\,>}(\omega)\; \{(V \;+\; W^{>}(\omega))\,\Pi^{>}(\omega) + V\,\Pi^{<}(\omega)\} \\ \Pi^{<}(\omega) &= \Pi^{f\,<}(\omega) \;+\; \Pi^{f\,<}(\omega)\; \{V\,\Pi^{>}(\omega) + (V \;+\; W^{<}(\omega))\,\Pi^{<}(\omega)\} \end{aligned} \tag{4.6}$$

in which all the four possible time directions of the two-time kernel $K^{(ph)}(\omega)$ – forward backward and the two time inversions– have been separated. The RPA kernel consists of a single interaction V which is the same for all four cases. Thus the (D)RPA equations can also be written in the compact form (2.28). This is no longer true when different contribution, such as $W^{>}(\omega)$ and $W^{<}(\omega)$, are added. In

Eq. (4.6), $W^{>}(\omega)$ represents the contribution of all the sixteen two-phonon diagrams, Fig. 4.3, in the forward direction. $W^{<}(\omega)$ corresponds to the backward-going term.

The details of the formalism needed to solve Eqs. (4.6) are discussed in Appendix A.3. The next section reports on the application of this formalism to ^{16}O.

4.2 Results

The contributions of two-phonon states were first studied by solving the ERPA equation (4.6) with an IPM propagator. This was the same input ansatz to the RPA calculations in Section 3.2.1, i.e. it was constructed from the harmonic oscillator (h.o.) orbitals that form the model space. A G-matrix evaluated at ω=-25 MeV was adopted, consistent with the calculations of Chapter 3. The standard RPA equation was solved first, in order to generate the ph phonons that entered the final calculation. In principle, only the lowest negative parity states of ^{16}O have the right quantum numbers and energies low enough to generate two-phonon contributions relevant for our purposes [28]. Other ph phonons would couple at too high energy and could not mix to form low-lying excitations. Therefore, in the present calculation we have limited the number of intermediate phonons to include only the most relevant ones. For each channel with quantum numbers J^{π} and T (up to angular momenta J=9 were present), we have kept at least the lowest three solution of the IPM/RPA equation. For the isoscalar 0^{+}, 1^{-}, 2^{+} and 3^{-} channels, however, up to five phonons were considered. After coupling these, only the intermediate two-phonon states with energy lower than 25 MeV were selected to be included in $W^{>}(\omega)$ and $W^{<}(\omega)$. This resulted in adding about 35 intermediate two-phonon configurations to each channel in ERPA equation. The excluded contributions are higher in energy and some stability tests showed that no change in the result for low-lying states occurs if these were included.

The same calculation was also performed with a different IPM propagator, obtained by solving the BHF equation, as well as with a dressed propagator as input, respectively.

4.2.1 Results for the Polarization Propagator

The results obtained from the h.o. input propagator are displayed in Fig. 4.5. The isoscalar eigenvalues obtained for energies below 15 MeV are displayed, for both the standard RPA and for the final ERPA calculation. The ERPA calculation produces lower energies for all the levels that are already obtained in RPA. Both

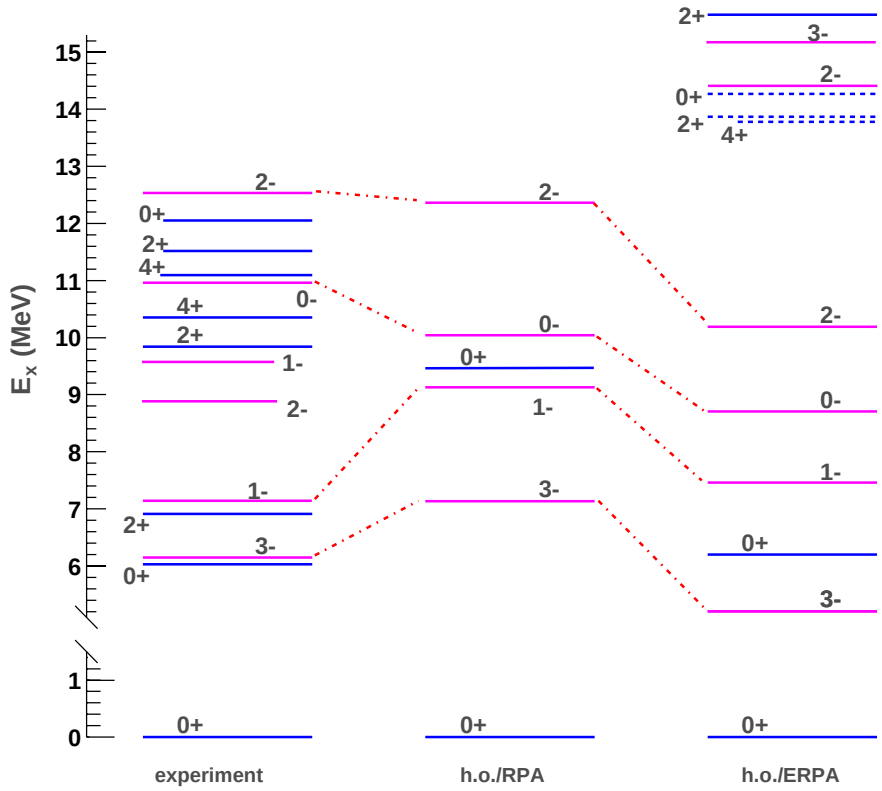

Figure 4.5: Results for the two-phonon ERPA propagator of ^{16}O with an h.o. IPM input propagator, last column. The spectrum in the middle is obtained by solving the standard RPA problem and is employed to generate two-phonon contributions to the ERPA equation. Note that these intermediate RPA results have already been discussed in Section 3.3.1. The excited states indicated by dashed lines are those for which the (E)RPA equation predicts a total spectral strength Z_{n_π} lower than 10%. The first column reports the experimental results.

3^-, 0^- and 2^- are shifted below the experiment by 1 MeV or more. The latter feature looks rather attractive since the dressing of the sp propagator, which has the effect to rise their eigenvalues, has not been taken into account. Moreover, the first 0^+ moves roughly to the right experimental energy. This appears to be rather fortuitous. Still, the fact that the correction for this case is as large as 3.5 MeV shows that correlations between ph and two-phonon states are possible and go in the right direction.

It is also worth considering the total ph spectral strength for a given state, that is obtained by summing over all the corresponding amplitudes, Eq. (A.20), as

$$Z_{n_\pi} \;=\; \sum_{\alpha\beta} \left| \mathcal{Z}^{n_\pi}_{\alpha\beta} \right|^2 \,. \tag{4.7}$$

Results for both the excitation energy and Z_{n_π} of the principal levels in Fig. 4.5 are given in Table 4.1. Note that Z_{n_π} is substantially bigger than one for the 3^- and 0^+ states and that it raises further for the ERPA results. This signals an increase of the collective character for these solutions. The ERPA equation generates a triplet of states at about 14 MeV, with quantum numbers 0^+, 2^+ and 4^+. However, their ph spectral strength is found to be very small. This indicates that these levels contain small admixtures of ph states and are almost exclusively bare two-phonon contributions. Also note that their quantum numbers and their energies correspond to those obtained by coupling two 3^- RPA phonons at 7.14 MeV. Experimentally, the first 2^+ is found at a lower energy and spectral strength for these states is known to have relevant ph components [75]. Thus the lack of mixing between ph and the other configurations is quite unsatisfactory. Very small spectral strength is found for most of the states that are not reproduced by standard RPA.

A second approximation for an IPM propagator was obtained by solving the Brueckner-Hartree-Fock equations including the energy dependence of the G-matrix. These results were employed as input to new RPA and two-phonon ERPA calculations. The principal eigenvalues are also shown in Table. 4.1. In general, the results of the ERPA equation agree with the case of an h.o. input. The principal negative parity levels are shifted down of about 1 MeV. A 0^+, 2^+ and 4^+ triplet is generated at twice the energy of the RPA 3^- phonon. These have a marked two-phonon character and fail to mix with ph contributions. In this case, the latter 0^+ appears to be a little more collective since it if found about 1 MeV below its partners and has a total strength of $Z_{0^+_2}$=0.197. Note that for the BHF propagator the standard RPA calculation is no longer able to reproduce a low-lying 0^+ state. Also, the low 3^- and 1^- levels are found a little higher in energy (about 1 MeV) with respect

$T=0$	h.o./RPA		h.o./ERPA		BHF/RPA		BHF/ERPA	
J^π	ε_{n_π}	Z_{n_π}	ε_{n_π}	Z_{n_π}	ε_{n_π}	Z_{n_π}	ε_{n_π}	Z_{n_π}
0^+	–	–	–	–	21.36	1.005	–	–
4^+			13.63	0.029			16.97	0.021
2^+			13.87	0.062			16.93	0.033
0^+			14.27	0.100			16.43	0.196
1^-	9.13	1.027	7.46	0.997	10.44	1.002	9.86	0.998
3^-	7.14	1.258	5.21	1.367	8.33	1.008	7.87	1.113
0^+	9.46	1.582	6.20	1.621	–	–	–	–

Table 4.1: Excitation energy and total spectral strengths obtained for the principal solutions of RPA and ERPA equations. Both the h.o. and BHF cases are displayed.

to the h.o. results. This is expected since the Hartree-Fock approximation tend to lower the ground state energy but not necessarily the energies of the excited states. This effect results in shifting the whole spectrum upward. Still, the behavior of the 0^+ state is strange and not well understood.

Similar results have been obtained by employing a dressed input propagator. Fig. 4.6 and Table 4.2 show the solution of the DRPA and ERPA obtained by using the output of the third iteration of Section 3.2. The principal negative parity isoscalar states are shifted down in energy, as expected, but the improvement is by less than 1 MeV. The low 3^- and 1^- levels remain above the their experimental energy at 8.74 and 9.92 MeV, respectively. At the same time a larger number of excited states is generated above 10 MeV. Most of them have two-phonon character and do not mix with ph states, as it would be required in order to generate the most relevant low lying states. The coupling of two low 3^- phonons of ^{16}O produces an almost degenerate triplet of states at around 16 MeV, which is twice the original phonon's energy. The instability of the 0^+ state appears in the two-phonon ERPA as well and no improvement is obtained.

The ERPA results for an h.o. input look very promising, since they give sizable corrections to several energy levels. However, this improvement tends to become negligible in the successive calculations. Presumably this happens because a sizable part of correlations, which in the first case are introduced by ERPA, are already accounted for by the BHF term (3.1) and the dressing of the input propagator. Nev-

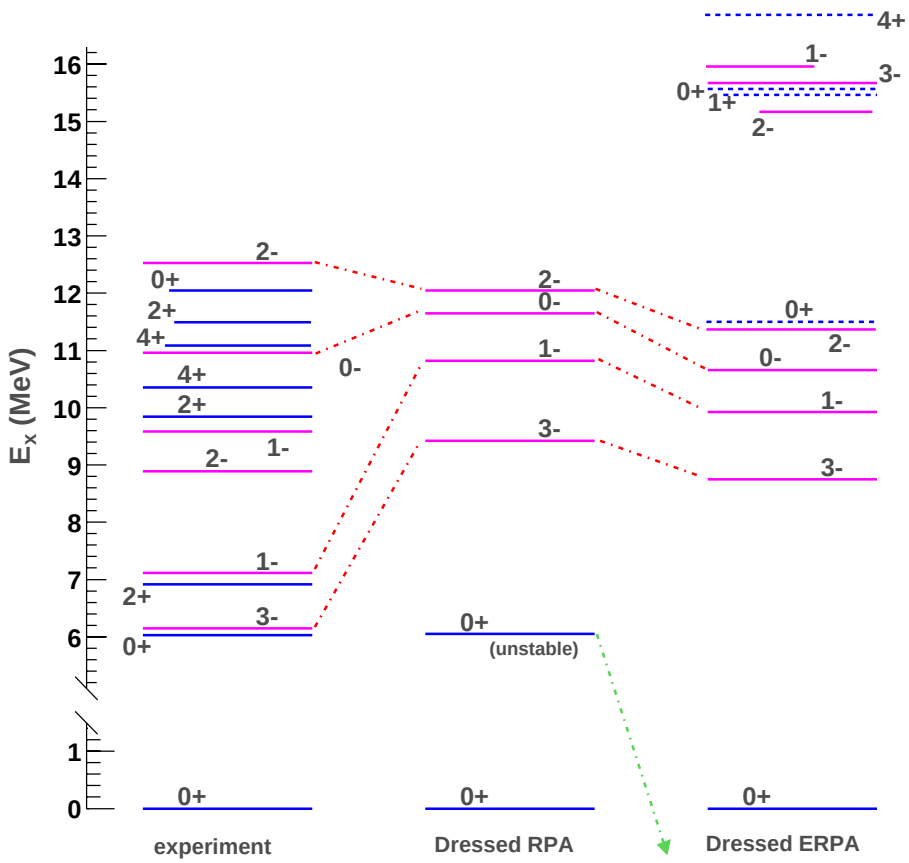

Figure 4.6: Results for the two-phonon ERPA propagator of ^{16}O with a dressed input propagator, last column. The spectrum in the middle is obtained by solving the standard DRPA, as in Section 3.3.1, and it is employed to generate two-phonon contributions to the ERPA equation. The excited states indicated by dashed lines are those for which the (E)RPA equation predicts a total spectral strength Z_{n_π} lower than 10%. The first column reports the experimental results.

$T=0$	3rd itr./DRPA		3rd itr./ERPA	
J^π	ε_n^π	Z_{n_π}	ε_n^π	Z_{n_π}
2^+			16.02	0.038
0^+			15.54	0.002
0^+			11.41	0.021
1^-	10.81	0.729	9.92	0.690
3^-	9.42	0.765	8.74	0.740
0^+	6.05	1.829	*unst.*	∞

Table 4.2: Excitation energy and total spectral strengths obtained for the principal solutions of RPA and ERPA equations. A dressed propagator has been employed.

ertheless it is clear that the DRPA do not completely solve the problem of ^{16}O [26] and that other correlation effects have to be present. Two-phonon contributions properly account for configurations at the 2p2h and higher level and therefore are expected to have some relevance. Although the results obtained for the lowest excited states are not attractive enough for the case of a dressed input propagator, it must be recognized that the ERPA calculation does represent an important step forward. Indeed the coupling of ph phonons allows one to generate a set of low lying states with quantum numbers that could not be obtained in the standard (D)PRA approach. This had not been achieved before. Obviously, the missing feature in the above calculation is the ability of mixing effectively ph and two-phonons states. Once this issue can be solved, improved results will be obtained from the ERPA approach.

As mentioned above, shell-model calculations require up to $4\hbar\omega$ contributions to properly generate the spectrum of ^{16}O. These surely involve 3p3h contributions that can be generated starting from the model space employed in the present work. Accordingly, time inversion diagrams of the type shown in Fig. 4.4 should be taken into account as well, since they properly make up for the effects of Pauli correlations at the 3p3h level [43]. Also, $4\hbar\omega$ components are seen to importance in allowing a coupling between different low energy contributions [70]. These would involve simple ph excitations in which a nucleon is brought up to states that are not included in the present work (6 major shells should be required). This suggest that an extension of the model space employed here, to include one more p and sd shells, may introduce

significant contributions to the interaction between ph and two-phonon terms. This may be the origin of the lack of mixing between these states and future work should address this problem [67].

It is worth nothing that other extensions of this formalism to include more than two intermediate phonons and/or to properly sum them to all orders in a Faddeev-Yakubovsky fashion do not appear to be relevant at present.

Chapter 5

Conclusions

The present theoretical description of the distribution of spectroscopic strength at low energies lacks important ingredients for a successful comparison with experimental data. One of these ingredients is a proper description of the coupling of sp motion to low-lying collective modes that are present in the system. Recent calculations for ^{16}O [19], for example, only include a TDA description of these collective modes. A new method has been proposed here to study the influence of pp and ph RPA correlations on the sp propagator for a system with a finite number of fermions. This method is formulated in the context of SCGF theory by evaluating the nucleon self-energy in terms of the 2p1h and 2h1p propagators. The description of the 2p1h (or 2h1p) excitations has been studied by using the Faddeev formalism, which is usually applied to solve the three-body problem. The Faddeev formalism is necessary since we consider the collective pp and ph RPA phonons as the basic building blocks to describe the 2p1h motion.

In deriving the set of Faddeev equations a formulation has been chosen which involves only a single diagonalization for the 2p1h fragments. The appearance of spurious solutions has also been discussed in some detail, showing that the inclusion of the contribution of certain diagrams is necessary to separate such spurious solutions from the physically meaningful ones. When this separation occurs, it is straightforward to project out the physical eigenstates from the Faddeev equations, thereby eliminating the spurious ones.

The computational scheme presented here employs only two-time propagators, thus leading to a tractable set of equations. At the same time the contributions of pp and ph RPA phonons have been consistently summed to all orders thereby including the physical effects that appear to be relevant for the study of the ^{16}O nucleus. Unlike previous calculations in which ph phonons have been included, the present formalism takes the Pauli-exchange correlations properly into account up to the 2p1h level.

This formalism has been applied to study 2h1p correlations at small missing

energies for the nucleus of ^{16}O. The application of the Faddeev method has allowed for the first time the treatment of the coupling of ph and hh collective modes within an RPA framework and to all orders in the nucleon self-energy. At first, the effects of including RPA correlations were studied for an input IPM propagator. The resulting spectral function shows a improvement of the absolute spectroscopic factors of about 3-4%, with respect to the TDA results. This is in better agreement with experimental data than all previous calculations. Additional encouraging results are obtained in the form of low-lying positive parity fragments. Fragmentation effects were then included by recalculating the RPA phonons using the so-obtained dressed sp propagator and iterating the procedure. The results show that substantial self-consistency can be reached already after a few iterations. The inclusion of fragmentation in the phonons leads to the appearance of an additional $p_{3/2}$ fragment at low energy, in agreement with experiment. At the same time screening effects tend to raise again the spectral strength of the $p_{1/2}$ fragment. The final values for the absolute spectroscopic factors are 72.5% for the $p_{3/2}$ quasihole and 77.5% for $p_{1/2}$. Other features, like the presence of positive parity $5/2^+$ and $1/2^+$ holes at -17 MeV, cannot be obtained when the present calculations are iterated.

In general the compensation between fragmentation and RPA effects leaves the theoretical results for the spectroscopic factors about 10-15% far from the experiment [45]. This indicates that further correlations at low energy are required to achieve a complete description of the experiment.

At the same time, the dressing of nucleons in the medium is seen to be crucial in determining the fragmentation pattern itself. The calculations have further identified the important role played by the low-lying ph states of ^{16}O. The low-lying 0^+ appears to be at least partially responsible for the splitting of the $p_{3/2}$ strength at low energy, whereas the low-lying 3^- state plays a decisive role in the presence of $d_{5/2}$ strength at low energy. The results for the spectral function are therefore very sensitive to the quality of the RPA (DRPA) description of the ph spectrum. It is well known that this description is as yet unsatisfactory but key ingredients for further improvements can be identified through the Baym-Kadanoff procedure based on self-consistent propagators. We therefore conclude that the present results show that further improvement in the understanding of the low-energy fragmentation can be gained by reproducing all the lowest ph collective modes. As a first step in this direction, we have developed an extension of the RPA formalism that accounts for contributions in which two ph phonons propagate at the same time. The results for ^{16}O show that two-phonon coupling actually reproduces a series of low-lying states

with quantum numbers that are observed experimentally. Though, the present approximation fails to describe the proper mixing between ph and two-phonon states. Further work is needed to address this point.

The Faddeev formalism employed here allows to include specific correlations corresponding to pp and ph phonons in a natural way. Extensions to the inclusion of more complicated excitations like the extended DRPA [59] and two-phonon contributions can be obtained in a convenient way by starting from the formalism presented in Section. 2.4 and Appendix B.

Appendix A

(E)RPA Formalism for Dressed Propagators

A.1 Dressed RPA Equation for the Kernel of Faddeev Equations

It is useful to give the explicit results for the DRPA appromation of the Faddeev kernels (2.40) and (2.41) as well as the normalization and closure relation satisfied by their solutions. This also allows to introduce the notation used in appendix B to discuss the Faddeev formalism. Only the pp-DRPA case is discussed here as an example. The ph-DRPA case is completely analogous.

The pp-DRPA approximation to the matrix $\tilde{\Gamma}^{(pp)}$ is obtained by choosing $K^{(pp)}_{\alpha\beta,\gamma\delta} = V_{\alpha\beta,\gamma\delta}$ in (2.40) and is shown in Fig. A.1. This equation is completely equivalent to (2.30) and the solutions of the two are trivially related by cutting the external legs of $g^{II}_{(D)RPA}(\omega)$. This can be easily seen by looking at both the diagrammatic form of the equations, shown in Figs. 2.7 and A.1, respectively. From these it is also evident that the following relation between $\tilde{\Gamma}^{(pp)}$ and g^{II}

$$\tilde{\Gamma}^{(pp)}_{\alpha\beta,\gamma\delta}(\omega) \;=\; V_{\alpha\beta,\gamma\delta} \;+\; \frac{1}{4}\, V_{\alpha\beta,\mu\nu}\; g^{II}_{\mu\nu,\epsilon\rho}(\omega)\; V_{\epsilon\rho,\gamma\delta}\;, \tag{A.1}$$

is valid in the DPRA case. By substituting Eq.(2.14) into (A.1), one obtains the following Lehmann representation for $\tilde{\Gamma}^{(pp)}(\omega)$

$$\begin{aligned}
\tilde{\Gamma}^{(pp)}_{\mu\nu,\alpha\beta}(\omega) \;&=\; V_{\mu\nu,\alpha\beta} \;+\; \sum_{n+} \frac{\left(\Delta^{n+}_{\mu\nu}\right)^{*}\, \Delta^{n+}_{\alpha\beta}}{\omega - \varepsilon^{\Gamma+}_{n+} + i\eta} \;-\; \sum_{k-} \frac{\Delta^{k-}_{\mu\nu}\, \left(\Delta^{k-}_{\alpha\beta}\right)^{*}}{\omega - \varepsilon^{\Gamma-}_{k-} - i\eta}\;, \\
&\equiv\; V_{\mu\nu,\alpha\beta} \;+\; \Delta\tilde{\Gamma}^{>}_{\mu\nu,\alpha\beta}(\omega) \;+\; \Delta\tilde{\Gamma}^{<}_{\mu\nu,\alpha\beta}(\omega)
\end{aligned} \tag{A.2}$$

in which $n+$ ($k-$) label the forward-going (backward-going) contributions and the following convention has been used to represent the excitation energies and spectroscopic amplitudes, in analogy to Eqs. (2.5)

$$\begin{aligned}
\Delta^{n+}_{\alpha\beta} \;&\equiv\; \langle \Psi^{A+2}_{n+} | c^{\dagger}_{\mu} c^{\dagger}_{\nu} | \Psi^{A}_{0} \rangle \frac{1}{2} V_{\mu\nu,\alpha\beta}\;, \\
\Delta^{k-}_{\alpha\beta} \;&\equiv\; V_{\alpha\beta,\mu\nu} \frac{1}{2} \langle \Psi^{A-2}_{k-} | c_{\mu} c_{\nu} | \Psi^{A}_{0} \rangle\;,
\end{aligned}$$

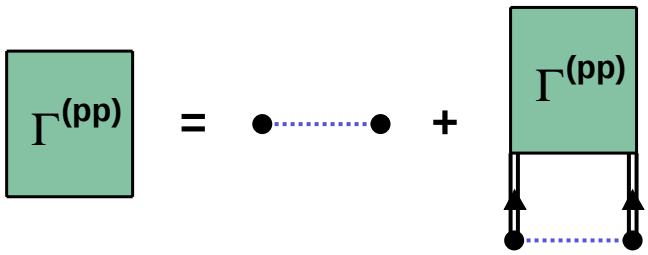

Figure A.1: DRPA equation for the $\tilde{\Gamma}^{(pp)}$ matrix. No implicit time direction is assumed in this diagram.

$$\begin{aligned} \varepsilon^{\Gamma+}_{n+} &\equiv E^{A+2}_{n+} - E^{A}_{0} \,, \\ \varepsilon^{\Gamma-}_{k-} &\equiv E^{A}_{0} - E^{A-2}_{k-} \,. \end{aligned} \tag{A.3}$$

Using the Lehmann representation (A.2) and extracting the poles $\varepsilon^{\Gamma+}_{n+}$ $(\varepsilon^{\Gamma-}_{k-})$ from the DRPA equation, one obtains the usual eigenvalue problem

$$\Delta^{n+(k-)}_{\alpha\beta} = \Delta^{n+(k-)}_{\gamma\delta} \; g^{(0)}_{\gamma\delta,\epsilon\rho}(\omega) \; \tfrac{1}{2} \; V_{\epsilon\rho,\alpha\beta}\Big|_{\omega=\varepsilon^{\Gamma+}_{n+} \; (\varepsilon^{\Gamma-}_{k-})} \,. \tag{A.4}$$

which can be derived either by starting from Eq. (2.30) or from the formulation of Fig. A.1.

The normalization condition is obtained as usual by considering the term of order zero in the above expansion. To state the result, it is useful to introduce the following quantities, that appear directly in the form (B.7) of the Faddeev equations,

$$U^{n+}_{n_1,n_2} = \frac{\mathcal{X}^{n_1}_{\alpha}\mathcal{X}^{n_2}_{\beta} \; \left(\Delta^{n+}_{\alpha\beta}\right)^*}{\sqrt{2}\,\left(\varepsilon^{\Gamma+}_{n+} - \varepsilon^{+}_{n_1} - \varepsilon^{+}_{n_2}\right)} \,, \tag{A.5}$$

$$H^{k-}_{n_1,n_2} = \frac{\mathcal{X}^{n_1}_{\alpha}\mathcal{X}^{n_2}_{\beta} \; \Delta^{k-}_{\alpha\beta}}{\sqrt{2}\,\left(\varepsilon^{\Gamma-}_{k-} - \varepsilon^{+}_{n_1} - \varepsilon^{+}_{n_2}\right)} \,, \tag{A.6}$$

$$J^{n+}_{k_1,k_2} = \frac{\left(\mathcal{Y}^{k_1}_{\alpha}\mathcal{Y}^{k_2}_{\beta} \; \Delta^{n+}_{\alpha\beta}\right)^*}{\sqrt{2}\,\left(\varepsilon^{\Gamma+}_{n+} - \varepsilon^{-}_{k_1} - \varepsilon^{-}_{k_2}\right)} \,, \tag{A.7}$$

$$V^{k-}_{k_1,k_2} = \frac{\left(\mathcal{Y}^{k_1}_{\alpha}\mathcal{Y}^{k_2}_{\beta}\right)^* \; \Delta^{k-}_{\alpha\beta}}{\sqrt{2}\,\left(\varepsilon^{\Gamma-}_{k-} - \varepsilon^{-}_{k_1} - \varepsilon^{-}_{k_2}\right)} \,. \tag{A.8}$$

These expressions represent the generalization to dressed propagators of the usual RPA components (the $\sqrt{2}$ has been inserted only in the pp case for convenience). In Eq. (A.5-A.8) the quantities $\mathcal{X}$ ($\mathcal{Y}$) and ε_n^+ (ε_k^-) represent the spectroscopic amplitudes and the poles of the forward-going (backward-going) part of the one-body propagator, Eqs. (2.5), while $\varepsilon_{n+(k-)}^{\Gamma+(-)}$ are the eigenvalues of the DRPA equation (A.4).

The normalization condition for the DRPA solutions, given in terms of the components (A.5-A.8), is the generalization of the normalization for the usual RPA [58] and can be put in matrix notation as

$$\begin{bmatrix} U^\dagger & J^\dagger \\ H^\dagger & V^\dagger \end{bmatrix} \begin{bmatrix} I & \\ & -I \end{bmatrix} \begin{bmatrix} U & H \\ J & V \end{bmatrix} = \begin{bmatrix} I & \\ & -I \end{bmatrix} , \tag{A.9}$$

while the closure relations are given by

$$\begin{bmatrix} U & H \\ J & V \end{bmatrix} \begin{bmatrix} I & \\ & -I \end{bmatrix} \begin{bmatrix} U^\dagger & J^\dagger \\ H^\dagger & V^\dagger \end{bmatrix} = \frac{1}{2} \begin{bmatrix} I - I^{ex} & \\ & I^{ex} - I \end{bmatrix} , \tag{A.10}$$

where U, H, J and V are the matrices containing the elements of Eqs. (A.5-A.8) and $\{n_1, n_2\}$ ($\{k_1, k_2\}$) and $\{n+\}$ ($\{k-\}$) label the row and column indices, respectively. In dealing with the formalism for the Faddeev equations, it is also useful to introduce the following two matrices:

$$T_{n_1,n_2}^{n+} = \frac{1}{\sqrt{2}} \mathcal{X}_\alpha^{n_1} \mathcal{X}_\beta^{n_2} \left(\Delta_{\alpha\beta}^{n+}\right)^* , \tag{A.11}$$

$$W_{k_1,k_2}^{k-} = \frac{1}{\sqrt{2}} \left(\mathcal{Y}_\alpha^{k_1} \mathcal{Y}_\beta^{k_2}\right)^* \Delta_{\alpha\beta}^{k-} . \tag{A.12}$$

which are trivially related to the components (A.5) and (A.8).

The matrix elements given in Eqs. (A.5-A.8) and (A.11-A.12) correspond to the matrices $H^{(3)}$, $U^{(3)}$, and $T^{(3)}$ introduced after Eq.(B.7) for the 2p1h Faddeev expansion (J, V, and W being the corresponding ones for the 2h1p expansion).

A.2 Interaction Boxes

The $\tilde{\Gamma}^{(pp)}$ matrix (2.40) obtained by solving the DRPA equation has the Lehmann representation given in Eq. (A.2). In obtaining the $\Gamma^{(3)}$ vertex given by Eq. (2.39) one needs to keep both the forward- and backward-going terms of (A.2). This implies that all three diagrams of Fig. 2.10 must be included. The main problem

encountered when working with dressed propagators is that the contribution of these three diagrams do not factorize in an expression of the form $G^{0>}\Gamma G^{0>}$ when $G^{0>}$ is represented by a propagator of the form

$$G^{0>}_{\mu\nu\lambda,\alpha\beta\gamma}(\omega) \;=\; \sum_{n_1,n_2,k} \frac{\left(\mathcal{X}^{n_1}_{\mu}\mathcal{X}^{n_2}_{\nu}\mathcal{Y}^{k}_{\lambda}\right)^{*}\;\mathcal{X}^{n_1}_{\alpha}\mathcal{X}^{n_2}_{\beta}\mathcal{Y}^{k}_{\gamma}}{\omega-(\varepsilon^{+}_{n_1}+\varepsilon^{+}_{n_2}-\varepsilon^{-}_{k})+i\eta}\;, \tag{A.13}$$

This factorization cannot be made because of the implicit sums over the particle and hole excitation indices (n, n', k) in Eq. (A.13). For example, the hole label k cannot change in Fig. 2.10 [29, 59, 76].

This difficulty can be overcome with a slight reformulation of the problem. We no longer regard $\Gamma^{(3)}$ and $G^{0>}$ only as functions of the model space indices (α, β, γ), but instead assign an additional dependence on the particle and hole indices. Thus promoting the (n, n', k) quantum numbers to external indices, the Lehmann representation of $G^{0>}$ (2.43) will contain at most one pole for every matrix element. As a consequence, all the components (2.33-2.35) appearing in the Faddeev equations have to be reformulated in the same way. The original propagators can then be retrieved at the end by summing the solutions over all the particle and hole fragments. With this procedure it becomes possible to write the sum of the three diagrams in Fig. 2.10 in terms a matrix product of two $G^{0>}$ (2.43) propagators and the following vertex

$$\begin{aligned}\Gamma^{(3)}_{\mu n_\mu \nu n_\nu \lambda k_\lambda,\alpha n_\alpha \beta n_\beta \gamma k_\gamma}(\omega) \;=\; & \tfrac{1}{2}\frac{\delta_{k_\lambda,k_\gamma}}{\sum_\sigma \left|\mathcal{Y}^{k_\lambda}_{\sigma}\right|^2} \\ \times\; \Bigg\{ & V_{\mu\nu,\alpha\beta} \;+\; \sum_{n+} \frac{\left(\Delta^{n+}_{\mu\nu}\right)^{*}\Delta^{n+}_{\alpha\beta}}{\omega-(\varepsilon^{\Gamma+}_{n+}-\varepsilon^{-}_{k_\lambda})+i\eta} \\ & +\; \sum_{k-} \frac{\left[\omega-\varepsilon^{+}_{n_\mu}-\varepsilon^{+}_{n_\nu}-\varepsilon^{+}_{n_\alpha}-\varepsilon^{+}_{n_\beta}+\varepsilon^{-}_{k_\lambda}+\varepsilon^{\Gamma-}_{k-}\right]\Delta^{k-}_{\mu\nu}\left(\Delta^{k-}_{\alpha\beta}\right)^{*}}{(\varepsilon^{\Gamma-}_{k-}-\varepsilon^{+}_{n_\mu}-\varepsilon^{+}_{n_\nu})(\varepsilon^{\Gamma-}_{k-}-\varepsilon^{+}_{n_\alpha}-\varepsilon^{+}_{n_\beta})} \Bigg\}\;,\end{aligned} \tag{A.14}$$

which corresponds to the expression for the pp interaction box (2.39). With this prescription, we are able to write an expansion that sums diagrams like those of Fig 2.10. This is achieved at the cost of an increased size of the matrices to be dealt with. After further manipulation, it is possible to avoid this complication by dropping the dependence on the model space indices $(\alpha,\ \beta,\ \gamma)$, as explained in Sec. B.1. The expressions for the ph interaction boxes $\Gamma^{(1)}$ and $\Gamma^{(2)}$ are derived in a completely analogous way.

A.3 Extended DRPA Equation with Two-phonon Contributions

In this work, the Extended DRPA calculation of Chapter 4 represents the most sophisticated approach to the Bethe-Salpeter Eqs.(4.1) and (2.40-2.41). For this reason it is helpful to give specific details on the formalism employed in solving Eq. (4.6). This will also help to complete the description of the standard DRPA outlined in Section A.1, as well as giving the details on how the 2p1h Faddeev kernels have been extended to include the solutions from ERPA.

In this appendix, we discuss the general case, where also time inversion diagrams, like the ones in Fig. 4.4, are included. Thus, the ERPA equations are given by

$$\begin{aligned}
\Pi^{>}(\omega) &= \Pi^{f\ >}(\omega) \ + \\
&\quad \Pi^{f\ >}(\omega) \ \{(V \ + \ W^{>}(\omega))\,\Pi^{>}(\omega) + (V \ + \ H^{>,<})\,\Pi^{<}(\omega)\} \\
\\
\Pi^{<}(\omega) &= \Pi^{f\ <}(\omega) \ + \\
&\quad \Pi^{f\ <}(\omega) \ \{(V \ + \ H^{<,>})\,\Pi^{>}(\omega) + (V \ + \ W^{<}(\omega))\,\Pi^{<}(\omega)\}
\end{aligned} \tag{A.15}$$

where the time inversion kernels $H^{>,<}$ and $H^{<,>}$ do not depend on energy.

The separation of the propagators $\Pi^{f}(\omega)$ and $\Pi(\omega)$ into forward and backward components is a consequence of adopting the prescription of Section A.2. Indeed particle and hole external lines turn into each other by time inversion and become quantities that depend on different quantum numbers due to the introduction of fragmentation indices $\{n, k\}$. For this reason, Eqs. (4.3) and (4.4) are only formal relations and the arrow can be substituted by an equal sign only after having summed over all the fragments. The free polarization propagator (2.27) naturally splits in two components that are purely forward and backward-going. The relevant Lehmann representations are

$$\begin{aligned}
\Pi^{f\ >}_{\alpha n_\alpha \beta k_\beta, \gamma n_\gamma \delta k_\delta}(\omega) &= \delta_{n_\alpha, n_\gamma}\delta_{k_\beta, k_\delta}\,\frac{\left(\mathcal{X}^{n_\alpha}_{\alpha}\mathcal{Y}^{k_\beta}_{\beta}\right)^{*}\ \mathcal{X}^{n_\alpha}_{\gamma}\mathcal{Y}^{k_\beta}_{\delta}}{\omega - \left(\varepsilon^{+}_{n_\alpha} - \varepsilon^{-}_{k}\right) + i\eta} \\
&\equiv G^{\dagger}\,\frac{1}{\omega - D + i\eta}\,G \ , \\
\\
\Pi^{f\ <}_{\alpha k_\alpha \beta n_\beta, \gamma k_\gamma \delta n_\delta}(\omega) &= -\,\delta_{k_\alpha, k_\gamma}\delta_{n_\beta, n_\delta}\,\frac{\mathcal{Y}^{k_\alpha}_{\alpha}\mathcal{X}^{n_\beta}_{\beta}\ \left(\mathcal{Y}^{k_\alpha}_{\gamma}\mathcal{X}^{n_\beta}_{\delta}\right)^{*}}{\omega + \left(\varepsilon^{+}_{n_\beta} - \varepsilon^{-}_{k_\alpha}\right) - i\eta}
\end{aligned} \tag{A.16}$$

$$\equiv \quad (G^*)^\dagger \, \frac{-1}{\omega + D - i\eta} \, G^* \quad , \tag{A.17}$$

where no summation is implied and a shorter notation for the unperturbed poles and residues has been introduced. The numbers D and G can be thought as matrices whose elements contain all the unperturbed poles and residues, respectively. Note that in this case D is diagonal and depends on the fragmentation indices $\{n, k\}$ only, while G is rectangular because its column indices also depend on the model space orbitals $\{\alpha\}$.

A little more complicated is the separation of the complete propagator (4.4), which involves the time direction of the outgoing lines. Since the RPA series contains contributions that can invert the sense of propagation of the ph diagrams, both forward and backward poles can appear in each component

$$\Pi^{>}_{\alpha n_\alpha \beta k_\beta, \gamma\delta}(\omega) \;=\; \sum_{n\neq 0} \frac{\left(\mathcal{Z}^{>\;n}_{\alpha n_\alpha \beta k_\beta}\right)^* \; \mathcal{Z}^n_{\gamma\delta}}{\omega - \varepsilon^\pi_n + i\eta} \;-\; \sum_{n\neq 0} \frac{\mathcal{Z}^{<\;n}_{\beta k_\beta \alpha n_\alpha} \; \left(\mathcal{Z}^n_{\gamma\delta}\right)^*}{\omega - \varepsilon^\pi_n - i\eta} \;, \tag{A.18}$$

$$\Pi^{<}_{\alpha k_\alpha \beta n_\beta, \gamma\delta}(\omega) \;=\; \sum_{n\neq 0} \frac{\left(\mathcal{Z}^{<\;n}_{\alpha k_\alpha \beta n_\beta}\right)^* \; \mathcal{Z}^n_{\gamma\delta}}{\omega - \varepsilon^\pi_n + i\eta} \;-\; \sum_{n\neq 0} \frac{\mathcal{Z}^{>\;n}_{\beta n_\beta \alpha k_\alpha} \; \left(\mathcal{Z}^n_{\gamma\delta}\right)^*}{\omega + \varepsilon^\pi_n - i\eta} \;, \tag{A.19}$$

where the obvious convention (see Eq. (2.12))

$$\begin{aligned} \mathcal{Z}^n_{\alpha\beta} \;&\equiv\; \langle \Psi^A_n | c^\dagger_\alpha c_\beta | \Psi^A_0 \rangle \;, \\ \varepsilon^\pi_n \;&\equiv\; E^A_n - E^A_0 \;, \end{aligned} \tag{A.20}$$

has been used.

In Eqs. (A.18) and (A.19) the spectroscopic amplitude splits in two contributions $\mathcal{Z}^>$ and $\mathcal{Z}^<$. These appears unchanged in both equations due to the time inversion symmetries obeyed by the ph states. In terms of the above definitions, Eq. (4.4) can be stated explicitly by applying the summation prescription of Sec. A.2

$$\mathcal{Z}^n_{\alpha\beta} \;=\; \sum_{n_1,k_2} \left[\mathcal{Z}^{>\;n}_{\alpha n_1 \beta k_2} + \mathcal{Z}^{<\;n}_{\alpha k_2 \beta n_1} \right] \;, \tag{A.21}$$

$$\Pi^{>}_{\alpha\beta,\gamma\delta}(\omega) \;=\; \sum_{n_1,k_2} \left[\Pi^{>}_{\alpha n_1 \beta k_2, \gamma\delta}(\omega) + \Pi^{<}_{\alpha k_2 \beta n_1, \gamma\delta}(\omega) \right] \;. \tag{A.22}$$

The contribution of two-phonon diagrams are

$$\begin{aligned} W^{>}_{\alpha n_\alpha \beta k_\beta, \gamma n_\gamma \delta k_\delta}(\omega) \;&=\; \sum_{n_a, n_b} \frac{\left(K^{>\;n_a n_b}_{\alpha n_\alpha \beta k_\beta}\right)^* \; K^{>\;n_a n_b}_{\gamma n_\gamma \delta k_\delta}}{\omega - \left(\varepsilon^\pi_{n_a} + \varepsilon^\pi_{n_b}\right) + i\eta} \\ &=\; K^{>\dagger} \frac{1}{\omega - E + i\eta} K^> \;, \end{aligned} \tag{A.23}$$

$$
\begin{aligned}
W^{<}_{\alpha k_\alpha \beta n_\beta, \gamma k_\gamma \delta n_\delta}(\omega) &= \sum_{n_a, n_b} - \frac{K^{<\ n_a n_b}_{\alpha k_\alpha \beta n_\beta} \left(K^{<\ n_a n_b}_{\gamma k_\gamma \delta n_\delta}\right)^*}{\omega + \left(\varepsilon^{\pi}_{n_a} + \varepsilon^{\pi}_{n_b}\right) - i\eta} \\
&= K^{<\dagger} \frac{-1}{\omega - E - i\eta} K^{<} \ , \qquad \text{(A.24)}
\end{aligned}
$$

where $\varepsilon^{\pi}_{n_a}$ and $\varepsilon^{\pi}_{n_b}$ are the energies of the intermediate ph phonons.

A.3.1 ERPA Matrix

The eigenvalue equation for the ERPA is obtained in the usual way, by substituting Eqs. (A.16) to (A.19) into (A.15) and then extracting the residues of the ph poles ε^{π}_{n}. The result is an eigenvalue equation in terms of the vectors $\mathcal{Z}^{>}$ and $\mathcal{Z}^{<}$.

To linearize the problem, we introduce the following components

$$
\begin{aligned}
X^{(1)}_{n_\alpha k_\beta} &\equiv \frac{1}{\omega - D + i\eta}\, G\ \{(V\ +\ W^{>}(\omega))\, \mathcal{Z}^{>}\ -\ (V\ +\ H^{>,<})\, \mathcal{Z}^{<}\}\ , \\
Y^{(1)}_{n_\alpha k_\beta} &\equiv \frac{1}{\omega + D - i\eta}\, G^*\, \{(V\ +\ H^{<,>})\, \mathcal{Z}^{>}\ -\ (V\ +\ W^{<}(\omega))\, \mathcal{Z}^{<}\}\ , \\
X^{(2)}_{n_\alpha k_\beta} &\equiv \frac{1}{\omega - E + i\eta}\, K^{>} \mathcal{Z}^{>}\ , \\
Y^{(2)}_{n_\alpha k_\beta} &\equiv \frac{1}{\omega + E - i\eta}\, K^{<} \mathcal{Z}^{<}\ , \qquad \text{(A.25)}
\end{aligned}
$$

$X^{(1)}$ and $Y^{(1)}$ are related to $\mathcal{Z}^{>}$ and $\mathcal{Z}^{<}$ respectively by

$$
\begin{aligned}
\mathcal{Z}^{>}_{\alpha n_\alpha \beta k_\beta} &= \mathcal{X}^{n_\alpha}_{\alpha} \mathcal{Y}^{k_\beta}_{\beta}\ X^{(1)}_{n_\alpha k_\beta} \ = \ G^{\dagger}\ X^{(1)} \\
\mathcal{Z}^{<}_{\alpha k_\alpha \beta n_\beta} &= \mathcal{Y}^{k_\alpha}_{\alpha} \mathcal{X}^{n_\beta}_{\beta}\ Y^{(1)}_{k_\alpha n_\beta} \ = \ (G^*)^{\dagger}\ Y^{(1)} \qquad \text{(A.26)}
\end{aligned}
$$

Eqs. (A.26) are the analogous of definitions (B.3) for the case of 2p1h Faddeev equations. In the present case, though, $X^{(1)}$ and $Y^{(1)}$ represent the ph amplitudes that appear in the standard RPA equations [58, 43] and must not be confused with the Faddeev amplitudes of Section B.1.1. Similarly $X^{(2)}$ and $Y^{(2)}$ are the 2p2h amplitudes introduced by the ERPA approach.

After some algebra, Eqs. (A.25) and (A.26) can be put in the form of a linear eigenvalue equation

$$
\omega \begin{pmatrix} X^{(1)} \\ X^{(2)} \\ Y^{(1)} \\ Y^{(2)} \end{pmatrix} = \mathbf{M} \begin{pmatrix} X^{(1)} \\ X^{(2)} \\ Y^{(1)} \\ Y^{(2)} \end{pmatrix} . \qquad \text{(A.27)}
$$

where the matrix $\mathbf{M}$ is defined as

$$\mathbf{M} = \begin{bmatrix} G\ V\ G^\dagger\ +\ D & G\ K^{>\dagger} & G\ [V\ +\ H^{>,<}]\ G^\dagger & \\ K^{>}\ (G^*)^\dagger & E & & \\ -G^*\ [V\ +\ H^{<,>}]\ G^\dagger & & -G^*\ V(G^*)^\dagger - D & G^*\ K^{<\dagger} \\ & & K^{<}\ (G^*)^\dagger & -E \end{bmatrix} . \quad \text{(A.28)}$$

The off diagonal 2×2 blocks in Eq. (A.28) describe diagrams in which the time direction of propagation is inverted. In the present case the only nonvanishing elements are the ones that involve the inversion of a single ph into a hp one, or vice versa. These correspond to the first-order term V, which represents the kernel of the bare RPA, and to possible contributions from more complex diagrams, $H^{>,<}$ and $H^{<,>}$. The last diagram of Fig. 4.4 is an example of the latter. Of course, time inversion diagrams that involve incoming and/or outgoing two-phonons contributions could be considered and included in the ERPA equations (A.15). Their contribution would then fill the empty spaces in Eq. (A.28). The calculations of Chapter 4 are aimed to explore the relevance of the coupling between two phonons to the presence of previously unexplained levels. These contributions were summed in a Tamm-Dancoff fashion and therefore no time inversion diagram was considered other than the traditional RPA one (the $H^{>,<}$ and $H^{<,>}$ were neglected as well).

It must be noted that if the terms involving the matrix $G\ K^\dagger$ are discarded in Eq. (A.28), the components $X^{(1)}$ and $Y^{(1)}$ decouple from $X^{(2)}$ and $Y^{(2)}$. In this case, Eqs. (A.15) reduce to the ph-DRPA one (2.28) and the matrix (A.28) would take the form of the standard RPA matrix [58]. Finally, by neglecting all the off-diagonal and time inversion contributions (i.e. also the term in V), one is left with the Dressed TDA equations.

The normalization condition is derived in the usual way, by extracting the contribution of order zero of the expansion around a pole and by employing the conjugate equation. One eventually obtains [43]

$$\sum_{i=1,2} \left(X^{(i)\dagger}\ X^{(i)}\ -\ Y^{(i)\dagger}\ Y^{(i)} \right) = 1\ , \quad \text{(A.29)}$$

where the inner product of the vectors $X^{(i)}$ and $Y^{(i)}$ is implied.

When the standard (D)RPA is used, as in Chapter 3, only solutions for the components $X^{(1)}$ and $Y^{(1)}$ are obtained. In this case the number of solutions is the same as the number of ph fragments that appear in Eq. (A.28). With the choice of the Faddeev kernel depicted in Section A.2, the matrix elements that appear in

Eq. (B.7) are simply related to amplitudes that diagonalize the DRPA equation

$$U^{n_\pi}_{n_1,k_2} = X^{(1)\ n_\pi}_{\ n_1,k_2} \ , \tag{A.30}$$

$$J^{n_\pi}_{k_1,n_2} = -Y^{(1)\ n_\pi}_{\ k_1,n_2} \ , \tag{A.31}$$

$$H^{n_\pi}_{n_1,k_2} = \left(Y^{(1)\ n_\pi}_{\ k_2,n_1}\right)^* \ , \tag{A.32}$$

$$V^{n_\pi}_{k_1,n_2} = -\left(X^{(1)\ n_\pi}_{\ n_2,k_1}\right)^* \tag{A.33}$$

which are analogous to Eqs. (A.5-A.8) for the pp(hh) case[1]. When the ERPA equations are solved, the situation is more complex since also two-phonon amplitudes enter Eq. (A.27) and a number of solutions bigger than the total number of ph fragments is found. One must, therefore, extend the row indices of Eqs. (A.30-A.33) to include the components $X^{(2)}$ and $Y^{(2)}$ as well. Then Eq. (A.29) becomes a special case of the ortho-normalization relation (A.9), which is valid again. From the latter one can derive the closure relation, analogous to Eq.(A.10). It worth noting that the components (A.30-A.33) can also be employed as a starting point to embed the solutions for ERPA phonons into the Faddeev formalism for Sec. 2.4 and Appendix B.

A.3.2 Matrix Elements for ph ERPA

In the following we give the explicit expression for the matrix elements of Eq. (A.28). The contributions originating from the standard (D)RPA equation are

$$\left(G\,V\,G^\dagger \ + \ D\right)_{n_1k_2,n_3k_4} = \mathcal{X}^{n_1}_\alpha \mathcal{Y}^{k_2}_\beta \ V_{\alpha\nu,\beta\mu} \ \left(\mathcal{X}^{n_3}_\mu \mathcal{Y}^{k_4}_\nu\right)^* \ ,$$

$$\left(G^*\,V\,(G^*)^\dagger \ + \ D\right)_{k_1n_2,k_3n_4} = \left(\mathcal{Y}^{k_1}_\alpha \mathcal{X}^{n_2}_\beta\right)^* \ V_{\alpha\nu,\beta\mu} \ \mathcal{Y}^{k_3}_\mu \mathcal{X}^{n_4}_\nu \ ,$$

$$\left(G^*\,V\,G^\dagger\right)_{k_1n_2,n_3k_4} = \left(\mathcal{Y}^{k_1}_\alpha \mathcal{X}^{n_2}_\beta\right)^* \ V_{\alpha\nu,\beta\mu} \ \left(\mathcal{X}^{n_3}_\mu \mathcal{Y}^{k_4}_\nu\right)^* \ ,$$

$$\begin{aligned}\left(G\,V\,(G^*)^\dagger\right)_{n_1k_2,k_3n_4} &= \mathcal{X}^{n_1}_\alpha \mathcal{Y}^{k_2}_\beta \ V_{\alpha\nu,\beta\mu} \ \mathcal{Y}^{k_3}_\mu \mathcal{X}^{n_4}_\nu \ = \\ &= \left\{\left(G^*\,V\,G^\dagger\right)_{n_4k_3,k_2n_1}\right\}^* \ ,\end{aligned}$$

[1]Here, $\{n_1,k_2\}$ and $\{n_\pi\}$ label row and column indices, respectively

with the relevant unperturbed ph energies

$$D_{n_1 k_2} = diag\{\varepsilon^+_{n_1} + \varepsilon^-_{k_2}\} \ . \tag{A.34}$$

The interaction between two-phonon intermediate states and the ph ones is given by

$$\begin{aligned}\left(K^> G^\dagger\right)_{n_a^\pi n_b^\pi, n_1 k_2} \ = \ & \frac{1}{2} \ \Big\{ \Big[\left(X^{(1)}{}^{n_a^\pi}_{n_\mu k_\rho} \ X^{(1)}{}^{n_b^\pi}_{n_1 k_\epsilon} \right)^* \ \mathcal{X}^{n_\mu}_\mu \mathcal{Y}^{k_\rho}_\rho \ V_{\mu\nu,\rho\epsilon} \ \mathcal{Y}^{n_\epsilon}_\epsilon \left(\mathcal{Y}^{k_2}_\nu\right)^* \\ & - \ \left(X^{(1)}{}^{n_a^\pi}_{n_\mu k_\rho} \ X^{(1)}{}^{n_b^\pi}_{n_\nu k_2} \right)^* \ \mathcal{X}^{n_\mu}_\mu \mathcal{Y}^{k_\rho}_\rho \ V_{\mu\nu,\rho\epsilon} \ (\mathcal{X}^{n_1}_\epsilon)^* \ \mathcal{X}^{k_\nu}_\nu \Big] \\ & + \ [n_a^\pi \leftrightarrow n_b^\pi] \Big\}\end{aligned}$$

where n_a^π and n_b^π are the quantum numbers of the two phonons that form the intermediate state. The quantities $X^{(1)}{}^{n^\pi}_{n_1 k_2}$ are the forward-going amplitudes of the intermediate phonons (A.25) or (A.26) and are obtained from the previous solution of the polarization propagator. Note that $K^> G^\dagger$ is symmetric under the exchange of the two indices n_a^π and n_b^π, as required by the boson character of the ph phonons. Due to the time inversion property of npnh states, the corresponding contribution for backward-going propagation is simply related to above one:

$$\left(K^< G^{*\dagger}\right)_{n_a^\pi n_b^\pi, k_1 n_2} \ = \ \left\{ \left(K^> G^\dagger\right)_{n_a^\pi n_b^\pi, n_2 k_1} \right\}^* \ . \tag{A.35}$$

Finally, the two-phonon unperturbed energies are given by

$$E_{n_a^\pi n_b^\pi} = diag\{\varepsilon^\pi_{n_a} + \varepsilon^\pi_{n_b}\} \ . \tag{A.36}$$

Appendix B

Details of the Faddeev Formalism

The quantities entering the Faddeev equations (2.42) depend on a large number of indices. Expressed in this form, the dimension of the problem can become excessively large even for a small model space. Thus, some further manipulations are needed to achieve a practical solution. The difficulty can be overcome by introducing a new set of spectroscopic amplitudes which depend only on the indices labeling the particle and hole fragments (n, n', k) [77, 51]. Thereby the problem is reexpressed by changing from the basis of sp states $\{\alpha\}$, used in definitions (2.22) and (2.33-2.35), to a new formulation constructed in terms of the fragments labeled by $\{n, k\}$. This procedure also allows to rewrite the eigenvalue and normalization conditions corresponding to Eqs. (2.42) in a more concise way. As long as the interaction elements $V_{\alpha\beta,\gamma\delta}$ are energy independent, all the solutions can then be obtained through a *single* diagonalization.

A second complication is the existence of spurious solutions. The Faddeev formalism introduces three different components that live in the same Hilbert space of the complete propagator (2.36) or (B.2). By solving a set of three coupled equations, one can in principle generate a larger number of solutions. Therefore, it is not surprising that about 2/3 of the eigenvalues of Eqs. (2.42) have no physical meaning.

Sections B.1 and B.2 describe the above manipulations and use the results to discuss the properties of spurious solutions. Following the choice of Section 2.4, only the 2p1h propagator will be discussed. The 2h1p case is analogous. This new formulation does not introduce any further approximation. Nevertheless, since it appears relevant for a practical solution of the problem it will be described in the following. Section B.3 gives some details of the practical implementation.

B.1 Solution of Faddeev Equations

B.1.1 Faddeev Amplitudes

The Lehmann representation of the Faddeev components $R^{(i)}_{\mu n_\mu \nu n_\nu \lambda k_\lambda, \alpha n_\alpha \beta n_\beta \gamma k_\gamma}$, contains all the poles ε^{Fd}_m of the 2p1h propagator, each with its own residue. One obtains for these components

$$R^{(i)}_{\mu n_\mu \nu n_\nu \lambda k_\lambda, \alpha n_\alpha \beta n_\beta \gamma k_\gamma} \;=\; \sum_m \frac{\left(\beta^{(i),m}_{\mu n_\mu \nu n_\nu \lambda k_\lambda}\right)^* \; b^m_{\alpha n_\alpha \beta n_\beta \gamma k_\gamma}}{\omega - \varepsilon^{Fd}_m + i\eta} \;+\; R^{(i)}_{free}(\omega) \;, \tag{B.1}$$

where the superscript m labels the solutions of Faddeev equations. In Eq. (B.1), $R^{(i)}_{free}$ represent components containing the same poles as $G^{0>}$ (2.43). The sum of these terms cancels exactly the contribution of the three freely propagating lines in Eq. (2.36), leaving in the Lehmann representation of the Faddeev propagator only those poles ε^{Fd}_m, that correspond to correlated 2p1h states [60, 37]. This is most easily demonstrated by applying the DRPA equations to both sides of Eq. (2.42).

The vectors $\beta^{(i),m}_{\mu n_\mu \nu n_\nu \lambda k_\lambda}$ represent the amplitudes of the three Faddeev components and sum up to the residues of the full propagator

$$b^m_{\alpha n_\alpha \beta n_\beta \gamma k_\gamma} \;=\; \sum_{i=1,2,3} \beta^{(i),m}_{\alpha n_\alpha \beta n_\beta \gamma k_\gamma} \;. \tag{B.2}$$

We now define new Faddeev amplitudes $x^{(i),m}_{n_1 n_2 k}$ which are related to the $\beta^{(i)}$'s in such a way that [77]

$$\beta^{(i),m}_{\alpha n_1 \beta n_2 \gamma k} \;=\; \mathcal{X}^{n_1}_\alpha \mathcal{X}^{n_2}_\beta \mathcal{Y}^k_\gamma \; x^{(i),m}_{n_1 n_2 k} \;, \tag{B.3}$$

where no summation is performed over the particle and hole indices n_1, n_2 and k. We also introduce the notation for the spectroscopic amplitude, analogous to Eq. (B.2)

$$x^m_{n_1 n_2 k} \;=\; \sum_{i=1,2,3} x^{(i),m}_{n_1 n_2 k} \;. \tag{B.4}$$

In general, $x_{n_1 n_2 k}$ and the components $x^{(i)}_{n_1 n_2 k}$ define four vectors $\mathbf{x}$ and $\mathbf{x}^{(i)}$ all belonging to the same linear space. It is useful to split up the latter in two spaces V_A and V_S containing all the vectors that are antisymmetric and symmetric with respect to the exchange of the two particle indices n_1 and n_2, respectively. Thus,

$$\mathbf{x} \;,\; \mathbf{x}^{(i)} \;\in\; V_A \otimes V_S \;. \tag{B.5}$$

We also define a vector $\mathbf{X}$ containing all the three components

$$\mathbf{X} \;=\; \left(\begin{array}{c} \mathbf{x}^{(1)} \\ \mathbf{x}^{(2)} \\ \mathbf{x}^{(3)} \end{array} \right) \;\in\; V_A^3 \otimes V_S^3 \;. \tag{B.6}$$

Here and in the following, we use the convention to denote vectors with lower case boldface and operators (matrices) with plain capital letters belonging to the space $V_A \otimes V_S$. Both vectors and matrices in the space $V_A^3 \otimes V_S^3$ are denoted by capital boldface letters. We will also use I for the identity matrix in the $V_A \otimes V_S$ space and the superscript ex to indicate the vectors obtained by exchanging the two particle indices (thus, I^{ex} is the operator exchanging n_1 and n_2 in Eqs. (B.3) and (B.4)).

B.1.2 Faddeev Hamiltonian

The eigenvalue equation for the Faddeev expansion can be obtained by substituting the Lehmann representation (B.1) into Eqs. (2.42) and extracting the residues ε_m^{Fd} of the poles. After some algebra, one obtains the following set of equations in terms of the $\mathbf{x}^{(i)}$ vectors

$$\mathbf{x}^{(i)} \;=\; \left[H^{(i)} H^{(i)\dagger} \;+\; U^{(i)} \frac{1}{\omega - D^{(i)}} T^{(i)\dagger} \right] \;\left(\mathbf{x}^{(j)} \;+\; \mathbf{x}^{(k)} \right) \quad i = 1,2,3 \;. \tag{B.7}$$

In Eq. (B.7), the components of the matrices $H^{(i)}$, $U^{(i)}$ and $T^{(i)}$ are related to the spectroscopic amplitudes of the DRPA propagators, as explained in Appendix A.1. The $D^{(i)}$'s are diagonal matrices containing the eigenvalues of the corresponding DRPA, coupled to the corresponding particle or hole pole of the freely propagating line.

One can now define block-diagonal matrices $\mathbf{H}$, $\mathbf{D}$, etc... which contain on the diagonal the matrices $H^{(i)}$, $D^{(i)}$, etc. These matrices act on the vectors $\mathbf{X}$ defined in (B.6). Using this notation one combines Eqs. (B.7) as follows

$$\mathbf{X} \;=\; \left[\mathbf{H}\mathbf{H}^\dagger \;+\; \mathbf{U} \frac{1}{\omega - \mathbf{D}} \mathbf{T}^\dagger \right] \;\mathbf{M}\;\mathbf{X} \;, \tag{B.8}$$

where we have also introduced the matrix

$$\mathbf{M} \;=\; \left[\begin{array}{ccc} & I & I \\ I & & I \\ I & I & \end{array} \right] \tag{B.9}$$

that takes into account the proper mixing between the Faddeev components.

By introducing the vector

$$\mathbf{Y} \equiv \frac{1}{\omega - \mathbf{D}} \mathbf{T}^{\dagger} \mathbf{M} \mathbf{X} \tag{B.10}$$

(which appears in Eq. (B.8)) and remembering that $\mathbf{D}$ is a diagonal matrix, it is possible to manipulate Eq. (B.8) into the usual form of an eigenvalue equation

$$\omega \mathbf{X} = \mathbf{F} \mathbf{X} \tag{B.11}$$

where we have introduced the Faddeev hamiltonian $\mathbf{F}$ [42], which is given by

$$\mathbf{F} = \left[\mathbf{I} - \mathbf{H}\mathbf{H}^{\dagger}\mathbf{M}\right]^{-1} \mathbf{U} \left\{\mathbf{T}\mathbf{M} + \mathbf{D}(\mathbf{U}^{-1}) \left[\mathbf{I} - \mathbf{H}\mathbf{H}^{\dagger}\mathbf{M}\right]\right\} . \tag{B.12}$$

The form (B.11) of the Faddeev eigenvalue equations is useful, since it reduces the problem to the diagonalization of a single (non-hermitian) hamiltonian.

The hamiltonian $\mathbf{F}$ can still correspond to a large matrix requiring a large amount of CPU time to diagonalize. As will be explained later in Sec. B.2, about 2/3 of its solutions are trivial and without physical meaning. Thus, it is not necessary to diagonalize the full Faddeev hamiltonian (B.12) but one can project it onto the space of physical solutions.

B.1.3 Symmetry Requirements and Normalization Conditions

As a consequence of the Pauli exclusion principle, the spectroscopic amplitudes for the 2p1h motion have to be antisymmetric with respect to the exchange of the two particle indices. This statement applies to the full spectroscopic amplitudes (B.2) and (B.4) but not to the single Faddeev components, which have more complicated exchange properties. To exhibit the correct symmetry requirements for the Faddeev components, it is useful to introduce the following exchange operator, which works on the space (B.6) of the three $\mathbf{x}^{(i)}$ components:

$$\mathbf{P} = \begin{bmatrix} & I^{ex} & \\ I^{ex} & & \\ & & I^{ex} \end{bmatrix} . \tag{B.13}$$

The form of matrix (B.13) takes into account that the component $x^{(1)}$ has to change into $x^{(2)}$ when the first two legs (i.e. the two particles) are exchanged. Since $\mathbf{P}$ satisfies the propriety $\mathbf{P}^2 = \mathbf{P}$, it has only eigenvalues $+1$ and -1 and the respective

eigenvectors are of the form

$$\mathbf{X}_{-1} \;=\; \begin{bmatrix} \mathbf{x}_a \\ -I^{ex}\,\mathbf{x}_a \\ \mathbf{x}_b - I^{ex}\,\mathbf{x}_b \end{bmatrix} \quad \text{and} \quad \mathbf{X}_{+1} \;=\; \begin{bmatrix} \mathbf{x}_a \\ +I^{ex}\,\mathbf{x}_a \\ \mathbf{x}_b + I^{ex}\,\mathbf{x}_b \end{bmatrix} , \tag{B.14}$$

in which $\mathbf{x}_a$ and $\mathbf{x}_b$ are any two vectors. One easily recognizes that the three Faddeev components of $\mathbf{X_{-1}}$ and $\mathbf{X_{+1}}$ give rise to antisymmetric and symmetric spectroscopic amplitudes, respectively, when they are inserted in Eq. (B.4).

Using the symmetry properties of the interaction boxes (2.38) and (2.39) and the definition of $\mathbf{M}$ (B.9), one can show that $\mathbf{P}$ commutes with the matrix multiplying $\mathbf{X}$ in Eq. (B.8) and therefore with the Faddeev hamiltonian (B.12). Thus, $\mathbf{P}$ and $\mathbf{F}$ must have a common set of eigenvalues. The relevant eigenvectors in the present case correspond to those of type $\mathbf{X_{-1}}$, as required by the Fermi-Dirac statistics.

The normalization condition is derived as usual by considering the Lehmann representation (B.1) for the components $R^{(i)}_{\mu\nu\lambda,\alpha\beta\gamma}(\omega)$ [55, 56]. One can expand around a given pole ε^{Fd}_m and consider terms to order zero and then make use of the conjugate of the eigenvalue equation (B.7). The result is a condition for the $\mathbf{X}^{(i)}$'s which only allows proper normalization for the antisymmetric component. These antisymmetric solutions $\mathbf{X_{-1}}$ satisfy the following condition

$$\mathbf{x}^\dagger\mathbf{x} \;-\; \sum_{i=1,2,3} \mathbf{y}^{(i)\dagger}\mathbf{y}^{(i)} = 2 \,, \tag{B.15}$$

where $\mathbf{x}$ is the spectroscopic amplitude appearing in Eq. (B.4) and the factor of 2 appears because a sum over all indices of $x^m_{n_1 n_2 k}$ (B.3) is implied, which also includes the exchange terms. Eq. (B.15) differs from the usual normalization of a wave function due to the subtraction of the additional terms

$$\mathbf{y}^{(i)} \;=\; \left[V^{(i)}H^{(i)\dagger} \;+\; J^{(i)}\frac{1}{\omega - D^{(i)}}T^{(i)\dagger}\right] \;\left(\mathbf{x}^{(j)} \;+\; \mathbf{x}^{(k)}\right) \;\; i = 1,2,3. \tag{B.16}$$

These contributions correspond to the diagrams shown in Fig. 2.11 which have been discarded in the present expansion.

B.2 Spurious Solutions

The Faddeev formalism is based on the introduction of different components $\mathbf{x}^{(i)}$, which belong to the same linear space of the total spectroscopic amplitude $\mathbf{x}$ (B.5). These components are the solutions of the Faddeev-eigenvalue equation (B.11),

which is formulated in a larger space in terms of the vectors $\mathbf{X}$ containing all three $\mathbf{x}^{(i)}$. Only one third of the solutions in this larger space have physical meaning while the others have to be discarded. This separation becomes more clear if one looks at how the final solution is obtained in terms of the single components, Eq. (B.2) or (B.4): one may obtain a set of components $\mathbf{x}^{(i)}$ that solve the Faddeev equations but that generates a vanishing spectroscopic amplitude $\mathbf{x} = \mathbf{x}^{(1)} + \mathbf{x}^{(2)} + \mathbf{x}^{(3)} = 0$. Obviously such solutions don't have physical meaning. Relevant details for treating this issue are discussed below.

B.2.1 Nature and Form of Spurious Solutions

The antisymmetric solutions of the Faddeev equations $\mathbf{X}_{-1}$ are determined from two independent vectors $\mathbf{x}_a$ and $\mathbf{x}_b$ as shown in Eq. (B.14). In particular, one has to specify both the symmetric and antisymmetric parts of the first vector ($\mathbf{x}_a$) and only the antisymmetric part of the second ($\mathbf{x}_b$). These solutions therefore belong to the space

$$V_F \equiv V_A \otimes V_A \otimes V_S \,. \tag{B.17}$$

The complete spectroscopic amplitudes $\mathbf{x}$ must also be antisymmetric under the exchange of the two particle indices, so they belong to V_A. Thus, Eq. (B.4) must be regarded as a projection from V_F to the smaller space V_A and therefore must have a nonvanishing kernel. We denote this kernel by V_{Sp} and refer to its vectors as *spurious states*, $\mathbf{Y}_{Sp}$. Although these states satisfy the Pauli requirements, they don't yield any contribution to the full 2p1h propagator and have by themselves no physical meaning. We also consider the space V_{Ph}, which is orthogonal to the kernel V_{Sp} and contains the antisymmetric states $\mathbf{Y}_{Ph}$ which generate nonvanishing spectroscopic amplitudes $\mathbf{x}$. The vectors belonging to V_{Ph} produce contributions to the 2p1h propagator and therefore in the following they will be referred as *physical states*.

Thus, the set of solutions $\mathbf{X}_{-1}$ (B.14) which satisfy the Pauli requirements can be divided in two subsets of physical V_{Ph} and spurious states V_{Sp}. Explicit orthogonal basis sets for these two spaces are given by

$$\mathbf{Y}_{Ph} = \begin{pmatrix} \mathbf{u} - \mathbf{u}^{ex} \\ \mathbf{u} - \mathbf{u}^{ex} \\ \mathbf{u} - \mathbf{u}^{ex} \end{pmatrix} \in V_{Ph} \quad \text{and} \quad \mathbf{Y}_{Sp} = \begin{pmatrix} -\mathbf{u} \\ +\mathbf{u}^{ex} \\ \mathbf{u} - \mathbf{u}^{ex} \end{pmatrix} \in V_{Sp} \,. \tag{B.18}$$

where the $\mathbf{u}$ represent unit vectors which belong to the space (B.5). Their compo-

nents are given by

$$u_{n_1 n_2 k} \;=\; \delta_{n_1,n'}\delta_{n_2,n''}\delta_{k,k'} \tag{B.19}$$

with n', n'' and k' fixed fragmentation indices which label all the possible $\mathbf{u}$. The vectors $\mathbf{u}^{ex} = I^{ex}\ \mathbf{u}$ are given by the exchange of the two particle indices n_1 and n_2. The physical states $\mathbf{Y}_{Ph}$ are characterized by the fact that they do not produce vanishing spectroscopic amplitudes while the spurious states $\mathbf{Y}_{Sp}$ do. Thus V_{Sp} completely represents the kernel of Eq. (B.4).

It is clear from Eq. (B.18) that the $\mathbf{Y}_{Ph}$ states span a space equivalent to the space of antisymmetric vectors $\mathbf{x}$ (B.4), thus $V_{Ph} \equiv V_A$. Analogously, the $\mathbf{Y}_{Sp}$ states depend on both the symmetric and the antisymmetric parts of the $\mathbf{u}$ vectors, which implies $V_{Sp} \equiv V_A \otimes V_S$. Therefore, the vectors (B.18) form a basis for the full antisymmetric Faddeev space V_F (B.17).

B.2.2 Spurious Eigenstates vs. Faddeev Kernel

In general, the physical and spurious states (B.18) defined here are not solutions of the Faddeev equations (B.11), they simply define a basis over which these solutions can be expanded. Nevertheless, for both the normal three-body Faddeev equations and the expansion proposed in this thesis, it can be seen that the spurious states $\mathbf{Y}_{Sp}$ (and only those) diagonalize the Faddeev hamiltonian. The eigenvalues correspond to the poles of the three freely propagating lines $\omega = \varepsilon^+_{n'} + \varepsilon^+_{n''} - \varepsilon^-_k$ (2.43). This feature serves as a sum rule on the solutions of the Faddeev equations and (unlike the case of 3-body systems) is not always satisfied when applying the formalism to particle and hole excitations. Instead this property depends on the diagrams included in the expansion and a proper set of diagrams needs to be employed in order to apply the Faddeev formalism. For the particular Faddeev expansion described here, this constraint is achieved by including the backward-going terms of DRPA phonons in the $\Gamma^{(i)}$ matrices and by using the closure relations (A.10), which turn out to play an important role. This result is important enough to outline its proof in the following. This also clarifies the relationship between the correct behavior of the spurious solutions and the backward-going DRPA diagrams.

The states $\mathbf{Y}_{Sp}$, defined in (B.18), actually represent a set of spurious solutions of the Faddeev Eqs. (2.42) and (B.7). Proof: consider a spurious state $\tilde{\mathbf{Y}}_{Sp}$ of the form (B.18), with $\tilde{\mathbf{u}}$ given by Eq. (B.19) and eigenvalue $\tilde{\omega}$. We now observe that the matrices U (A.5) and T (A.11) differ from each other only by an energy

denominator. In particular, we have

$$-\frac{1}{\tilde{\omega}-\mathbf{D}}\,\mathbf{T}\rightarrow\mathbf{U}\ , \tag{B.20}$$

were $\mathbf{U}$, $\mathbf{T}$ and $\mathbf{D}$ are defined in Sec. B.1.1. If the eigenvalue is given by $\tilde{\omega}=\varepsilon^{+}_{n'}+\varepsilon^{+}_{n''}-\varepsilon^{-}_{k}$, the equivalence of the left- and right-hand side holds *only* for the matrix elements having the same indices (n',n'',k'). Indeed, only in that case the denominator $\tilde{\omega}-\mathbf{D}$ will be equal to the one in Eq. (A.5). On the other hand, we see from Eq. (B.19) that the components of $\tilde{\mathbf{u}}$ are nonzero only for the same indices. This allows the substitution of the $\rightarrow$ in Eq. (B.20) by an equal sign when acting on the vector $\tilde{\mathbf{Y}}_{Sp}$. Substituting Eq. (B.20) into Eq. (B.8) and using the closure relations of the DRPA, we obtain the equation

$$\tilde{\mathbf{Y}}_{Sp}\ =\ -\ \mathbf{M}\,\tilde{\mathbf{Y}}_{Sp}\ , \tag{B.21}$$

which is valid only for the specific state $\tilde{\mathbf{Y}}_{Sp}$, labeled by the indices (n',n'',k'). The last equation is satisfied for a spurious states of the form (B.18) but not for the corresponding physical states $\tilde{\mathbf{Y}}_{Ph}$. Thus, we have obtained a set of spurious solutions of the Faddeev equations which form an orthogonal basis of V_{Sp}.

In this proof, we note that the closure relation (A.10) can be applied to derive Eq.(B.21) because of the presence of the backward-going term $\mathbf{HH}^{\dagger}$ in Eq. (B.8), which comes directly from the last diagram of Fig. 2.10.

B.2.3 Physical Solutions

In general the solutions of the Faddeev eigenvalue equation (B.11) do not automatically separate into the physical and spurious states defined below Eq. (B.17). Nevertheless, we have just shown that the states of V_{Sp} are proper eigenstates of the Faddeev hamiltonian for the expansion presented in this thesis. This feature always occurs for the three-body problem but is not guaranteed when working with quasiparticle and quasihole excitations unless a proper set of diagrams is considered. When this condition is satisfied, there exists a set of spurious solutions of the Faddeev equation (B.11) which spans the space V_{Sp} completely. The projection of the Faddeev hamiltonian (B.12) onto the physical and spurious subspaces V_{Ph} and V_{Sp} then takes the form

$$\mathbf{F}\ =\ \left[\begin{array}{cc}\langle Ph|\mathbf{F}|Ph\rangle & 0\\ \langle Sp|\mathbf{F}|Ph\rangle & \langle Sp|\mathbf{F}|Sp\rangle\end{array}\right]\ . \tag{B.22}$$

It should be noted that the physical states $\mathbf{Y}_{Ph}$, belonging to V_{Ph}, differ from the spurious ones $\mathbf{Y}_{Sp}$ ($\in V_{Sp}$) not only because they give rise to physically meaningful spectroscopic amplitudes but also because they are not solutions of the Faddeev equations (B.11). In general, a physically meaningful eigenvector of (B.22), $\mathbf{X}_{physical}$, is a mixture of states belonging to both V_{Ph} and V_{Sp}, due to the mixing term $\langle Sp|\mathbf{F}|Ph\rangle$. Thus,

$$\mathbf{X}_{physical} \;=\; c_1\;\mathbf{Y}_{Ph} + c_2\;\mathbf{Y}_{Sp}\;, \tag{B.23}$$

with c_1 and c_2 some constants. In other words, a spurious component $\mathbf{Y}_{Sp}$ is also generated which will be automatically projected out when computing the spectroscopic amplitude $\mathbf{x}$ (B.5).

It is important to recognize that such spurious contributions are indeed needed since they account for the differences of the three Faddeev components (B.3). The relation between the usual Faddeev components for a given physical or spurious state can be inferred from the basis sets (B.18). There it is shown that all the Faddeev components $\mathbf{x}^{(i)}$ of a state $\mathbf{Y}_{Ph}$ or $\mathbf{Y}_{Sp}$ are equal, up to a sign. As a consequence, if a general solution is a pure physical state $\mathbf{Y}_{Ph}$, all its Faddeev components cannot differ from each other in a significant way. Having a mixing between physical and spurious states allows the possibility of obtaining two independent Faddeev components. This result corresponds to the physical ingredients of the calculations whic (in this thesis) involve identical ph phonons for the components $\mathbf{x}^{(1)}$ and $\mathbf{x}^{(2)}$ but a pp phonon for $\mathbf{x}^{(3)}$.

When all the Faddeev components are summed to generate the full $\mathbf{x}$ in (B.4), the contribution of the spurious states cancels out. Thus, for any nonspurious solution of the Faddeev equations, only the contribution from physical states $\mathbf{Y}_{Ph}$ is needed to determine the 2p1h propagator. By looking at Eq. (B.22), it is easy to see that these contributions can be directly obtained by diagonalizing the upper-left block

$$\omega_m\;\mathbf{Y}^m_{Ph} \;=\; \langle Ph|\mathbf{F}|Ph\rangle\;\mathbf{Y}^m_{Ph}\;, \tag{B.24}$$

where m is used to label the solutions. The solutions of Eq. (B.24) are sufficient to determine the 2p1h propagator. For some applications one may need the individual components $\mathbf{x}^{(i)}$. In that case, the contribution from spurious states $\mathbf{Y}_{Sp}$ can be determined by solving the remaining part of the Faddeev equations

$$\omega_m\;\mathbf{Y}^m_{Sp} = \langle Sp|\mathbf{F}|Ph\rangle\;\mathbf{Y}^m_{Ph} + \langle Sp|\mathbf{F}|Sp\rangle\;\mathbf{Y}^m_{Sp}\;. \tag{B.25}$$

We note that if the upper-right block of Eq. (B.22) is not zero, a mixing between the $\mathbf{Y}_{Ph}$ and $\mathbf{Y}_{Sp}$ states occurs for all the eigenstates of the Faddeev hamiltonian.

In this situation, the spurious eigenvalues will differ from the unperturbed energies and all of the solutions of the Faddeev equations will contain a component $\mathbf{Y}_{Ph}$. The Faddeev formalism would therefore become useless, since it would no longer be possible to discern between "good" and "bad" solutions. We have shown how the correct behavior of spurious solutions is related to the presence of backward-going contributions of the DRPA Γ-matrices (see Fig. 2.10). In case these diagrams are neglected, the spurious states $\mathbf{Y}_{Sp}$ no longer diagonalize the Faddeev hamiltonian. Such diagrams may give a small contribution to the description of low-lying states but they are essential to make the whole formalism presented here completely consistent. As a general rule, when deriving expansions based on the Faddeev equations, it should be kept in mind that not all possible sets of diagrams can be effectively summed to all orders. Instead, one must first check the consistency of the set of diagrams with respect to the behavior of spurious solutions.

B.3 Notes on Numerical Calculations

In the practical application to the nucleus of ^{16}O, the set of physical states V_{Ph} had different dimensions for each separate sp channel of the Dyson equation. The maximum number of sp states turned out to be about 3,000. The dimension of the corresponding Faddeev Hamiltonian $\mathbf{F}$ (B.12) was therefore $\sim$9,000, before projection on the subspace V_{Ph}. Some complications also arise from the fact that $\mathbf{F}$ is not (in general) Hermitian and that we are looking for a full diagonalization of Eq. (B.24), in order to generate the total occupation number for fragments at intermediate missing energies.

From a numerical point of view, the main issue consists in evaluating the Faddeev Hamiltonian $\mathbf{F}$ and all the matrix elements of its projection $\langle Ph|\mathbf{F}|Ph\rangle$. Eq. (B.12) can be rewritten has

$$\mathbf{F} = \mathbf{A}^{-1}\ \mathbf{B}\ , \tag{B.26}$$

where

$$\mathbf{A} \equiv \left[\mathbf{I} - \mathbf{H}\mathbf{H}^{\dagger}\mathbf{M}\right] \quad \text{and} \quad \mathbf{B} \equiv \mathbf{U}\ \left[\mathbf{T}\mathbf{M}\ +\ \mathbf{D}(\mathbf{U}^{-1})\mathbf{A}\right]\ . \tag{B.27}$$

The matrices $\mathbf{U}$ and $\mathbf{H}$ are block diagonal in both the 3-dimensional space of Faddeev components and in each channel of the corresponding ph and pp DRPA equations (see Eq.(2.30)). In the present application, every block had dimension of at most 100 states (after performing the angular momenta reduction) and therefore it could be easily inverted numerically. As a consequence, $\mathbf{B}$ can be evaluated algebraically in terms of the inverse of each block in $\mathbf{U}$.

More complicated is the issue of inverting the matrix **A**. Using the conventions introduced after Eq. (B.6) one finds

$$\mathbf{A} = \begin{bmatrix} I & -H^{(1)}H^{(1)\dagger} & -H^{(1)}H^{(1)\dagger} \\ -H^{(2)}H^{(2)\dagger} & I & -H^{(2)}H^{(2)\dagger} \\ -H^{(3)}H^{(3)\dagger} & -H^{(3)}H^{(3)\dagger} & I \end{bmatrix} \tag{B.28}$$

which is no longer block diagonal, due to the Faddeev mixing between ph and pp channels. Still one may notice that the 2×2 block in the upper left corner and the 1×1 block in the lower right refer to separately to ph and pp channels. After performing angular momenta coupling and projecting on the spaces of spurious and physical states, one finds that these two blocks can be expressed in block diagonal form as well. Thus, they can be inverted separately in a mixed algebraic-numerical way, with a negligible expense of computer time. In the present work, the inverse of the full matrix **A** was obtained inverting the 2×2 ph block and then applying a partitioning technique [78]. This procedure still requires a certain amount of computer time but avoids the inversion of the complete 9,000×9,000 matrix (B.28). The main amount of CPU time was therefore spent on the direct diagonalization of Eq. (B.24).

The closure relation for the RPA equations (A.10) gives a relation between the contribution from **U** and **H**. Schematically (i.e. apart from symmetry factors and exchange contributions) one has $-H^{(i)}H^{(i)\dagger} = I - U^{(i)}U^{(i)\dagger}$, where the $U^{(i)}$'s refer to the main contributions to the Faddeev kernel and the matrices $H^{(i)}$ represent the contribution to "Z-diagrams" like the last one of Fig. 2.10. As discussed in the previous section, the latter have been included mainly to guarantee the correct behavior of spurious solutions. Here we see that, by applying the RPA closure relations, one can reexpress the whole Faddeev Hamiltonian only in terms of the $U^{(i)}$ contributions. The effects needed to fix the behavior of spurious solution are effectively accounted for due to the fact that the $U^{(i)}$'s are not unitary. Obviously, as long as ph and pp (D)RPA phonons are employed to construct the Faddeev kernel, the two approaches are completely equivalent.

When one goes beyond the DRPA scheme, as was attempted in Chapter 4, it is not clear which set of Feynman diagrams should be employed in order to deal with spurious eigenstates. Still, the projection of **F** on the the V_{Ph} space can be performed in a formal way. In this situation, the two approaches to evaluate the matrix **A** in terms of either **U** or **H** are not equivalent but represent two different approximations that can be compared to assert the quality of the separation between physical and spurious states.

Bibliography

[1] B. E. Vonderfecht, W. H. Dickhoff, A. Polls, and A. Ramos, Phys. Rev. C **44**, R1265 (1991).

[2] W. H. Dickhoff and H. Müther, Rep. Prog. Phys. **55**, 1947 (1992).

[3] G. A. Rijsdijk, K. Allaart, and W. H. Dickhoff, Nucl. Phys. **A550**, 159 (1992).

[4] A. E. L. Dieperink and P. de Witt Huberts, Ann. Rev. Nucl. Part. Sci. **40**, 239 (1990).

[5] I. Sick and P. de Witt Huberts, Commun. Nucl. Part. Phys. **20**, 177 (1991).

[6] L. Lapikás, Nucl. Phys. **A553**, 297c (1993).

[7] C. J. C. Onderwater *et al.*, Phys. Rev. Lett. **78**, 4893 (1997).

[8] C. J. C. Onderwater *et al.*, Phys. Rev. Lett. **81**, 2213 (1998).

[9] G. Rosner, Prog. Part. Nucl. Phys. **44**, 99 (2000)

[10] M. Leuschner *et al.*, Phys. Rev. C **49**, 955 (1994).

[11] J. M. Udías, J. A. Caballero, E. Moya de Guerra, J. R. Vignote, and A. Escuderos, Phys. Rev. C **64**, 024614 (2001).

[12] M. Radici, A.Meucci, and W. H. Dickhoff, arXiv:nucl-th/0205013, submitted to Phys. Rev. C.

[13] H. Müther and W. H. Dickhoff, Phys. Rev. C **49**, R17 (1994).

[14] M. Radici, S. Boffi, S C. Pieper, and V. R. Pandharipande, Phys. Rev. C **50**, 3010 (1994).

[15] A. Fabrocini and G. Co', Phys. Rev. C **63**, 044319 (2001).

[16] A. E. L. Dieperink and T. de Forest, Jr. Phys Rev. C **10**, 543 (1974).

[17] D. Van Neck, M.Waroquier, A. E. L. Dieperink, S C. Pieper, and V. R. Pandharipande, Phys. Rev. C **57**, 2308 (1998).

[18] K. Amir-Azimi-Nili, H. Müther, L. D. Skouras, and A. Polls, Nucl. Phys. **A604**, 245 (1996).

[19] W. J. W. Geurts, K. Allaart, W. H. Dickhoff, and H. Müther, Phys. Rev. C **53**, 2207 (1996).

[20] W. J. W. Geurts, K. Allaart, W. H. Dickhoff, and H. Müther, Phys. Rev. C **54**, 1144 (1996).

[21] C. Giusti, F. D. Pacati, K. Allaart, W. J. W. Geurts, W. H. Dickhoff, and H. Müther, Phys. Rev. C **57**, 1691 (1998).

[22] H. Müther and P. Sauer, in *Computational Nuclear Physics* ed. by K.-H. Langanke, et al. (Springer Berlin, 1993).

[23] M. O. Distler, in Proc. Fifth Workshop on *Electromagnetically induced two-hadron emission*, eds. P. Grabmayr *at al.* (Univ. Lund, published on CD, ISBN: 91-631-1612-X, 2001), p. 336.

[24] D. Van Neck, M. Waroquier, and J. Ryckebusch Nucl. Phys. **A530**, 347 (1991).

[25] G. A. Rijsdijk, W. J. W. Geurts, K. Allaart, and W. H. Dickhoff, Phys. Rev. C **53**, 201 (1996).

[26] P. Czerski, W. H. Dickhoff, A. Faessler, and H. Müther, Phys. Rev. C **33**, 1753 (1986).

[27] G. E. Brown, and A. M. Green, Nucl. Phys. **75**, 401 (1966).

[28] W. H. Dickhoff, in *Condensed Matter Theories. Vol. 3*, ed. J. S. Arponen, R. F. Bishop and M. Manninen (Plenum, New York 1988) p. 261.

[29] J. Yuan, Ph.D. thesis, Washington University, St. Louis, 1994.

[30] W. H. Dickhoff, in *Nuclear Methods and the Nuclear Equation of State*, ed. M. Baldo (World Scientific, Singapore, 1999) p. 326.

[31] P. Danielewicz, Ann. of. Phys. **197**, 154 (1990).

[32] P. Danielewicz and P. Schuck, Nucl. Phys. **A567**, 78 (1994).

[33] A. D. Jackson, A. Lande, and R. A. Smith, Phys. Rep. **86**, 55 (1982).

[34] P. Schuck, F. Villars, and P. Ring, Nucl. Phys. **A208**, 302 (1973).

[35] M. Hjorth-Jensen, arXiv:nucl-th/9811101.

[36] L. D. Faddeev, Sov. Phys. JETP **12**, 1014 (1961).

[37] W. Glöckle, *The Quantum Mechanical Few-Body Problem* (Springer, Berlin, 1983).

[38] C. Barbieri and W. H. Dickhoff, Phys. Rev. C **63**, 034313 (2001).

[39] C. Barbieri and W. H. Dickhoff, in Proc. Fifth Workshop on *Electromagnetically induced two-hadron emission*, eds. P. Grabmayr *at al.* (Univ. Lund, published on CD, ISBN: 91-631-1612-X, 2001), p. 108.

[40] S. K. Adhikari and W. Glöckle, Phys. Rev. C **19**, 616 (1979).

[41] J. W. Evans and D. K. Hoffman, J. Math. Phys. **22**, 2858 (1981).

[42] P. Navrátil, B. R. Barrett, and W. Glöckle, Phys. Rev. C **59**, 611 (1999).

[43] M. G. E. Brand, K. Allaart, and W. H. Dickhoff, Nucl. Phys. **A509**, 1 (1990)

[44] J. Fujita and H. Miyazawa, Prog. Theor. Phys. **17**, 360 (1957); S. A. Coon and W.Glöckle, Phys. Rev. C **23**, 1790 (1981); J.Carlson, V. R. Pandharipande and R. B. Wiringa Nucl. Phys. **A401**, 59 (1983).

[45] C. Barbieri and W. H. Dickhoff, Phys. Rev. C **65**, 064313 (2002).

[46] A. L. Fetter and J. D. Walecka, *Quantum Theory of Many-Particle Physics* (McGraw-Hill, New York, 1971).

[47] A. A. Abrikosov, L. P. Gorkov and I. E. Dzyaloshinski, *Methods of Quantum Field Theory in Statistical Physics* (Dover, New York, 1975).

[48] J. W. Negele and H. Orland, *Quantum Many-Particle Systems* (Perseus Books, Massachusetts, 1988).

[49] L. P.Kadanoff and G. Baym, *Quantum Statistical Mechanics* (Benjamin, New York, 1962).

[50] R. D. Mattuck, *A Guide to Feynman Diagrams in the Many-Body Problem* (Dover, 1992).

[51] J. P. Blaizot and G. Ripka, *Quantum Theory of Finite Systems* (MIT Press, Cambridge MA, 1986).

[52] G. Brown, *Many-Body Problems* (North Holland, Amsterdam, 1972).

[53] H. Lehmann, Nuovo cimento **11**, 342 (1952).

[54] J. Winter, Nucl. Phys. **A194**, 535 (1972).

[55] W. Hengeveld, W.H. Dickhoff and K. Allaart, Nucl. Phys. **A451**, 269 (1986).

[56] S.D. Yang and T.T.S. Kuo, Nucl. Phys. **A456**, 413 (1986).

[57] P. C. Martin and J. Schwinger, Phys. Rev. **115**, 1342 (1959).

[58] P. Ring and P. Schuck, *The Nuclear Many-body Problem* (Springer, New York, 1980).

[59] W. J. W. Geurts, K. Allaart, and W. H. Dickhoff, Phys. Rev. C **50**, 514 (1994).

[60] C. J. Joachain *Quantum Collision Theory*, (North-Holland, Amsterdam, 1975).

[61] P. Schuck and S. Ethofer, Nucl. Phys. **A212**, 269 (1973).

[62] A. Polls, H. Müther, and W. H. Dickhoff, Phys. Rev. C **51**, 3040 (1995).

[63] R. Machleidt, Adv. Nucl. Phys. **19**, 191 (1989).

[64] M. G. E. Brand, K. Allaart, and W. H. Dickhoff, Phys. Lett. **B214**, 483 (1988)

[65] S. C. Pieper and V. R. Pandharipande, Phys. Rev. Lett. **70**, 2541 (1993).

[66] R. Brockmann, Phys. Rev. C **18**, 1510 (1978); H. Müther, R. Machleidt, and R. Brockmann, Phys. Rev. C **42**, 1981 (1990);

[67] C. Barbieri, W. H. Dickhoff, in preparation.

[68] R. B. Firestone, *Table of Isotopes*, eds. S. Shirley *at al.* (Wiley, 1996).

[69] E. P. Roth, Ph.D. thesis, Washington University, St. Louis, 2000.

[70] W. C. Haxton, and C. J. Johnson, Phys. Rev. Lett. **65**, 1325 (1990).

[71] F. Azjenberg-Selove, Nucl. Phys. **A523**, 1 (1991).

[72] F. Azjenberg-Selove, Nucl. Phys. **A460**, 1 (1986).

[73] G. Baym and L. P. Kadanoff, Phys. Rev. **124**, 287 (1961).

[74] G. Baym, Phys. Rev. **127**, 1391 (1962).

[75] T. N. Buti *et al.*, Phys. Rev. C **33**, 755 (1986).

[76] W. J. W. Geurts, Ph. D. Thesis, Free University, Amsterdam (1996).

[77] S. Amari, private communication (1996).

[78] W. H. Press, S. A. Teukolsky, W. T. Vetterling, and B. P. Flannery, *Numerical Recipes* (Cambridge University Press, 1975). Section 2.7.